UNIVERSITÀ DEGLI STUDI DI PADOVA

Sede Amministrativa: Università degli Studi di Padova

Dipartimento di Biologia

SCUOLA DI DOTTORATO DI RICERCA IN: BIOSCIENZE E BIOTECNOLOGIE

INDIRIZZO: BIOCHIMICA E BIOFISICA

CICLO: XXVIII

Spectroscopic Studies of the Super Relaxed State of Skeletal Muscle: a Possible Target for Obesity and Type 2 Diabetes Treatments.

Direttore della Scuola: Ch.mo Prof. Paolo Bernardi

Coordinatore di Indirizzo: Ch.mo Prof. Fabio Di Lisa

Supervisore: Dr.ssa Marcella Canton

Co-supervisore: Ch.mo Prof. Carlo Reggiani

Dottorando: Leonardo Nogara

"The hearth is the strongest muscle."

February, 1st 2016

Index

1. Summaries

1.1. Brief summary

Myosin and muscles have been studied since the beginning of the last century. The high amount of myosin and its optimized purification protocol started the huge field of the molecular motors around 50 years ago. The importance of myosin is not only due to its physiological role but also for its large contribution to the general biochemistry knowledge. Since myosin is a molecular motor, it represented an important step in the connection between chemistry and physics as fields of studies applied to biology. Myosin, as the fulcrum of biochemical conversion of energy into physical work, is the perfect example of the intimate connection between biochemistry and biophysics.

Several techniques have been used to study molecular muscle functions, and so, myosin function. Some of them are common but very powerful, as fluorescence. Some others are less used in biology, such as electronic paramagnetic resonance (EPR). Back in the 1980s, the first papers about EPR measurements on muscle fibers were published. Muscle fibers, and myosin filaments, are not an ordinary biological sample because of their physiological microscopic and macroscopic order. In such samples, EPR, being sensitive to orientation, becomes really informative. EPR was first used on muscle samples to describe the freedom of the myosin head in all the different physiological states it has to go through to complete a cycle. Using these and other techniques, scientists have been working on myosin, characterizing most aspects of the muscle motor protein. There are several models which try to describe the myosin cycle. They may be really detailed and complex. Generally, they all agree on the steps that the myosin has to go through to perform a power stroke. Recently, a new state of myosin has been identified. This state has been called the “Super Relaxed” (SRX) of myosin because when myosin enters this state the ATPase activity is very low.

In this thesis, we aim to characterize myosin behavior especially by studying the stability and the structural details of the super relaxed state.

First we wanted to explore the super relaxed state by modifying one of its components. We expressed mutants of a subunit associated with myosin and that has an important role in the stability of the super relaxed state. The protein has been exchanged into muscle fibers. The idea is to find a way to sense whether the myosin is in the super relaxed state or not. By collecting data on the effects of these mutants labeled with several probes, we were able to identify the mutant/probe couple able to sense the super relaxed state. We used that fluorimetric assay in a high throughput screening, we were looking for a molecule that was able to destabilize the state. Our belief is that the muscle tissue is a good target for increasing basal metabolism in humans, lowering the stability of the slow ATPase state to improve life quality of people affected by obesity and diabetes. A molecule has been identified and it has been shown to be a good leading compound for further pharmacological studies.

1.2. Breve sommario

Sin dall'inizio dello scorso secolo la miosina ed il tessuto muscolare sono stati oggetto di ricerca scientifica. Circa 50 anni fa, l'abbondanza della miosina ed il perfezionamento dei protocolli di purificazione hanno contribuito ad iniziare lo studio del grande campo dei motori molecolari. L'importanza della miosina non è solo dovuta al suo ruolo fisiologico, ma anche per il suo grande contributo alla crescita delle conoscenze biochimiche. La miosina è un motore molecolare ed ha rappresentato e rappresenta tuttora un importante anello di congiunzione tra chimica e fisica in quanto campi di studio applicabili alla biologia. La miosina è il fulcro della conversione di energia chimica in lavoro nel tessuto muscolare ed è l'esempio perfetto della intima connessione fra biochimica e biofisica.

Per lo studio delle funzioni molecolari del muscolo e della miosina si sono utilizzate numerose tecniche. Alcune di queste sono ormai piuttosto comuni, e anche molto potenti, quali la fluorescenza. Alcune altre sono meno conosciute in ambito biologico, come l'electron paramagnetic resonance (EPR) o risonanza paramagnetica elettronica, detta anche risonanza di spin elettronico. I primi lavori che vedono protagonista l'EPR su campioni di muscolo risalgono agli anni 80. Le fibre muscolari ed i miofilamenti sono campioni biologici particolari perchè sono fisiologicamente caratterizzati da un elevatissimo ordine microscopico e macroscopico. In tali campioni, l'EPR, essendo sensibile all'orientamento spaziale della molecola paramagnetica che porta l'elettrone spaiato, diventa realmente informativo. L'EPR è stato usato su campioni muscolari per descrivere la libertà di movimento della miosina durante i differenti stati del ciclo di interazione con l'actina. Usando questa ed altre tecniche, gli scienziati hanno studiato la miosina, ottenendo una profonda caratterizzazione di questo motore molecolare. Ci sono diversi modelli che descrivono tutti gli stati o passi che la miosina deve attraversare per completare un ciclo di interazione con l'actina. Recentemente, è stato identificato un nuovo stato della miosina. E' stato denominato stato "Super Relaxed State" o SRX per via del fatto che è caratterizzato da una attività ATPasica molto bassa.

Lo scopo di questa tesi è di caratterizzare il comportamento della miosina specialmente per quanto riguarda la stabilità e i dettagli strutturali dello stato Super Relaxed.

Il lavoro sperimentale è iniziato con lo studio sullo stato SRX attraverso la modifica di uno dei suoi componenti. Abbiamo espresso mutanti di una proteina associata alla miosina, la catena leggera regolatoria o fosforilabile, che svolge un ruolo fisiologicamente importante per la stabilità dello stato. La proteina mutata è stata sostituita alla forma naturale in fibre muscolari. Lo scopo è di trovare un insieme di proteina mutante marcata con una sonda in grado di identificare quando lo stato SRX è presente. Abbiamo sviluppato quindi un saggio fluorimetrico e abbiamo effettuato un "high throughput screening" al fine di trovare una molecola in grado di destabilizzare lo stato rilassato. Il tessuto muscolare può essere un ottimo bersaglio per aumentare il metabolismo basale, destabilizzando lo stato SRX a basso consumo di ATP e quindi aumentando moderatamente la spesa energetica. Come possibile applicazione, questo potrebbe avere un impatto positivo sulla salute delle persone affette da obesità e diabete di tipo 2. Abbiamo identificato una molecola candidato e abbiamo dimostrato che ha le caratteristiche per essere un buon punto di partenza per sviluppare ulteriori studi farmacologici.

2. Introduction

2.1. Muscle from a molecular point of view

2.2.1. The skeletal muscle

The body contains more than 660 different skeletal muscles. Muscle tissue is an important part of the body in terms of size. It is becoming more and more important and it is slowly beginning to be considered as an organ, more than mere tissue. A skeletal muscle is organized as thousands of cylindrical cells, wrapped in fibrous connective tissue, called muscle fibers. The main characteristic of a muscle fiber is its ability to contract and, by doing so simultaneously with other fibers, force is generated along the fiber long axis by the whole muscle. Each fiber is wrapped by a thin layer of connective tissue called endomysium, a bundle of about 150 fibers is surrounded by connective tissue to form a fiber bundle or fasciculum. The entire muscle is contained in the epimysium, a fibrous layer of connective tissue. The ends of the muscle are connected by the tendons, strong and dense connective tissue structures, to the periosteum, the bone outer covering. Under the endomysium, each muscle fiber is surrounded by the sarcolemma, a thin, elastic membrane that encloses the fiber cellular contents. It contains a plasma membrane, which conducts the depolarization wave to trigger a contraction, and a basement membrane, containing protein and strands of collagen fibrils fused with the endomysium and the tendon. Between the basement and plasma membrane there are the muscle myogenic cells, known as satellite cells. Satellite cells are normally quiescent and they activate upon damaging of the muscle tissue, starting the regenerative process. The cytoplasm of muscle fibers contains enzymes, fat and glycogen particles to supply energy to muscle contraction, those substrates are used by mitochondria. Since muscle fibers are formed as fused myoblasts, approximately 250 nuclei per millimeter of fiber are present, expressing genes and regulating muscle growth. The sarcoplasmic reticulum is an extensive network of tubular channels which provides structural integrity to the cell. The transversal component of the sarcoplasmic reticulum is responsible for the even propagation of the depolarization wave within all the fibers through the inner T-tubule system to initiate muscle action. The

membrane of the longitudinal component of the sarcoplasmic reticulum contains calcium channels which allow Ca2+ release from the cisternae and calcium pumps that take up Ca^{2+} from the cytoplasm. The combined action of calcium channels and calcium pumps regulates the concentration of calcium surrounding the filaments.

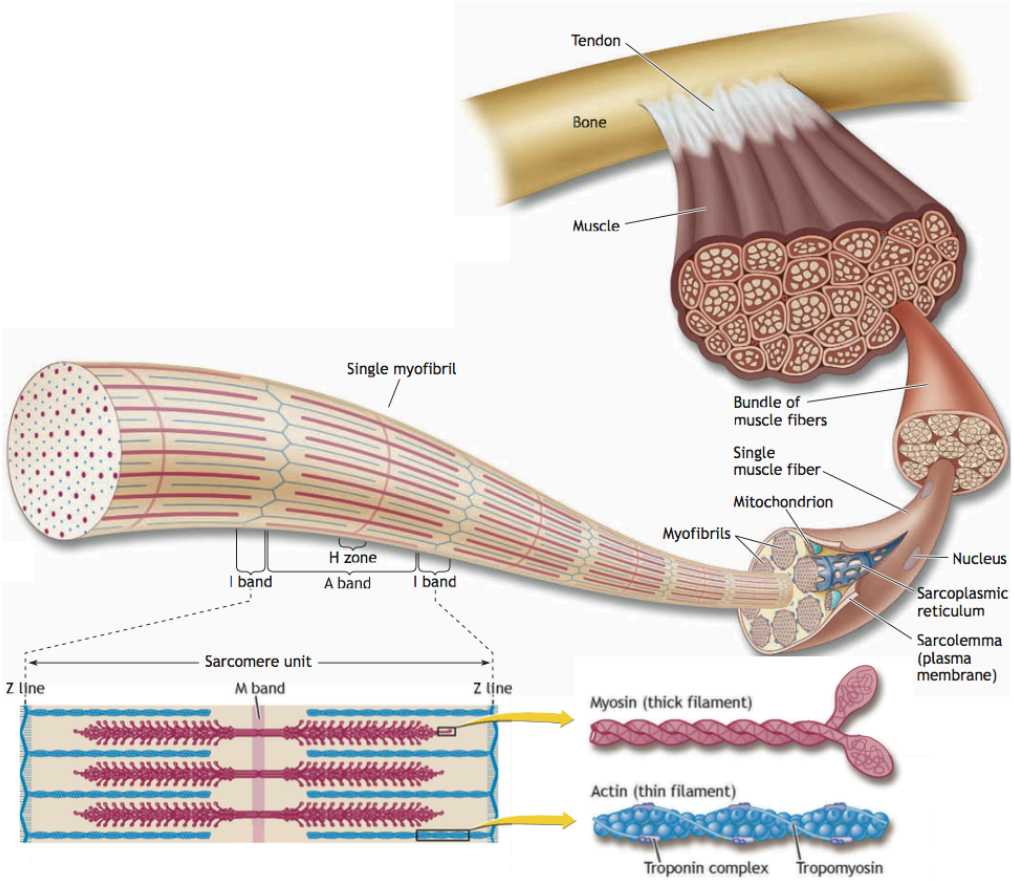

Figure 2.1. Muscle structure, macroscopic to microscopic (Source: McArdle, 2010[1]).

Arteries and veins lie parallel to muscle fibers to provide the nutrients supply. The vessels divide into numerous arterioles, capillaries and venules to form a network in and around the endomysium. Muscles are able to raise their metabolism hundreds times going from resting to strongly contracting. To support this enormous energy needs, extensive branching of blood vessels is needed. Between 200 and 500 capillaries deliver blood to each square millimeter of active muscle cross section, with up to four capillaries directly contacting each fiber[1]. Muscles have a rich innervation, being linked to central nervous system by motor efferent nerves and by sensitive afferent nerves. Each fiber receives a branch a motor nerve in a complex synaptic junction, called end plate or neuromuscular junction. The command to start a contraction originates, in form of action potential in the motor

neuron, runs along the motor axon and reach through the branching of the motor axon a number of muscle fibers, which together form the "motor unit".

2.1.2. The sarcomere

At low magnification, a skeletal muscle appears striated, white bands and black bands are alternating along the length of the fiber. Those small structures, approximately 2.5-3µm long (resting physiological length) are called sarcomeres. The darker zone is called A band, while the lighter is called I band. In the middle of the I band there is the Z line, it is connected to the sarcolemma providing stability to the entire structure. The sarcomere consists of the basic repeating unit between two Z lines and it is the functional unit of a muscle fiber. The center of the A band contains the H zone, a region where actin filaments are not present. Inside the H zone, in the M line there are the protein structures necessary to keep in register the thick filament.

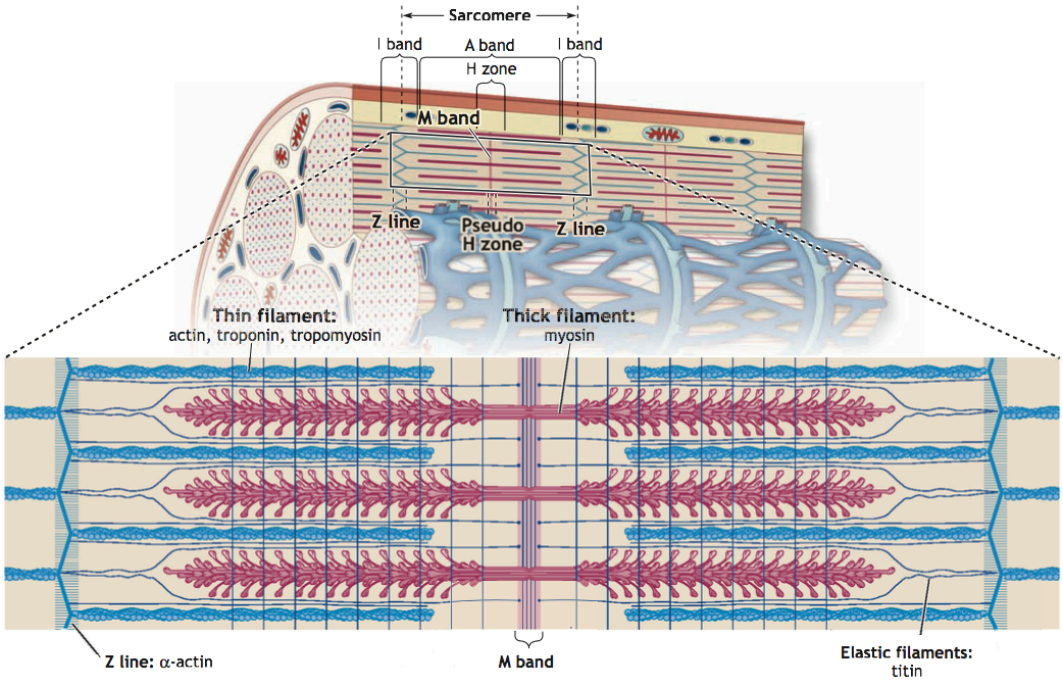

Figure 2.2. Sarcomere structure (Source: McArdle, 2010[1]).

Skeletal fibers are constituted for approximately 75% of their mass by water and 20% by proteins. The remaining 5% are due to salts, high-energy phosphates, urea, lactate, calcium, magnesium, and phosphorus. Organic molecules such amino acids, fats and carbohydrates are part of this 5%, too. Myosin represents approximately

60% of the total amount of proteins in a muscle fiber, and, together with actin and tropomyosin, they are the most abundant muscle proteins.

Techniques such as electron microscopy and X-ray diffraction have been used to reveal the microscopic details of a muscle fibers. A single multinucleated fiber contains smaller functional units that lie parallel to the fiber axis, called myofibrils. Myofibrils are 1μm in diameter and are made of smaller subunits called filaments. There are two filaments, the so called thin one is made of actin and tropomyosin, the thick filament is mainly composed by myosin molecules. Since both filaments are ordered structures of proteins, muscle fibers are so ordered that it is possible to collect diffraction patterns when observed with an X-ray beam. Myosin and actin account for 85% of the total protein content of the myofibril. Myosin is the molecular motor, the key element of muscle contraction. During the powerstroke, myosin binds to an ordered array of actin molecules, the thin filament. About a dozen of other structural proteins are less abundant but play important roles. Tropomyosin and the troponin complex lie on the thin filament and they are responsible for the control of calcium-triggered muscle contraction.

2.1.3. Muscle contraction

Muscle contraction is a wonderful example of several biological systems interconnected and finely regulated. The first of the many steps that need to be done to start muscle contraction is calcium release triggered by a depolarization signal coming from the nervous system. Within this frame, it is interesting to appreciate that contraction intensity is related to the frequency of the electrical stimulation. A fully contracting muscle is receiving a stimulation which is in the order of 60-100 Hertz. The impressive amount of work needed to support a depolarization, calcium release and uptake that have to occur up to 100 times in a second is possible only in a finely tuned and perfectly structured machinery.

In skeletal muscle, calcium is stored in the sarcoplasmic reticulum. To release this calcium, a depolarization wave comes from the peripheral nervous system, triggers the release of acetylcholine at the neuromuscular junction level and propagates again as depolarization through a structure called T-tubule. The T-tubule system runs perpendicular to the myofibrils, two vesicles, part of the sarcoplasmic

reticulum and called cisternae, lie parallel to the T-tubule, one for each side, forming a structure called triad. The triad is a repeating pattern of two vesicles and a T-tubule in the middle, one for each side of the Z line. The triads and the T-tubule system form a micro transportation network, they spread the action potential from the fiber outer membrane to deep inside the structure and generate a widely spread release of calcium from sarcoplasmic reticulum to the cytosol where myofibrils lie.

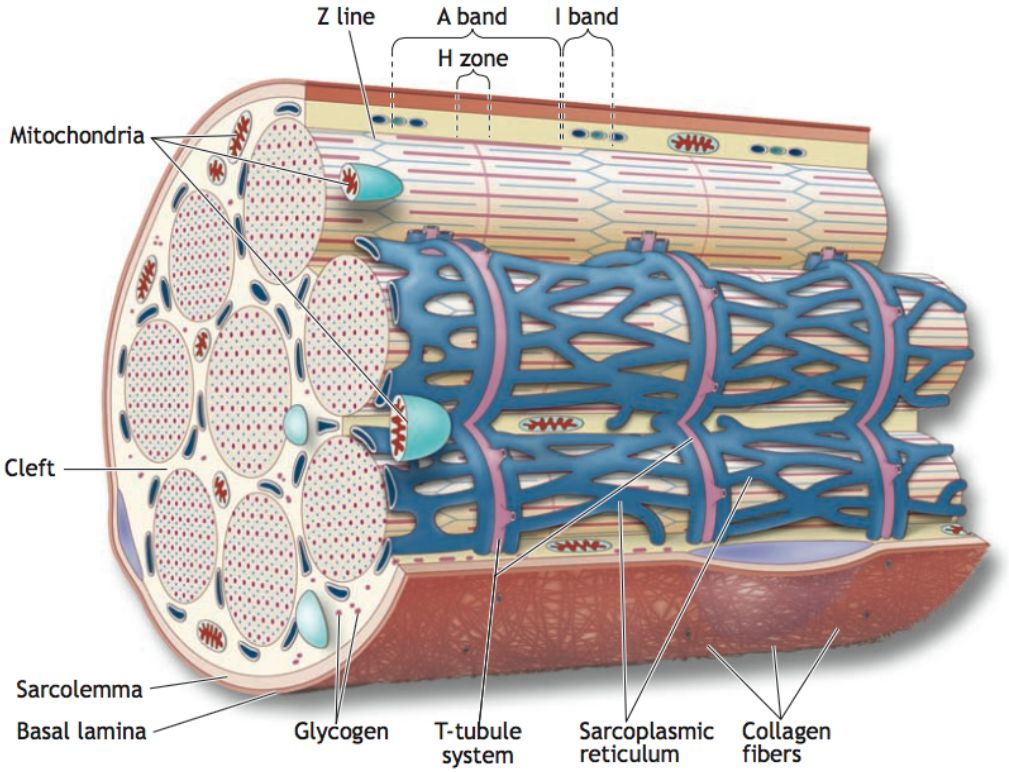

Figure 2.3. Muscle fiber microscopic structure: T-tubule system, mitochondria and membranes organization (Source: McArdle, 2010[1]).

When calcium flows in the surrounding of the myofibril, it binds to troponin C, an element of the troponin complex, and it causes a structural rearrangement of the protein[2]. When calcium is bound to troponin C, the troponin complex stops to hold tropomyosin in the "blocked" state and the molecule can now move to a "mobile" position, tropomyosin is pushed away to its, third, "open" position by myosin contacting actin in the thin filament[3,4]. Tropomyosin arrangement follow a helical order, the N-terminus of a molecule binds to the C-terminus of the next tropomyosin. This conformation allows the movements of the protein to be highly cooperative in the presence of calcium.

The most accepted model of muscle contraction has been proposed in the 1950s by Hugh Huxley and Sir Andrew Fielding Huxley[5] and it is called the sliding-filaments model. The model describes muscle shortening as the result of a sliding of thin and thick filaments that pass each other without changing their length. Myosin is the molecular motor that, by hydrolysing ATP, provides force to drive the sliding movement. Several studies support this model; a strong point is force development when compared to sarcomere length. At very long sarcomere lengths there is no overlap between the thick and the thin filament and force is very small, while with the decrease of the sarcomere length the force increases up to a maximum when the overlap is complete. A further decrease of the sarcomere length results in a drop in force production since the overlap is, again, not optimal. Myosin is an actin-activated ATPase, so, in muscle contraction, it plays an enzymatic role as well as a structural role. The thick filament is formed by approximately 300 myosin molecules all bound together with their filamentous part (the tail) in a sort of a bundle. Actually, myosins are dimers, the two heavy chains have a coiled coil structure, the tail, buried in the thick filament, while the two heads are protruding out of it and extending towards the thin filaments.

During a contraction, each myosin head can attach and detach from its binding site on the actin filament several times. During the attached state, the change in shape or isomerization of the head corresponds to a powerstroke and cause a translation of the actin filament of up to 10 nm. Skeletal muscle myosin it is not a processive molecular motor, the two heads do not cooperate in contraction and they bind to actin only for one tenth of the time of an ATPase cycle[6]. Since skeletal myosin is not processive nor cooperative, the sliding of the filaments occurs as a smooth, regular movement, thus the shortening of the fiber is even. Myosin touches actin for a very short time because myosins binding the thin filament for too long would slow down the contraction speed.

2.1.4. Relaxed muscle

Muscle contraction ends, when calcium is pumped back into the sarcoplasmic reticulum mainly by specialized ATPase enzyme called SERCA. When the calcium concentration is low enough, the ions still bound to the troponin complex are released and tropomyosin slides back into the "blocked" position, not allowing myosin to attach actin anymore. Since actin is not available anymore for myosin to bind, myosin bends back to the core of the thick filament, in the so called "Interactive J motif". The structure and details on the relaxed thick filaments have earned, recently, a great interest. According to the classical model, myosins in the relaxed state were characterized by a disordered condition in which it hangs in the space between the filaments, hydrolyzing ATP with a slow time constant. The model was fully functional from the mechanical point of view of a single myosin but it was not fulfilling the metabolic requirements of a living organ. Back in 1978, when the ATPase activity of resting frog muscles was compared with the purified frog myosin, a discrepancy in the values obtained was observed. The ATPase activity measured in a resting muscle, measured by oxygen consumption, was in the order of 0.0024 s-1 [7, 8] while it was in the order of 0.011 s-1 in purified myosin subfragment-1[9]. In both cases experiments were done on frog muscles. The fact that the ATPase activity is 4.5 times higher in the purified myosin compared to the muscle leaded to the idea that a component was missing in the purified protein which was inhibiting the activity in the intact muscle. Recently, a new state of the resting muscle has been proposed[10]. The state was called "Super Relaxed" (SRX) because it shows an ATPase activity much lower than the classic disordered relaxed state. As explained in the rest of this thesis, the SRX state may be that inhibiting factor.

2.1.5. Myosin structure

Myosin in the thick filament is organized in dimers. As said, myosin is a molecular motor which is able to convert the chemical energy stored in ATP in movement. ATP binds to myosin in the nucleotide binding pocket, in the head region. Myosin is an actin activated ATPase and the actin binding site is on the other side respect to the nucleotide binding pocket. How is it possible that the actin binding activates ATP

hydrolysis on the other side of the myosin head? And even more, how is the energy converted into movement even further in the structure? To do its action, myosin undergoes several structural rearrangements. Myosin interacts with actin in a weak binding state (ionic binding) and then, once the cleft is closed on actin and the binding to actin has become strong (hydrophobic binding), the protein structure acquires a high energy level with the contribution of ATP hydrolysis. After the release of the hydrolysis product, the new low energy level is reached and the powerstroke is performed. In order to perform the power stroke, myosin amplifies the internal structural rearrangements by using a rigid lever-arm.

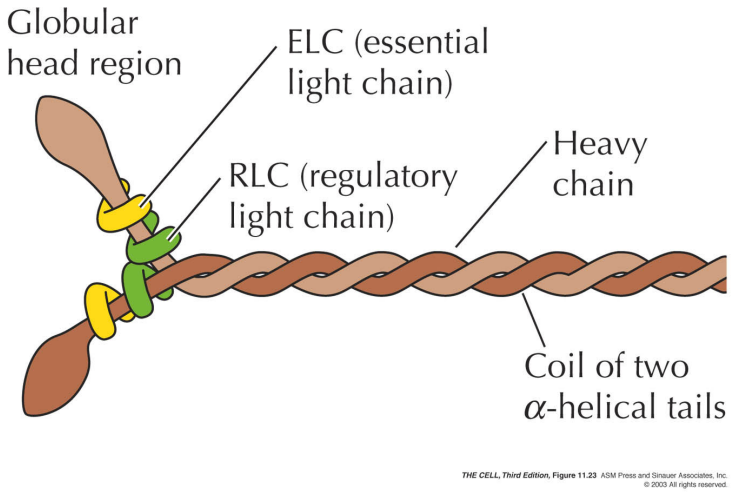

Figure 2.4. Myosin structure. Source: THE CELL, Third Edition.

The lever arm is a single chain of amino acids 85 Ålong and, even if it is an alpha helix, it is not rigid enough for itself, it needs two accessories proteins called the light chains (Figure 2.4.). The two light chains are calmodulin-like proteins which bind to the heavy chain to stabilize the structure and to give to the lever-arm the right stiffness. If the light chains are extracted from myosin, the sliding speed drops down[11]. The essential light chain (ELC) binds the lever arm heavy chain right just close to the myosin head and has a structural and functional role. Recently, researchers proposed that the N-terminus of the ELC may reach the thin filament and have a role in myosin dynamics as well[12]. The regulatory light chain (RLC) binds to the heavy chain more distally compared to the ELC, i.e. more close to the tail, and, as the name suggests, it has a regulatory function due to the phosphorylation site at its N-terminus. RLC phosphorylation is known to be involved in the post-tetanic potentiation (PTP). PTP is the mechanism which is responsible for the potentiation

of the contraction after an intense contractile action. Calcium flowing into the muscle fiber cytosol binds to calmodulin, activated calmodulin binds to its binding domain on the myosin regulatory light chain kinase (MLCK), activating the enzyme. MLCK is the enzyme responsible for phosphorylation of the N-terminus of the RLC. It is known that RLC phosphorylation (pRLC) is associated with stronger contraction. The effect of pRLC is to increase the fraction of crossbridges contacting the thin filament at all calcium concentrations, thus potentiating contraction[13]. Equilibrium between the phosphorylated form of RLC and the non-phosphorylated one depends on the frequency of the contraction and on the activity of myosin light chain phosphatase (MLCP) which removes the phosphorylation. MLCK is more abundant in fast-glycolytic fibers and less abundant in slow-oxidative fibers, MLCP abundance is the opposite.

2.2. The SRX state

In 2010 a new state of myosin has been proposed and described as a population of myosin in a state with very low ATPase activity and called the "Super Relaxed State" (SRX)[10]. The SRX state has been added to the model of the actin-myosin interaction cycle, so that myosin, once hydrolyzed the ATP molecule can "bounce" to the thin filament to develop force or move to the closed structure of the SRX state, whether the thin filament is not available.

In order to have a comprehensive view over the process, it is necessary to introduce the concept of myosin populations. In every moment, several myosin populations coexist in the fibers. A change in the state of the muscle shifts the equilibrium between populations, moving myosins from one to another. As discussed above, muscle structure, at the protein level, leads to the idea that cooperativity plays an important role in managing the overall organization. The best picture of muscle and myosin behavior would be composed of all these components, several dynamic populations which are in equilibrium between each other and changes in the equilibrium occur with strong cooperative mechanisms.

2.2.1. Measuring the stability of the SRX in skinned muscle fibers.

The measurement of the SRX state in muscle fibers is complicated by a number of factors. Measuring the ATP turnover of myosin in skinned muscle fibers is challenging because others ATPases are still present in the sample. Skinned muscle fibers are obtained by treating fibers with detergents, usually Triton X-100, or solution containing 50% glycerol. These conditions solubilize partially the plasma membrane and the sarcoplasmic membrane, allowing solutions and substances to diffuse into the fiber. Skinned fibers are not viable anymore, they do not have a metabolism and they do not express proteins, but they are able to contract and they are reliable from the mechanical point of view. Permeabilized fibers have their membranes partially solubilized, so ATPases like SERCA and sodium potassium pump can work continuously and consume ATP. In steady-state assays, these faster ATPases dominate the slower SRX myosin. It is even more challenging when the aim is to detect the most inhibited state, so, its ATP consumption is approximately a order of magnitude smaller than that of myosin in the disordered relaxed state. The key experiment in the paper by Stewart et al.[10] was the chasing of muscle fibers with a fluorescent ATP analogue, mantATP. A muscle fiber is mounted in a flow cell on the stage of an inverted fluorescent microscope. Fiber is in rigor solution, when the fiber is in focus the buffer is exchanged with a rigor solution containing 250μM mantATP, the fluorescent ATP analogue. MantATP has been shown to bind to myosin with higher affinity than that of ATP, and to be hydrolyzed with similar kinetics as ATP[14, 15].

In muscle fibers exposed to mantATP, myosin is able to detach from the thin filament and, since calcium is absent, it goes into the more stable conformations, the relaxed or the SRX state. The fiber is incubated in mantATP for several minutes so that all the myosin heads are able to bind the molecule. The mantATP also binds to other ATPases and, non-specifically, to other structures in the fiber. After incubation the fiber is chased with a relaxing solution containing normal ATP. The mantATP still bounded to the proteins is hydrolyzed by the ATPases at different rates and the relative mantADP diffuses out of the fiber. The decay in fiber fluorescence occurs in two phases: the fast initial phase occurs in 20-30 seconds while the slower second phase with a time constant of about 4 minutes (see Figure 2.5.).

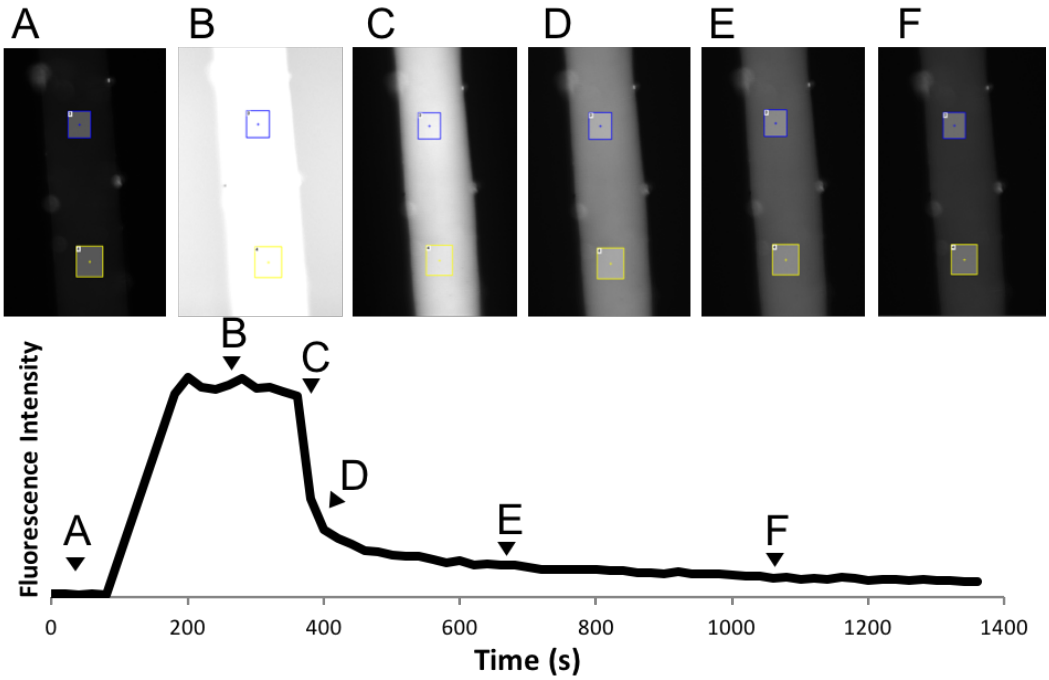

Figure 2.5. mantATP chasing experiment. *A*, fluorescence of the fiber with no fluorescent nucleotide mantATP. *B*, fiber in mantATP solution. *C*, chasing with ATP. *D* to *F*, decrease in fluorescence intensity due to hydrolysis of the bound mantATP and diffusion of mantADP out of the fiber.

The first phase of fluorescence decay consists of free nucleotides that were either non-specifically bound mantATPs or mantADPs as product of hydrolysis by fast ATPases. These disordered myosin heads and other enzymes present in the fiber have fast turnover rate, so that mantATP is hydrolyzed and released in less than 20 seconds and diffusion of free nucleotides out of the fiber occurs in about 10 seconds. The slower phase has been shown to be largely due to the slow turnover and release of mant-nucleotides from myosin that is in the SRX[10]. The data could be adequately fit by a function consisting of 2 exponential decays, one with a short lifetime and one with a longer lifetime. The populations of the two phases are called P1 and P2 and their lifetimes T1 and T2 (see Figure 2.6.).

The mantATP chasing is a powerful experiment but it has an important drawback. All the data points have to be normalized by the fluorescence before the chasing and that value contains the fluorescence of mantATP bound to other ATPases as well as non-specific sites (i.e. hydrophobic sides of proteins, membrane fragments). Since that value is not only considering myosin but also other ATPases and unspecifically bound mantATP, it is overestimated.

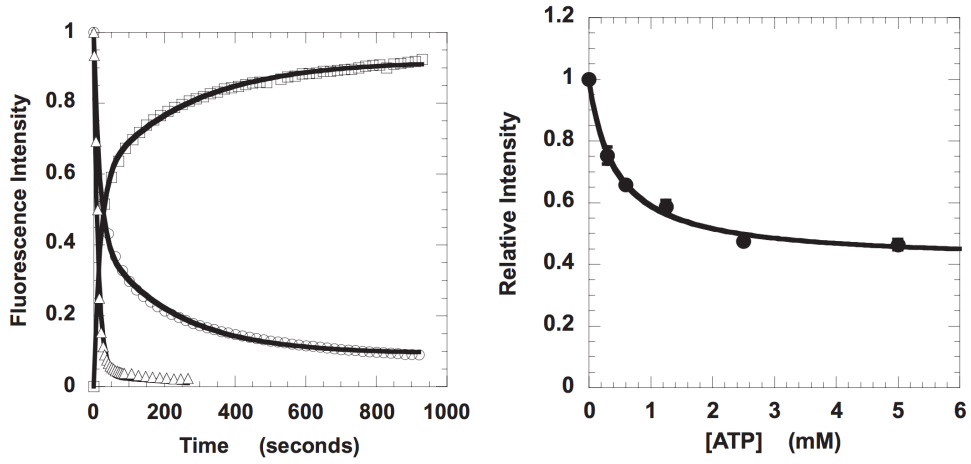

Figure 2.6. Left panel: mantATP chasing of rabbi skeletal muscle fibers. Incubation with mantATP and chasing with ATP (○). Incubation with ATP and chasing with mantATP (□). Incubation with mantATP and chasing with ADP(△).The data were fit with a double exponential function. The fits are defined as follows: ATP chase P1=0.58±0.01, T1=19±1s, P2=0.34±0.01, T2=258±12s; mantATP chase, P1=0.58±0.01, T1=16±1s, P2=0.33±0.01, T2=216±36s; ADP chase, P1=0.94±0.01, T1=12±1s, P2=0.05±0.01, T2=175±30s. **Right panel:** Determination of the fraction of mant nucleotides bound specifically to ATP binding sites in the fiber. The data of this figure were fit to a simple competition model (solid line), which defined the fraction of mant nucleotides bound nonspecifically to the fiber as 0.41 ± 0.02, and the ratio of the apparent affinities of ATP to mantATP, as 0.57 ± 0.07. [10]

Normalizing the other values to an overestimated value would result in an underestimated amount of myosins in the SRX state (P2). As explained by Stewart et al.[10], assuming that all of the specifically bound mant nucleotides are bound to myosin, a value of P2 of 0.33 represents a larger fraction, 0.56 of the fluorescence arising from binding to myosin. This implies that about 40% of the fluorescence of the first time point is generated by mantATP not bound to myosins.

2.2.2. The structure of the SRX state

Several evidences have been provided in support of the idea that the thick filament is an ordered structure in relaxing solution[16, 17]. A complete structural model of the thick filament identifies the backbone of the filament as an aggregate of the myosin tails, i.e. the alpha-helical coiled coil myosin rods. The packing is based on a regular pattern of charge on the 28 amino-acid repeat occurring in the myosin tail. At the surface of the thick filament, myosin heads are arranged in three rows, organized at an angle of 120° to each other and regularly spaced with a periodicity of 14.3nm

along the filament axis. A first picture of a relaxed myosin from relaxed smooth muscle, chicken gizzard, has been published in the late 90s, the structure has been called Interactive Heads Motif (IHM)[18].

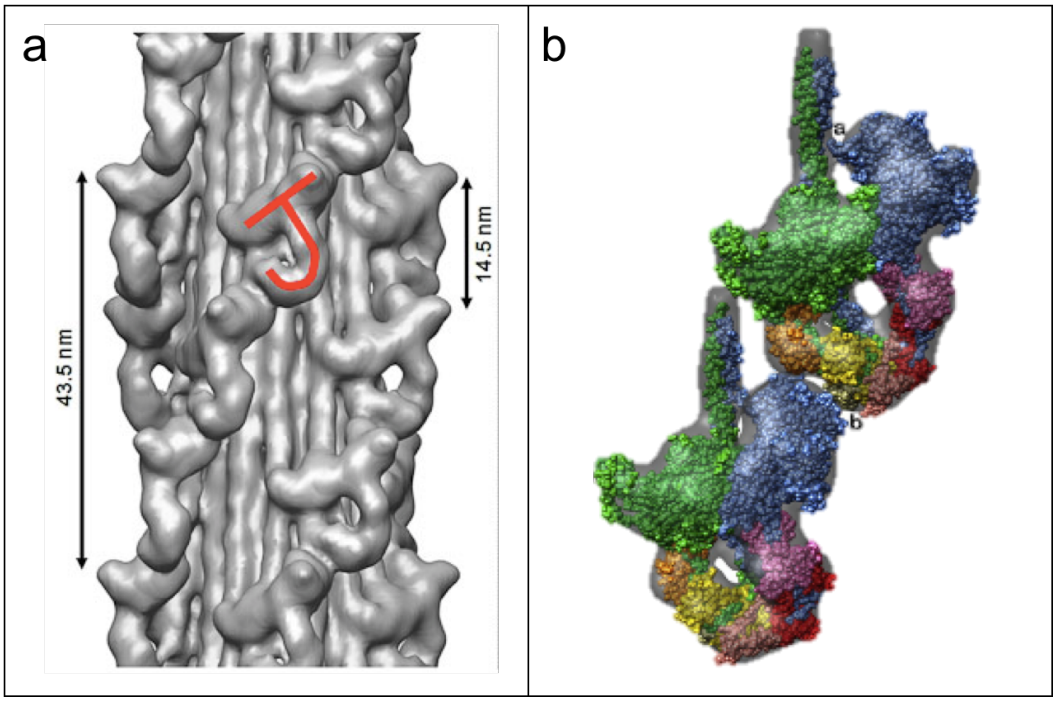

Figure 2.7. a) Interactive J motif highlighted in the cryo-3d electron density map of the tarantula thick filament. **b)** Fitting of myosin (green and blue), essential (orange and purple) and regulatory light chains (yellow and pink) structures into the electron density map, inter-complex contacts are possible in this model. [19]

In 2005 and 2008 a new model of the structure of the resting thick filament has been published based on a cryo-3d electron density map. The new model shows the heads in a closed conformation, bound back to the core of the filament[19, 20, 21]. The structure has been defined as the "J motif" because of the shape that the two myosin heads form with their light chains (see Figure 2.7.). The complex is formed by the myosin dimer, the lever arm is closed back to the thick filament, which presents a sequence of J complexes placed in an helicoidal order. According to the model, in the J motif myosin heads are touching each other, and at least one of them is binding to the heavy chain as well. Another surface which may be relevant is the one formed by the regulatory light chains at the bottom of the J. The 3d density map provides information about a number of interfaces that may be important for the stability of the complex. Some protein-protein interfaces are within the myosin dimer, while some other interfaces are inter-dimers. This kind of organization leads to the hypothesis that cooperativity drives the equilibrium of the in-out transition. A

surface that may be particularly important is the one formed by the regulatory light chains, at the very bottom of each J motif. Actually, in their paper, Cooke and coworkers showed that RLC phosphorylation affects the SRX state stability but with a low incidence. SRX state population is decreased by just about 30% (P2 goes from 30% to 20%) by going from approximately 0% to 80% of RLC phosphorylation[10]. In order to stabilize the complex, all the surface interactions have to subtract a certain amount of energy. In other words, to reach the lowest and more stable energy level, all protein-protein contacts must be formed. The RLC N-terminus region is characterized by a large number of positive residues, the negative charge applied by a phosphorylation in that region may change its conformation, destabilizing the RLC-RLC surface, thus, pushing the whole complex out of the low-energy state. The chasing experiment shown in Stewart et al.[10] gives support to the view that P2 changes with the change in RLC phosphorylation (see Figure 2.8. A and B).

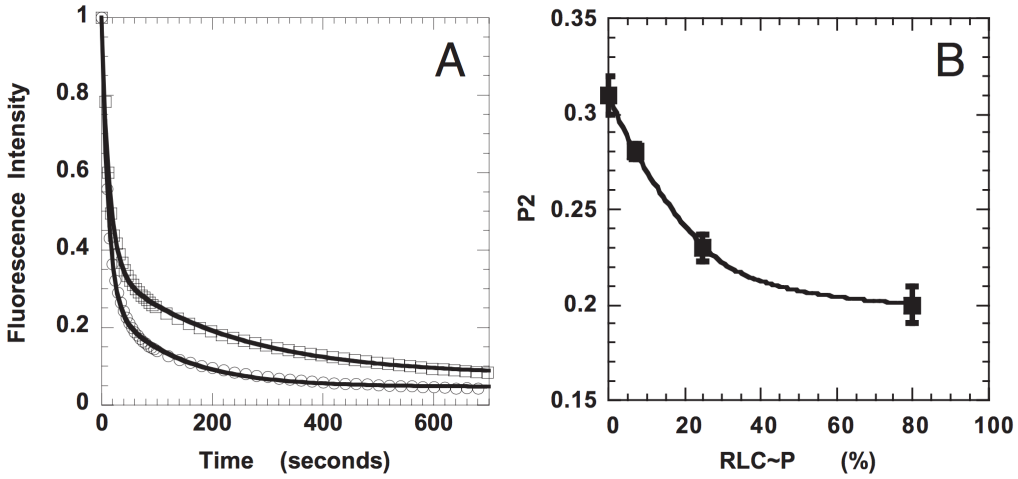

Figure 2.8. A) Chasing of mantATP in rabbit skeletal muscle fiber at 7% RLC phosphorylation (top trace) and 85% RLC phosphorylation (bottom trace). Fits to the data are defined as follows: 7% phosphorylation, P1=0.64±0.01, T1=14±1s, P2=0.28±0.01, T2=230±40s; 85%phosphorylation, P1=0.73±0.01, T1=11± 1 s, P2 = 0.22 ± 0.01, T2 = 125 ± 6 s. **B)** P2 as a function of RLC phosphorylation[10]. Temperature 24°C.

The strength of protein-protein interactions depends from the temperature, making the interaction stronger at approximately 37°C, the physiological temperature, and becoming weaker with the decreasing of the temperature. In Figure 2.9. two chasing experiments are compared on control fibers. The upper trace was performed at 30°C while the lower trace is the result of the experiment at 12°C. The population of myosin in the SRX state is 0.33 at 30°C and it dropped to 0.16 at 12°C.

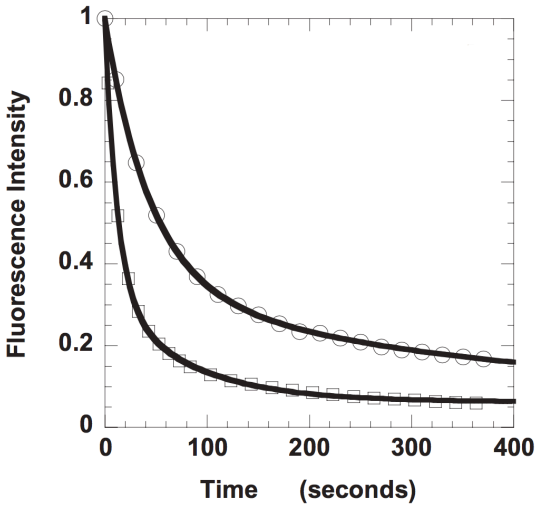

Figure 2.9. Chasing of mantATP in rabbit skeletal muscle fiber at 30°C (top trace) and 12°C (bottom trace). The fits to the data are defined as follows: 12°C, P1 = 0.80 ± 0.01, T1=26±1s, P2=0.16±0.01, T2=138±10s; 30°C, P1=0.57±0.02, T1=28±2s, P2 = 0.33 ± 0.02, T2 = 246 ± 35 s.

2.3. Electron Paramagnetic Resonance

Electron Paramagnetic Resonance is a technique which allows to characterize unpaired electrons, like free radicals. By using paramagnetic probes, also known as spin labels, it is possible to add stable unpaired electrons into biological samples which otherwise would not give any signal. EPR is a particularly valuable technique because it allows protein and biological samples to be studied in an aqueous environment and at physiologic temperatures, giving information about conformational changes of macromolecules. The most common technique is known as Continuous Wave EPR (CW-EPR). In CW-EPR the sample is irradiated with an electromagnetic radiation at a constant frequency, while the magnetic field sweeps continuously. The resonance is reached when the difference in energy among the levels, caused by the magnetic field, matches the frequency of the microwaves radiation applied to the sample. When resonance is reached, energy is absorbed by low-energy electrons in order to move to the high-energy spin state. The absorption or the release of energy by electrons is registered by the instrument and the signal is shown as the first derivative of the absorption (see Figure 2.10.).

EPR principles are very similar to those of Nuclear Magnetic Resonance (NMR). Both techniques are able to detect a difference in spin, for NMR is of nuclear spins while for EPR is of electrons spins.

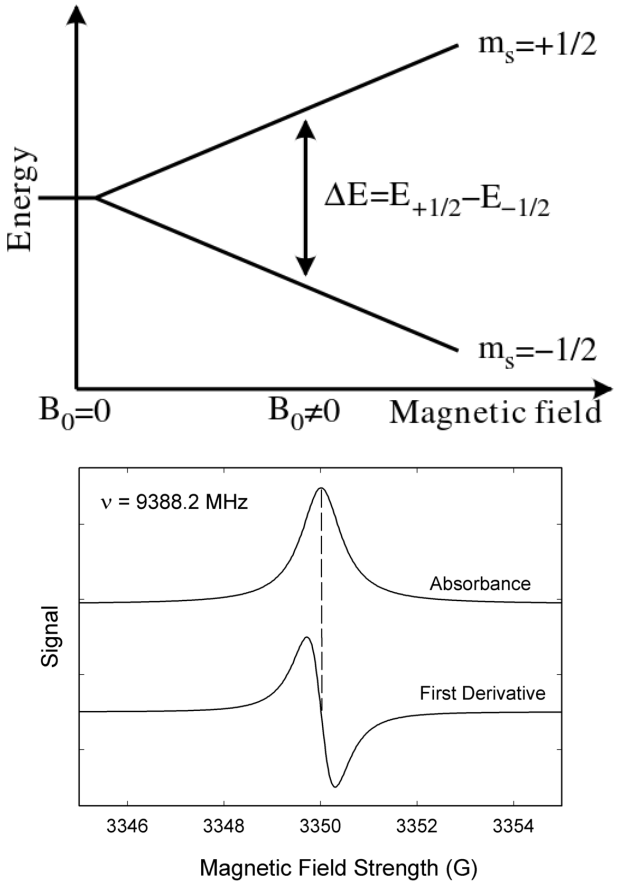

Figure 2.10. Splitting of the electrons population due to the external magnetic field, absorbance and first derivative of the absorbance as EPR signal of a transition from the low energetic state to the high energetic state.

In the absence of an external magnetic field, the energetic difference among the two spin orientation is so small that electrons can freely move from one state to the other. The splitting of the states is achieved by applying an external magnetic field and it is proportional to the intensity of the magnetic field.

To label biological samples that do not contains unpaired electrons spin probes can be used. Common spin probes are made by functionalizing in different ways a TEMPO molecule (see Figure 2.11. A). TEMPO is a molecule containing a stable unpaired electron, its ringed structure and the four methyl groups contribute to stabilize the radical (see Figure 2.11. B).

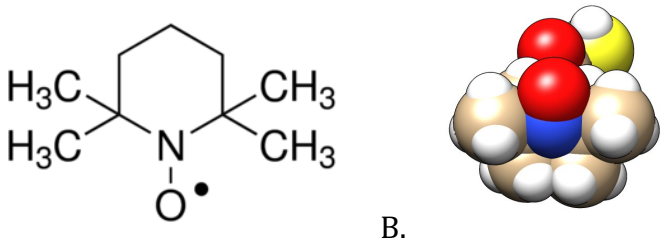

A. B.

Figure 2.11. A) TEMPO molecule. **B)** TEMPO molecule 3D structure, front view. Obtained using UCSF Chimera software[22].

The electron is not only sensitive to the external magnetic field but also to magnetic fields caused by surrounding nucleus. In the case of the TEMPO molecule, the electronic magnetic moment interacts with the nuclear magnetic moment of the nitrogen nucleus (^{14}N). This effect is called "hyperfine interaction". Depending on the direction of the spins, the energy required for the transition can be higher (spin quantum numbers are both positive) or lower (spin quantum numbers are both negative). Since spin quantum number for electrons can be equal to M_S=+½, -½ and nitrogen nucleus can have a spin quantum number of M_I=+1, 0, -1; each of the energy levels achieved by the electrons due to the external magnetic field split into two levels.

The allowed transitions in this system are now three:

- from M_S=-½ to M_S=+½ while M_I=+1 (*k*);
- from M_S=-½ to M_S=+½ while M_I=0 (*l*), the original transition;
- from M_S=-½ to M_S=+½ while M_I=-1 (*m*).

Transitions in which both electron spin quantum number and nucleus spin quantum number change are not allowed by selection rules. The transitions occur at different energy and so at different magnetic field intensity. In the first derivative spectrum, they appear as three peaks. Since the spin quantum number of nitrogen is added and subtracted by the original transition energy, the side peaks are at the same distance from the central peak.

The spectrum reported in Figure 2.12. represents the case of free spin probe in solution. The shape of the spectra can be affected by a number of factors. The rotational correlation time is an example of how EPR is sensitive to freedom of movements.

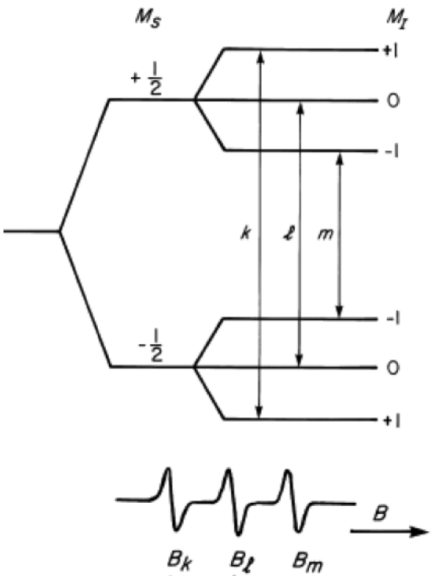

Figure 2.12. Energetic levels in a nitroxide molecule representing the energy splitting due to hyperfine interaction.

Figure 2.13. shows how the signal changes when the rotational correlation time goes from approximately 1ns to 1μs. The range shown in the picture is the one of CW-EPR, the one used in this work. There are other techniques, like Saturation Transfer EPR, that are sensitive to rotational correlation times smaller than 1μs.

Figure 2.13. Changes of the EPR spectra of a nitroxide probe respect to the rotational correlation time.

Spectral changes seen in Figure 2.13. can be obtained by measuring a free spin probe in several solutions with crescent viscosity. EPR is also sensitive to orientation.

Spectra can be analysed to obtain a cone angle in which the probe moves (see Figure 2.14.).

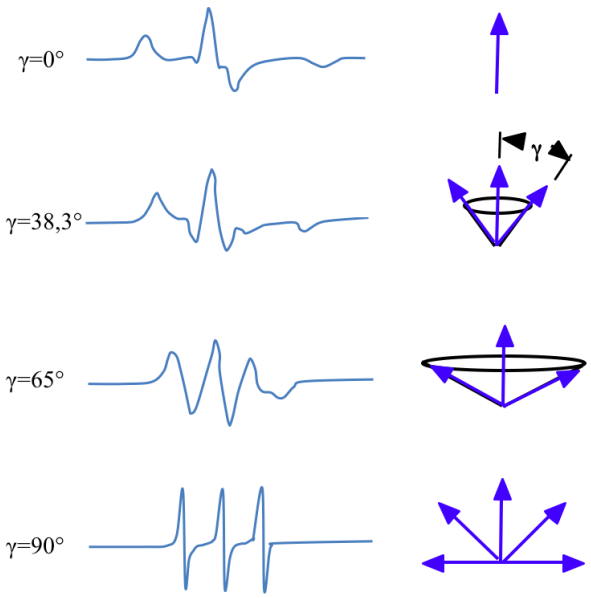

Figure 2.14. Changes in the EPR spectra of a nitroxide probe depending on the amplitude of the cone angle in which the probe is free to move.

2.3.1. Protein labelling

In order to have a paramagnetic signal, the sample must contain unpaired electrons. In case of biological sample, unpaired electron are often oxygen reactive species. For those samples, EPR is used to measure amounts of the oxygen reactive species. Skinned muscle fiber samples do not contain paramagnetic species. Spin probes can be used to introduce paramagnetic molecules in a biological sample. As reported, TEMPO derivatives have been commercialized and can be used according to situations. Several kind of spin probes are available. In the experiment reported in the present thesis, we used three different molecules: MTSL, IASL and MSL (see Figure 2.15.).

MTSL (or MMTS) is used for its small size but it has an important drawback, it reacts with a cysteine forming a disulfide bond and it can detach in a reducing environment. Even if IASL and MSL do not suffer the detaching issue, all paramagnetic probes are affected by reducing agents. In a reducing environment the paramagnetic probe would be quenched and the signal would be lost. IASL is characterized by a high mobility, the TEMPO is bound to the protein through a

mobile leash containing four bonds free to rotate. The molecule has a high flexibility and it can sneak around protein structures and adapt to different environments. These kind of probes are called "floppy". As an example, IASL has been used in a paper by Thomas and Cooke (1980) to label myosin cysteine 707[23] which has a surface exposed to the solvent of only 12 Å² instead of the usual 70 Å² of a surface cysteine[24]. The significant drawback of a floppy probe is that in many situations the probe would report only dramatic changes in the surrounding environment because the molecule masks small differences in its large freedom of movements. MSL is considered a well-ordered probe. In MSL, TEMPO is functionalized with a maleimide ring which is highly reactive with cysteine. The molecule can only rotate around one bond. As reported in Sale et al.[24] the desired probe behavior depends on the information that probe has to report: a well-ordered probe is desired to study backbone and domain dynamics, while a floppy probe is desired to study the extent of steric restriction of the side chain by its local protein environment.

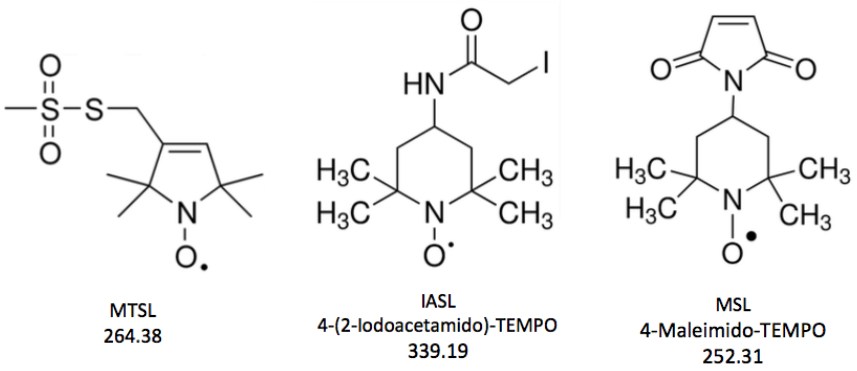

Figure 2.15. Structure of common paramagnetic probes.

The spin probes we used are small molecules that react with cysteine. They are approximately the same size of a big amino acid side chain. Figure 2.16. compares the structure of MSL and a tryptophan, even if the size is comparable, the amino acid has a more flat shape than the "balloon" shape of the spin probe. Figure 2.17. shows the reaction of a MTSL molecule with a cysteine. Each of these probes react with cysteines and so the flexibility is due also to the two bonds between the α and β carbons and the β carbon and the sulphur atom.

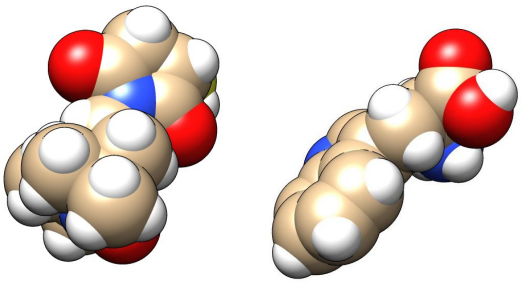

Figure 2.16. Size comparison of a MTSL molecule and the ammino acid tryptophan. Side view. Obtained using UCSF Chimera software[22].

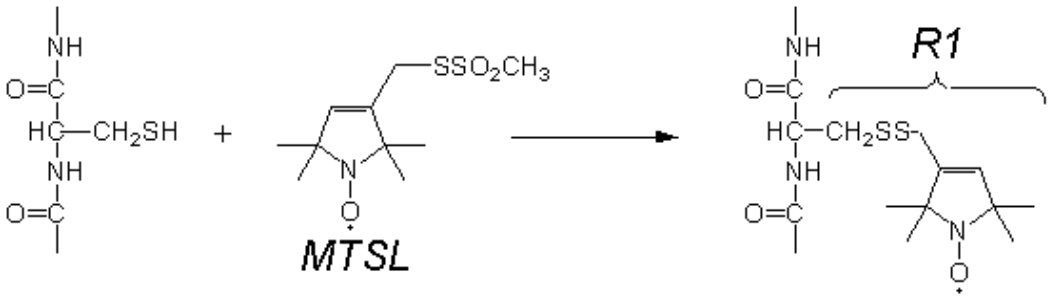

Figure 2.17. Scheme of the reaction between a MTSL spin label and the cysteine of a protein.

The reliability of EPR results have often been questioned because the behavior of the probe would be considered as the behavior of the labelled protein too easily. The assumption that the probe is solid with the labelled protein is not correct and it should always been considered that the timescale of molecular movements are orders of magnitudes shorter than the protein movements. To overcome the issue of excess of mobility, bi-functional probe have been developed, so that they will bind to two different residues in the same alpha helix.

As shown by Figure 2.18., which refers to probe attached to a myosin regulatory light chain (RLC), the free probe in solution has a three sharp peaks (panel a), the same probe bound to the RLC changes the shape to a less mobile situation (panel b). The addition of more constraints by exchanging the protein into a muscle fiber, gives an immobilized spectrum (panel c). An immobilized probe gives a spectrum that is characterized by a positive peak in the low field region (left side) and a corresponding low peak in the high field region (right side).

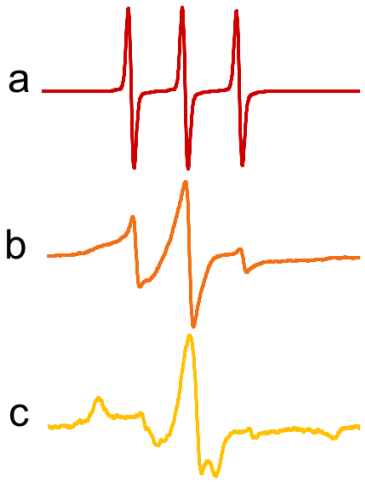

Figure 2.18. EPR spectra of a MMTS spin label free to move in aqueous solution **(a)**, bound to a RLC in solution **(b)**, bound to a RLC exchanged into muscle fibers **(c)**. The spectra show that the probe is experiencing higher constrains, going form a very mobile (solution) to an immobilized situation (in fiber).

2.3.2. EPR machine

The EPR machine is essentially composed by two magnets to generate the external magnetic field (Figure 2.19.). In the middle of those magnets, where the parallelism of the field lanes is maximum, there is the resonator. The resonator is a cavity in which the sample is positioned, so it can experience the magnetic field. The resonator is connected through a waveguide to the microwave source, also called "bridge". In CW EPR, microwaves are generated in the bridge, they go through the waveguide to the resonator and, when the system is tuned, the waves sum up to reach higher power without leaving the cavity. Energy is proportional to frequency, so, energy absorbed by the system leads to waves with different frequencies which do not resonate anymore and leave the cavity. The bridge is able to separate the waves coming back which are then sent to the detector. The detector compares the signal coming from the sample with a reference arm which is coming from the bridge to measure differences. A consolle is controlling the whole system. Since EPR is prone to signal-to-noise issues, the measures are taken at 100kHz and the resulting signal is measured at the same frequency, this allows to cut the noise which does not have a precise frequency.

Figure 2.19. EPR machine**.** Picture scource: http://epr.chem.wisc.edu/sites/epr.chem.wisc.edu/files/styles/large/public/EPR_Bruker_0.jpg?itok=KUaCmFKc

2.4. Fluorescence spectroscopy

Fluorescence spectroscopy is a technique which analyse fluorescence from a sample. Fluorescence is an emission of energy in form of light of a sample that has been previously excited with a light with a higher energy level. Absorption is the process which drives an electron from the ground state (S0) to an excited state (S1) by adsorbing an amount of energy which is equal to the energetic difference among S0 and S1 levels. Energy is delivered to the system in form of photons and it is characterized by a wavelength which is proportional to the energy delivered. Higher frequency and shorter wavelengths are more energetic than lower frequency and longer wavelength. High energy photons are absorbed by the S0 system, pushing electrons in the S1 excited state. Small amounts of energy are lost as thermal relaxation among the levels of the excited S1 system and a photon is emitted when the electron jumps back to the S0 system. Since some energy is lost in non-radiative transitions, the wavelength of the emitted radiation is less energetic than the exciting one and it has a longer wavelength. This phenomenon is known as Stokes shift (Figure 2.20.).

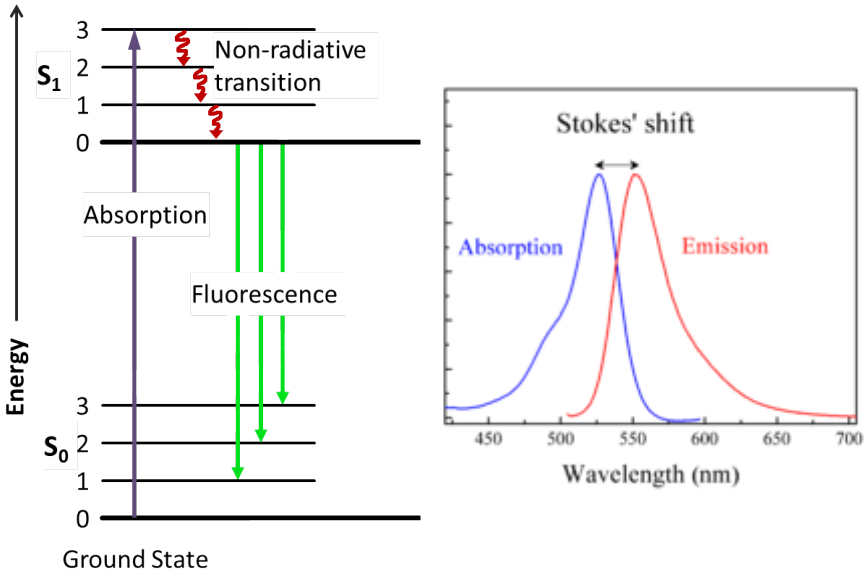

Figure 2.20. left panel) Jablonski diagram showing the energy level S0 (ground state) and S1 (excited state) of a molecule. Each state has several vibrational levels ("0" to "3"). Picture adapted from wikipedia.en
right panel) Absorption and emission spectra of a fluorophore. Source**:** https://upload.wikimedia.org/wikipedia/commons/thumb/3/3f/Stokes_shift-_Rh6G.png/300px-Stokes_shift-_Rh6G.png

Absorption and emission can be measured for each molecule, since the energetic levels of both S0 and S1 are different from system to system, the shape of the excitation and emission spectra can be different (Figure 2.20.). The spectra are not sharp peaks because of the contribution of nonradiative transition in the S0. Nonradiative transitions are more efficient and occur much faster than the radiative fluorescence emission, so, in spontaneous fluorescence, the electron leaves the excited state from the level 0 of S1 to reach one of the vibrational levels of the S0. Nonradiative transitions are vibrational processes which dissipate energy to the surrounding environment as a form of heat. Because of these and others processes, the absorbed light is not completely emitted as fluorescence. The number of photons emitted divided by the number of photons absorbed is defined as quantum yield. The maximum value of quantum yield is 1, since it would mean that all the absorbed photons are emitted.

Fluorescence is a powerful technique which allows to study changes in protein conformations in a physiological environment and aqueous buffers. Probes can be sensitive to environment or not, depending on the chemical structure of the

molecule. Fluorescent probes that are sensitive to polarity (Figure 2.21.) of surrounding environment change their emission spectra in response to hydrogen bonds, acid-base chemistry or charge-transfer interactions. Quantum yield of environment sensitive probes is highly affected by the surroundings.

Dyes covalently linked to proteins follow conformational changes and report polarity differences of the surrounding environment, which is especially useful to detect protein-protein interaction. Indeed, the different exposure of the dye at the solvent or at the hydrophobic core of the protein causes a shift to shorter wavelengths, in the blue side of the spectra.

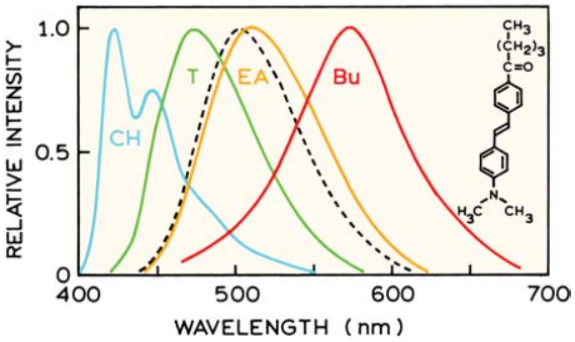

Figure 2.21. Corrected fluorescence emission spectra of DOS in cyclo-hexane (CH), toluene (T), ethyl acetate (EA), and butanol (Bu). The dashed line shows the emission of DOS from DPPC vesicles. Revised from Lakowicz et al.[25]

A powerful aspect of fluorescent spectroscopy is the mechanism known as Förster resonance energy transfer (FRET)[26]. FRET is an energy transfer which occurs between two different systems. In order to obtain energy transfer, the system has to contain two light-sensitive molecules called “donor” and “acceptor”. The essential condition needed to have FRET is that part of the “donor” emission spectra must overlap the “acceptor” excitation spectra. Other conditions are based on how close the two molecules are and on the orientation of the molecules (Figure 2.22.).

The orientation variable is not highly controllable in biological systems, while the distance is the key element. FRET efficiency (E) is defined as the fraction of energy transfer event occurring per donor excitation event.

E is described as a function of distance in the following formula:

$$E = \frac{1}{1 + (R/R0)^6}$$

with R0 being the Förster distance of this pair of donor and acceptor. R0 is the distance at which the energy transfer efficiency is 50%. An example of the behavior of the system is reported in Figure 2.23.

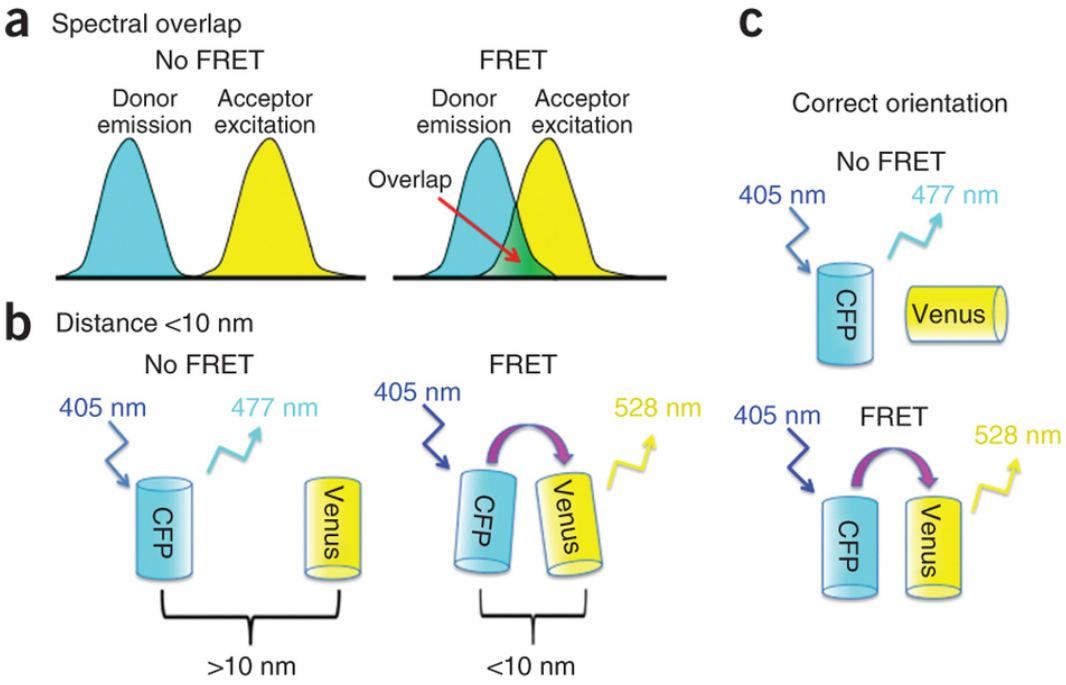

Figure 2.22. Conditions to obtain FRET: a) overlap between donor emission and acceptor excitation, b) distance between the two systems, c) molecule orientation. Adapted from Broussard et al.[27]

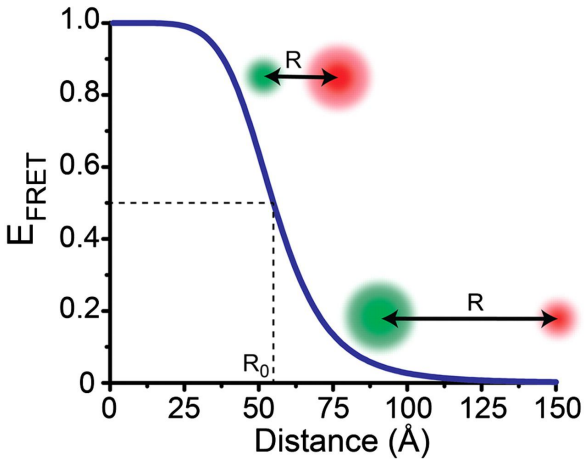

Figure 2.23. FRET efficiency plotted as a function of distance between donor and acceptor. Adapted from Roy at al.[28]

The figure shows a donor-acceptor couple with a R0 of approximately 55 Å. FRET technique allows to measure distances by estimating the efficiency of the transfer. Since the efficiency of transfer depends on the reciprocal of the sixth power of the distance (R) between the donor and acceptor fluorophores, FRET technique is more sensitive close to the R0 distance.

2.5. Obesity and type 2 diabetes

Overweight and obesity are conditions defined by a body mass index (BMI) between 25 and 30 (overweight) or above 30 kg/m2 (obesity) which recognize their origin in an imbalance between energy intake and energy expenditure. Sedentary lifestyles with insufficient physical activity and excessive caloric intake with food or a combination of the two are generally the causes of the increased BMI. According to the World Health Organization, worldwide obesity has more than doubled since 1980, in 2014 39% of adults aged 18 years and over were overweight and 13% were obese. The growing rate of this disorder is so relevant that obesity is recognized as the largest and fastest growing public health problem in the developed and developing world[29]. Of particular concern is the associated epidemic of obesity in children and adolescents. The current amount, around 10% of the population, is predicted to double by 2025 with persistence into adulthood[30, 31, 32]. Obesity is related to several others comorbidities such as type 2 diabetes, metabolic syndrome, hypertension, dyslipidemia, myocardial infarction, stroke, certain cancers, sleep apnea and osteoarthritis.

Diabete mellitus (DM) is a metabolic disorder characterized by high levels of blood glucose over a prolonged period. An abnormal high glucose level is persistent because of lack of insulin or because of an insulin-resistance condition. The first condition is known as “type 1” diabetes while the second one is named “type 2” diabetes. Type 2 DM is the commonest form since it counts about 90% of the cases[34]. Diabetes type 1 results from the autoimmune destruction of insulin-producing cells in the pancreas and it is unrelated to diet and lifestyle, while diabetes type 2 is strongly correlated with those factors which are also responsible of overweight and obesity, with an additional genetic component[35]. Physical inactivity, sedentary

lifestyle, cigarette smoking and abundant alcohol consumption are factors known to be strongly correlated to the onset of type 2 diabetes. Development of type 2 diabetes and increase of BMI go together often, although not always. It is estimated that the 366 million diabetic people in 2011 would be almost double by 2030 with insurgence moving towards developing countries which are acquiring a westernized lifestyle. Diabetes causes, over time, increased risk of heart disease and stroke, it is the leading causes of kidney failure. DM also causes alterations in microcirculation which may lead to nerve damage, infections and, eventually, limb amputation and diabetic retinopathy. The overall risk of dying among people with diabetes is at least double the risk of their peers without diabetes[36, 37, 38, 39].

Obesity and type 2 DM have a huge overall impact in terms of health issues and financial consequences[32]. Despite the large diffusion of obesity, an effective treatment is still missing. Diet and exercise help but it is hard and expensive to provide a personal trainer assistance to such a big part of the population and it has been demonstrated that the long-term efficacy of the auto-treatment is very low[40, 41, 42]. Bariatric surgery is much more effective in terms of weight loss but it may lead to surgical complications as frequent need of reoperation and it is suggested only for severe cases. In the 50s and 60s, most of the non invasive treatments were centrally acting sympathomimetics. Those compounds proved to have dangerous side effects especially at the cardiovascular system level. Another class of compounds, developed in the mid 90s, acted as cannabinoids receptor antagonist, suppressing appetite and weight gain. Such compounds have been retired from the market because of several studies reporting patients with psychiatric problems (depression, anxiety and suicide). A more recent approach to the problem has been developed by exploiting the action of multiple co-agonists hormone. Peptides such as glucagon like peptide 1 (GLP-1) have been identified as components of the endogenous satiety cascade. Treatments based on the effect of GLP-1 agonists and co-agonists are currently under intense studies. In 2012 the only approved treatment in Europe was based on the activity of a lipase inhibitor named Orlistat. The weight loss achieved by Orlistat treatment is modest (3kg in 12

months)[43] and the adverse effects are limited but uncomfortable such as diarrhoea, abdominal pain and dyspepsia[29, 44].

All the cited approaches aim at the reduction of energy intake, either by an appetite suppressing action or by limiting lipids absorption. Despite the fact that several "metabolic boosters" are commercially available, no pharmaceutical treatments have been developed to increase energy consumption. The future of obesity treatments may be characterized by the synergic co-action of several molecules, both increasing the energy expenditure and decreasing its intake. Uncoupling proteins have, recently, gained and, in a picture of increased energy consumption[45], muscles as the larger machinery in the body should have an important role[46, 47].

3. Aim of the thesis

The general aim of my work was the characterization of SRX state of myosin. In the first place to develop an assay to detect the presence of SRX and in the second place to find a molecule able to destabilize the SRX complex.

Therefore, the first part of the thesis reports my work on the RLC (Regulatory Light Chain) mutants and their effect on the stability of the SRX state when those proteins are exchanged into muscle fibers. My goal was to find a mutant which carries a cysteine in the right position to sense the SRX state when labelled with a paramagnetic or a fluorescent probe. I tried several matches of mutants and probes, measuring the stability of the SRX state by mantATP chasing and the fluorescent signal response to RIGOR-ATP cycle by fluorescent microscope analysis in flow cell. Structural changes were also measured by paramagnetic signal changes at the EPR machine.

The second step was to find a molecule able to disrupt the SRX complex. For this goal the identified mutant was used for the development of the high throughput screening. We collaborated with the Small Molecule Discovery Center (SMDC) at the University of California, San Francisco, we measured the effects of 2240 FDA approved molecules on RLC-C5 MDCC exchanged skeletal muscle fibers. The results were analyzed using a personalized Fiji[48] macro.

The effect of the identified molecule on the SRX state was confirmed by ATPase, tension and mantATP chasing measurements. The behavior was then characterized by measuring the activity in muscle fibers and by doing the mentioned experiments using components of the leading compound.

4. Results

4.1. Spectroscopic Studies of the Super Relaxed State of Skeletal Muscle

4.1.1. Introduction to the study of the Super Relaxed State in Skeletal Muscle fibers

The super-relaxed state of myosin (SRX) in which the myosin ATPase activity is strongly inhibited has been observed in a variety of muscle types. We selected as experimental model the rabbit psoas from which thin fiber bundles were dissected. It has been proposed that myosin heads in SRX state are inhibited by binding to the core of the thick filament in a structure known as the "interacting heads motif" (IHM). This contrasts with the disordered relaxed state (DRX), in which myosin heads are not organized around the core of the thick filament and have an ATPase rate that is an order of magnitude greater. In the IHM the two regulatory light chains (RLCs) bind to each other. To study the interaction between the RLCs, we designed a series of single cysteine mutants of the RLC, attached either paramagnetic or fluorescent probes, and exchange them into rabbit fast skeletal muscle fibers.

4.1.2. Design and selection of RLC mutants

As explained previously in the Introduction (Paragraph 2.2.2 The structure of the SRX state), RLC is important in the physiologic control of the SRX state complex, and, for this reason, it is the protein of choice for explore the SRX state using mutants. Furthermore, several robust protocols for RLC exchange into muscle fibers have already been defined in previous studies[49].

We were interested in studying the SRX state by using paramagnetic and fluorescent probes. Our aim was to find a residue in a key position, such that, when labelled, the probe would sense a different surrounding environment whether the SRX state complex is formed or not, so, whether myosin is in the ordered or disordered relax state. To spot residues in interesting positions we analyzed the recently published

model of the myosin in the SRX state which can be found in the Protein Data Bank (PDB, identification code 3DTP)[20].

The RLC sequence used in the 3DTP structure is the one from Tarantula skeletal muscle. Since we had decided to work with mammalian muscles, the RLC sequences of tarantula and mouse were aligned to discover conservation patterns and similarities among the two orthologs. RLC is a very conserved protein, a wider alignment is available in the Supplementary Materials section (8.1. RLC multi alignment). The tarantula sequence, as those from invertebrates, has a longer N-terminus region which seems to be very mobile and, therefore, it is not present in the 3DTP structure. Except the extra N-terminus, the alignment shows a high level of conservation (see Figure 4.1.).

The conservation patterns among RLCs are not only present in the core of the protein but also on the surface. It is useful to keep in mind that muscle contraction, in tarantula, is regulated by RLC phosphorylation while in mouse it is regulated by calcium binding to the Troponin complex on the thin filament. It may be surprising to find that such different forms of activation share proteins with so high similarity.

```
tarantula   1 MGDDEKKEKKKKSKKKAEEEGGDAPAAPPAPKPPSQKRRAQRSGSNVFAMFTQHQVQEFK 60
mouse       1 ----------------------------MAPK-KAKRRAGAEGSSNVFSMFDQTQIQEFK 31
                                          ***  :::* . ...****:** * *:****

tarantula  61 EAFQLIDQDKDGFISKNDIRATFDSLGRLCT-EQELDSMVAEAPGPINFTMFLTIFGDRI 119
mouse      32 EAFTVIDQNRDGIIDKEDLRDTFAAMGRLNVKNEELDAMMKEASGPINFTVFLTMFGEKL 91
              *** :***::**:*.*:*:* ** ::*** . ::***:*: ** ******:***:**:::

tarantula 120 AGTDEEDVIVNAFNLFD-EGDGKCKEETLKRSLTTWGEKFSQDEVDQALSEAPIDGNGLI 178
mouse      92 KGADPEDVITGAFKVLDPEGKGTIKKQFLEELLTTQCDRFSQEEIKNMWAAFPPDVGGNV 151
               *:* ****. **:::* **.*. *:: *:. ***  ::***:*:.:  :  * *  * :

tarantula 179 DIKKFAQILTKGAKEEGA 196          Legend: Mutants
mouse     152 DYKNICYVITHGDAKDQE 169                 A helix
                * *::. ::*:*  ::                    D helix
                                                    Calcium binding residues
```

Figure 4.1. Alignment of the skeletal muscle RLC of mouse and tarantula. Mutants are highlighted in green, helix A in yellow, helix D in purple and the calcium binding residues are underlined.

From the mouse-tarantula RLC alignment it is possible to notice that there is a conserved amino acids cluster on the N-terminal lobe, looking right at the other regulatory light chain according to the model of the IHM.

The presence of a cluster of conserved residues on the outside surface of a protein suggests that they may have a role in protein-protein interactions. This cluster provided a method for choosing residues for probe sites. The model structure of the IHM suggests that the interface between the two RLCs is formed around the A helix, aa 30 to 40 (mouse sequence numbering), and the N-terminus of the D helix 76 to 88[19, 20]. The ideal mutant will be at the border of the interface, will not destabilize the IHM and will sense changes in the SRX versus the DRX.

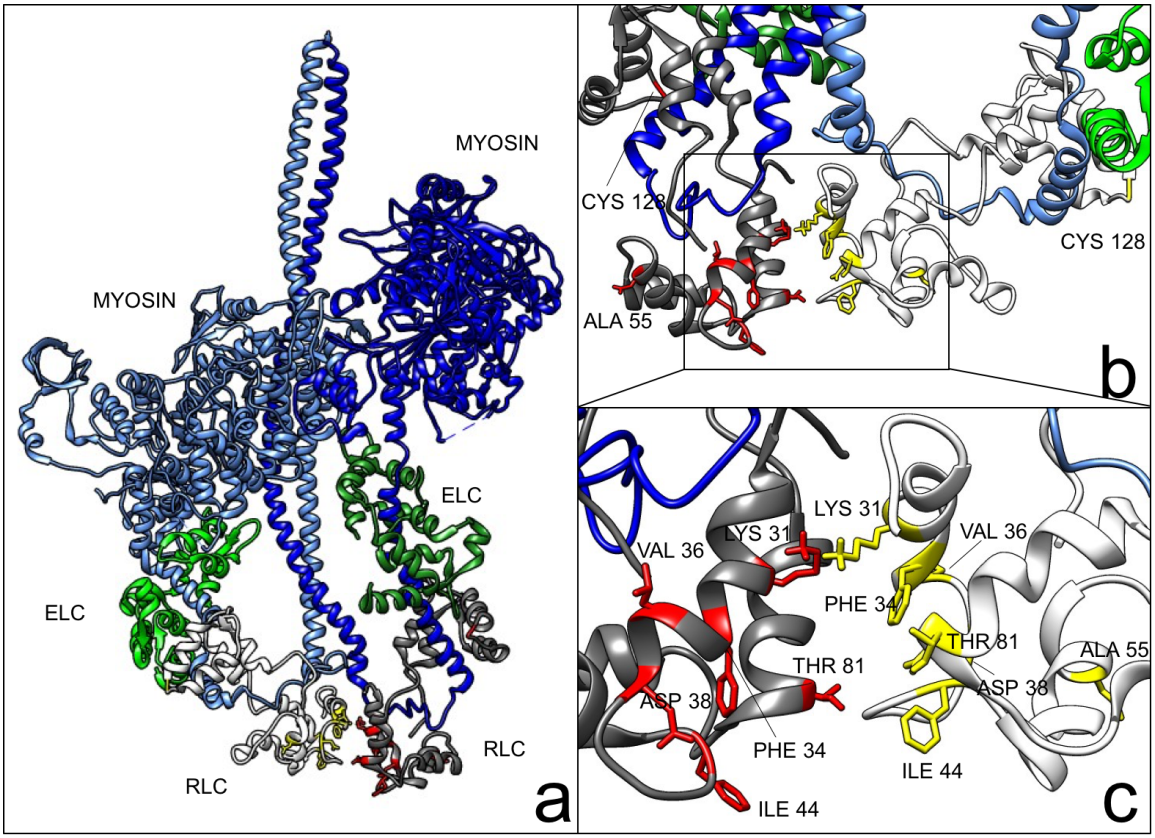

Figure 4.2. a) Complete model of the 3DTP structure (myosin in blue and light blue, ELCs in green and light green, RLCs in white and grey). **b)** RLC-RLC surface. **c)** Zoom into the RLC-RLC surface. Mutants are highlighted with the numbers according to the mouse sequence. Obtained using UCSF Chimera software[22].

Three sets of mutants were designed, the first set is at the very N-terminus, the second one is in the surface region of the proposed interface. The third one is in the C-lobe serving as a control. The first set has been designed with the idea that the N-terminus plays an important role in the stability of the IHM structure. A recent paper suggests that the N-terminus undergoes a structural change when phosphorylated[49]. The fact that phosphorylation affects the stability of both the SRX and the IHM, suggests a role of the N-terminus in the stability of the

complex[10, 20, 50, 51, 52]. The extra N-terminus found on the invertebrate RLCs, compared to the mammalian RLCs, may explain the higher stability of the IHM in tarantula muscles, compared to rabbit muscles [51, 52]. As in both mouse and tarantula the N-terminus is characterized by several positively charged residues, we explored the behavior of that region with the A6C mutant and we also checked if the positively charged residues were necessary for the stability of the complex by preparing the K5C mutant (mouse mutants and numbering). Some recent papers propose the N-terminus to be structured as an alpha-helix when phosphorylated, while being disordered in the non-phosphorylated form. With the possibility that the N-terminus assumes an alpha-helix secondary structure[49, 53, 54, 55] the K5C and the A6C mutants become interesting also to assess whether the phosphorylated state changes the probe environment. In an alpha helix, one residue would be approximately 100° tilted respect to the other. Unfortunately, due to time limitations, we could not perform experiments using phosphorylated RLC.

The second set (K31C, F34C, V36C, D38C, I44C, T81C) is located in the interface region according to the IHM structure (3DTP), and all the mutations were within or close to the cluster of conserved residues (see Figure 4.2.). Mutants were picked also based on their calcium binding capacity, in particular, D38C and I44C are responsible for calcium coordination in the EF-hand of the RLC N-terminal lobe. By mutating those residues, we wanted to explore whether (i) the calcium binding site was showing structural changes as well as (ii) different affinities for calcium ions may have an effect over the SRX state. An additional construct has been prepared as a control since one of the endogenous cysteines, C128, is far from the putative RLC-RLC interface.

4.1.3. Effect of RLC mutants on the SRX state

Mutants RLCs were prepared as described in the Methods (5.1.3. Molecular biology and protein purification). Fibers were exchanged with labeled and unlabeled mutant RLCs (see Figure 4.3.). They were incubated in mantATP and chased with ATP according to the protocol described in the Introduction (2.2.1. Measuring the stability of the SRX in skinned muscle fibers). Figure 4.4. shows the decay of fluorescence intensity during the chase phase normalized by the fiber fluorescence

prior to the chase. The fraction of the fluorescence intensity that decays with the longer lifetime, P2, provides a measure of the stability of the SRX. The lifetime of this phase, T2, is also an important property of the SRX.

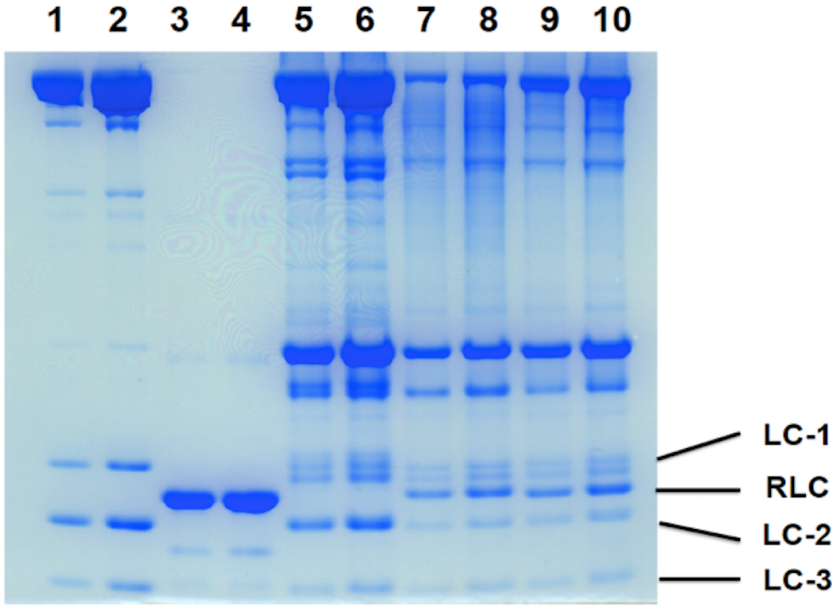

Figure 4.3. SDS page. 1, 2) purified myosin. 3,4) purified RLC mutant. 5, 6) control skeletal muscle fiber. 7, 8, 9, 10) Four fiber exchanged with mutated RLC. The mutated RLC is 3kDa heavier than the wt because of the purification tag.

The effect on the SRX was determined by the location of the mutant and by the nature of the label, as shown in Figure 4.4. and Table 4.1.. Figure 4.4. shows representative chase results for three samples. For the control sample (top trace) there is a fraction of the fluorescence that decays slowly during the chase, which represents 37% of the total fluorescence and has a lifetime of 248 seconds. This component arises from the slow release of nucleotides from myosin heads in the SRX. Although this component represents 37% of total fluorescence it represents a greater fraction of the myosin heads. There is a fraction of probes, 40%, that are bound non specifically to the fiber, which are released in the first 23-30 seconds[10]. Thus only 60% of the total fluorescence arises from probes bound to myosin and the proportion of the myosin that is in the SRX can be calculated as 37/0.6 = 62%. While the top trace of Figure 4.4. shows a control fiber, the lowest trace shows the chase of fibers exchanged with RLC-C44 labeled with BIMANE. Virtually all the fluorescence, 99%, is released in the fast phase. The population of the SRX in these fibers is close to zero.

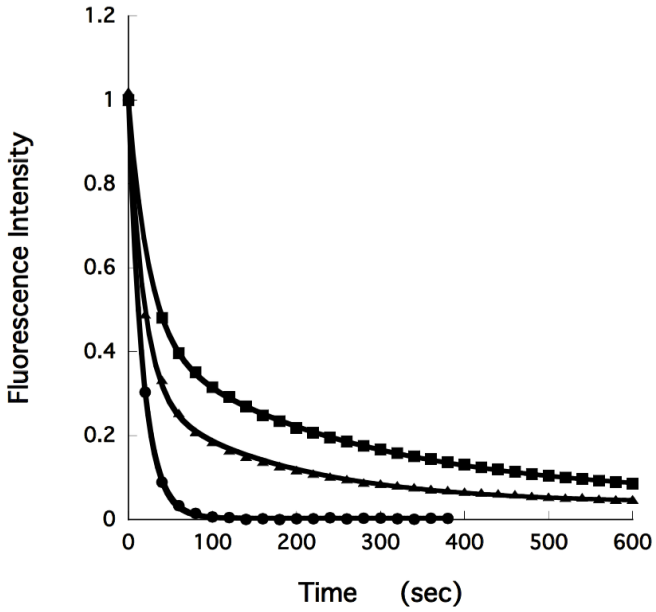

Figure 4.4. top trace) mantATP chasing of a control fiber, **intermediate trace)** mantATP chasing of RLC-C6 MDCC exchanged fiber, **bottom trace)** mantATP chasing of a RLC-C44 BIMANE exchanged fiber.

The intermediate trace in Figure 4.4. shows the chase of fibers exchanged with RLC-C6 labeled with MDCC. There is a slow decay of fluorescence that represents 26% of the total. The lifetime of this decay, 172 seconds, is shorter than that observed in the control fibers. Both the population and the lifetime show that the SRX in these fibers is destabilized relative to that observed in the control fibers. In general when the SRX is destabilized both the lifetime and the population decrease proportionally. However this is not always observed as discussed below in more detail. For each mutant and for each label, the results for a number of fibers were averaged and are summarized below in Table 4.1.

Table 4.1. shows the fraction of fluorescence (P2) that decays slowly during the chase phase, which is proportional to the population of the SRX, as discussed above. As reported in the top row of Table 4.1. the mutations alone have a minimal effect on the stability of the SRX as measured by the population, P2. For only one of the mutants, RLC-C38, did the mutation alone destabilize the SRX, decreasing the value of P2 to 0.21, a decrease of about 35% from control. In the D38C mutation, cysteine takes the place of an aspartic acid that coordinates to calcium in the EF hand at the N-terminal lobe of all RLCs.

Table 4.1. P2 values of the mutants, labeled and unlabeled. Values estimated by mantATP chasing.

LABEL	C5	C6	C31	C38	C44	C81	C128
NONE	0.26 ± 0.02	0.27 ± 0.04	0.28 ± 0.02	0.21 ± 0.02	0.31 ±0.02	0.31 ± 0.02	0.31 ± 0.02
MMTS	0.23 ± 0.03	0.25 ± 0.02	0.29 ± 0.02	0.10 ± 0.03	0.07 ±0.02	0.24 ± 0.02	0.28 ± 0.05
IASL	0.15 ± 0.04	0.10 ± 0.02	0.31 ± 0.02	/	/	0.19 ± 0.04	0.29 ± 0.01
MSL	0.19 ± 0.04	0.25 ± 0.02	0.20 ± 0.01	/	/	0.27 ± 0.02	0.31 ± 0.01
BIMANE	0.22 ± 0.03	0.16 ± 0.03	0.36 ± 0.04	0.08 ± 0.02	0.03 ± 0.03	0.32 ± 0.02	0.29 ± 0.03
MDCC	0.25 ± 0.02	0.26 ± 0.01	0.32 ± 0.01	/	/	0.36 ± 0.02	0.28 ± 0.03
MIANS	0.13 ± 0.03	0.20	0.10 ± 0.04	/	/	0.17 ± 0.04	0.34 ± 0.02

In some cases, the attachment of probes to the single cysteines decreases the population of the SRX, as measured by P2, shown in Table 4.1. Some of the probes are small molecules, MMTS and BIMANE, some probes have intermediate size, MSL and IASL and some probes are large but attached by a flexible leash, as MDCC, or large but not flexible, as MIANS. The large probes were expected to provide the most interference. In all cases, the pattern of interference produced by the attachment of probes provides information on the role of the various sites in the interface formed by the two RLCs in the SRX. As a control was used C128, which was one of the native cysteines, and located far from the putative interface. None of the probes attached to C128 affect the population of the SRX, as expected for a control. Two of the probe sites, D38C and I44C cannot tolerate even the smallest of the probes, MMTS or BIMANE. These sites are located in the region of a structural motif known as an EF hand, which binds to divalent cations, either Mg^{2+} or Ca^{2+}. In fact the mutant D38C was the site that produced the greatest effect on the value of P2 in the absence of an attached probe as discussed above. The second mutation in this region, I44C, is also in the EF hand structure. Although it does not coordinate the divalent cation and is not completely conserved, it forms part of the structural motif that binds the divalent cation. The data for RLC-C44 are almost identical to the data obtained for RLC-C38, with the exception that for RLC-C44 the mutation alone did not inhibit P2. These observations underline the importance of the presence of the divalent cation in the stability of the SRX. The sites K31C and T81C are within both the cluster of conserved residues and the proposed interface. Both of these sites tolerated the

smallest probes or the flexible probes, while larger and stiff probes partially affected the stability of the complex, see Table 4.1. The sites on the N-terminal region tolerated many but not all of the probes, with little correlation between probe properties and their effect.

In general, the destabilization of the population of the SRX is accompanied by a corresponding decrease of T2. While there is a lot of scatter in the values of T2 there is a clear correlation between P2 and T2, as shown in Figure 4.5.

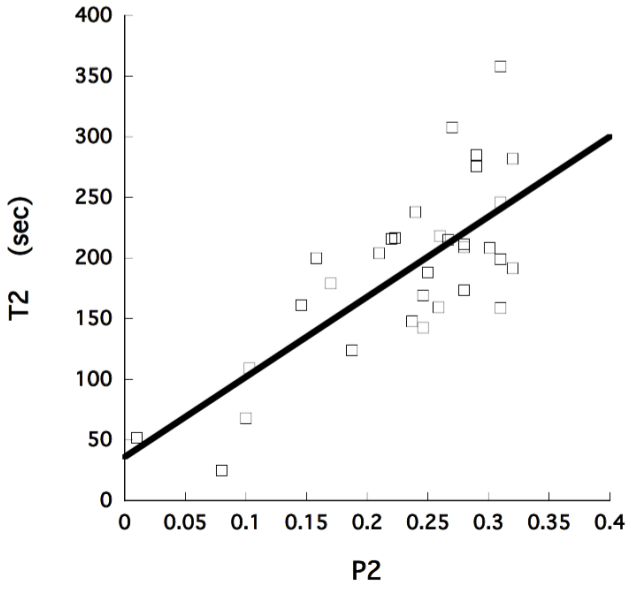

Figure 4.5. T2 plotted as a function of P2. The data show a correlation between the two values, so that the amount of myosin in the SRX state is proportional to the time constant and, so, the stability of the whole structure. The data suggests cooperativity as an important parameter in the system.

4.1.4. Changes in the spectra of fluorescent probes on the RLC.

Both fluorescent probes and paramagnetic probes are able to sense differences in the surrounding environment in different ways. Paramagnetic probes can sense differences in terms of the mobility and orientation of the probe. Fluorescent probes sense the hydrophobicity of the environment, mainly characterized by the side chains of the residues that are close to the probe in the protein structure. We were able to detect spectroscopic changes using both fluorescent and paramagnetic probes.

It was expected that fluorescent probes that are within or close to the RLC-RLC interface in the IHM would change their fluorescence spectra in relation to a transition from the DRX or the rigor state into the SRX. The probes described here are all environmentally sensitive, e.g., their quantum yields are altered by changes in the polarity of the surrounding medium. All of the probes were examined for spectral changes in a protocol that typically started in rigor, ATP was then added to populate the SRX followed by GTP to populate the DRX, see below. The rationale of the protocol is the following: *i*) it is known that in rigor all myosin heads are attached strongly to actin and thus the population of the SRX is zero (however there may still be some structure in the RLCs). *ii*) The chase experiments have shown that in the ATP relaxed state approximately 60% of the myosin heads are in the SRX, leaving the remaining 40% in the DRX[10] *iii*) Studies using X-ray diffraction found that myosin heads were more disordered in fibers relaxed by GTP[56]. This was confirmed by showing that in fibers relaxed in GTP the population of the SRX and T2 were decreased by a factor of 3, relative to that observed for fibers relaxed in ATP[10]. Thus in the presence of GTP, fibers are mechanically relaxed with 90% of the myosin heads in the DRX and 10% in the SRX. In our protocol, the addition of ATP to fibers in rigor 50-60% of the myosin heads caused the transition from a rigor state to a more ordered SRX. The sequent addition of GTP, two thirds of these heads move to a disordered, but still relaxed state. The signal was also reversed to the low fluorescence state by washing out the ATP with rigor buffer.

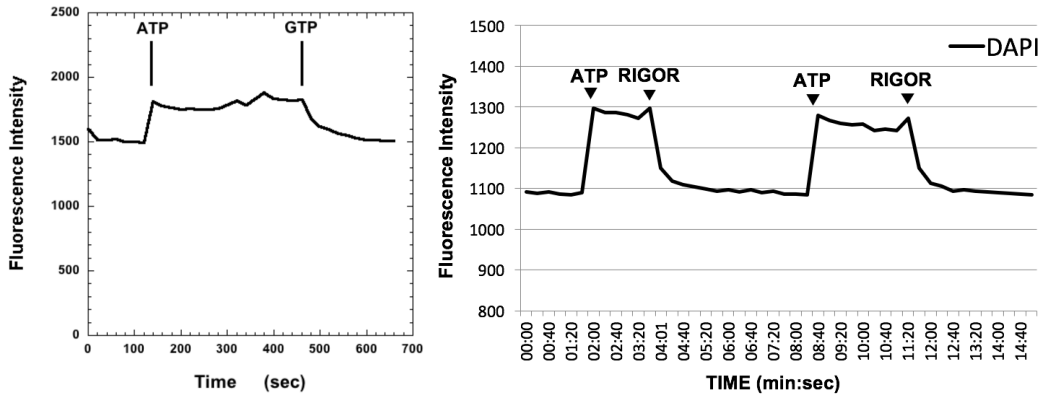

Figure 4.6. left panel) Change in the fluorescence signal of a muscle fiber exchanged with RLC-C31 MDCC in a flow cell. The experiment started in rigor buffer, then relaxing solution (ATP) and GTP solution, **right panel)** Change in the fluorescence signal of a muscle fiber exchanged with RLC-C6 MDCC in a flow cell. The experiment started in rigor buffer, then the relaxing solution and then the same procedure again.

The changes in fluorescence are shown for MDCC attached to RLC-C31 in figure Figure 4.6. (left panel) and for RLC-C6 MDCC (right panel). Data collected for selected mutants are in Table 4.2. As shown in Figure 4.6. fluorescence intensity increases by about 15% in the transition from the rigor state to the ATP relaxed state and then decreases by a similar amount in the transition to the GTP relaxed state (left panel) or back to rigor (right panel). The first conclusion is that the spectral intensity is similar in rigor and in fibers relaxed in GTP. This was generally observed for all the probes that gave spectral changes (see Table 4.2.). This suggests that the increased fluorescence intensity comes from the transition of myosin heads from a disordered state, either rigor or the DRX, into the SRX, where the RLC-RLC interface is formed in the Interacting Head Motif (IHM). Although the magnitude of the change is small (15%), the actual change for each head making the transition into the SRX is larger. As exchange of RLC-31C-MDCC into the fibers slightly inhibits the SRX, only about 50% of the myosin heads make the transition into the SRX upon addition of ATP to rigor fibers. Thus the actual change in the intensity for each labeled head is close to 30%.

Table 4.2. Summary of the fluorescence changes of selected mutant and probe combinations measured according to the change in buffers specified in the first column.

LABEL	C5	C6	C31	C81
BIMANE				
RIGOR>ATP	-8% ± 2%	-5%	+15 ± 3%	+14 ± 3%
ATP>GTP	<2%	+2%	-25 ± 3%	-17 ± 5%
MDCC				
RIGOR>ATP	+18% ± 4%	+21%	+15 ± 4%	<2%
ATP>GTP	-19% ± 4%	-11%	-14 ± 4%	<2%
MIANS				
RIGOR>ATP	-8% ± 2%	-6 ± 2%	<3%	<3%
ATP>GTP	+3%± 2%	+5 ± 1%	<3%	<3%

An important result was obtained labelling the RLC-C5 with maleimide coumarin (MDCC) and a similar behavior has been recorded for RLC-C6 MDCC (data not shown). Fluorescence spectra of RLC-C6 MDCC fibers have been measured in a fluorimeter. Figure 4.7. (upper panel) shows the blue shift that the probe is

experiencing by going from free MDCC in relax buffer (purple trace), bound to the RLC and exchanged into fibers, in rigor and relax buffer (respectively, green and red traces). The same sample has also been measured in a fluorescent microscope using an excitation filter (DAPI filter: 387/11nm) and two different emission filters (DAPI: 440/40nm and GFP: 525/30).

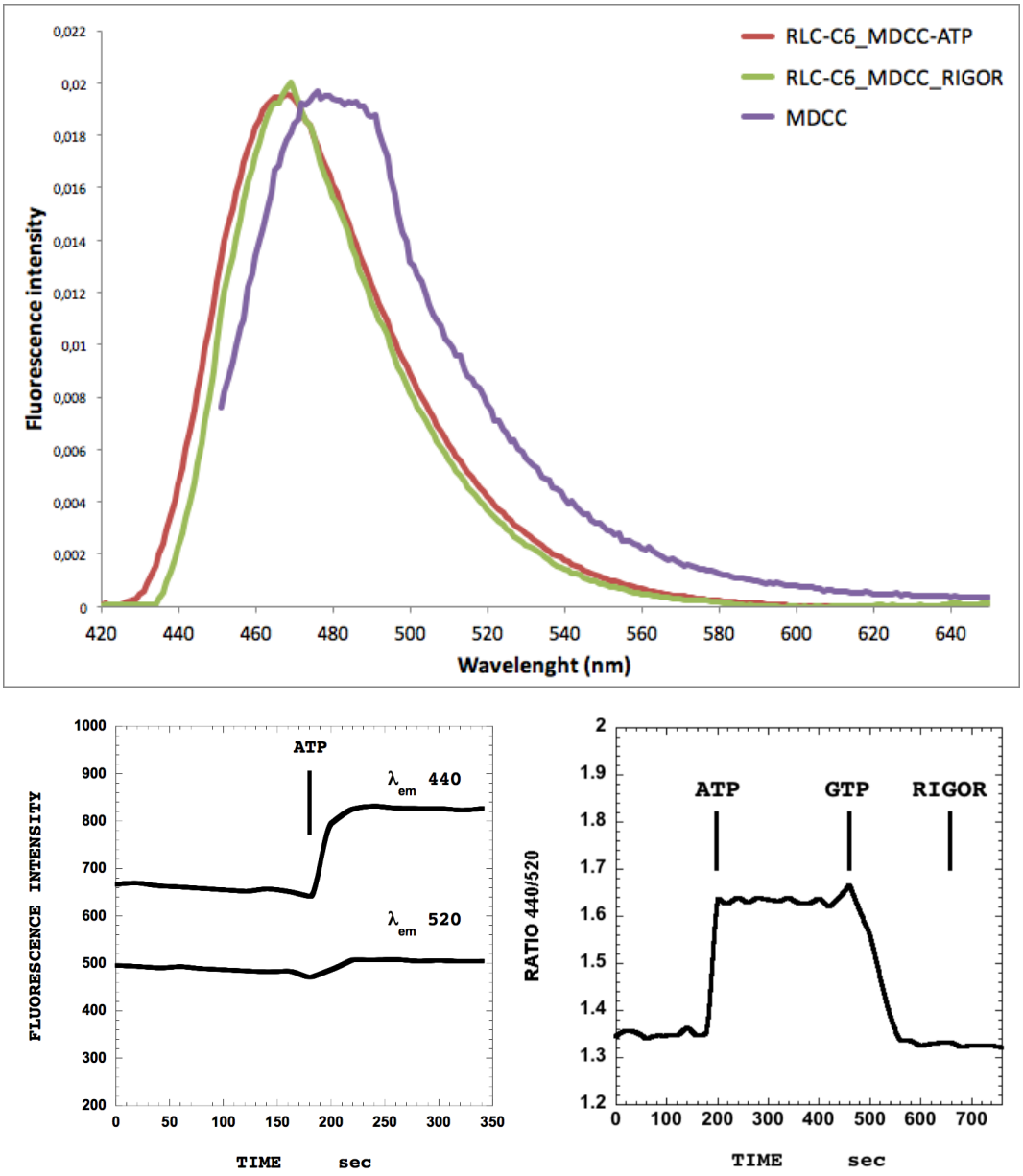

Figure 4.7. upper panel) Fluorescence emissions of MDCC in rigor buffer (purple trace), RLC-C6 MDCC exchanged muscle fiber in rigor buffer (green trace) and relaxing buffer (red trace); **bottom-left panel)** Signal changes of RLC-C6 MDCC fiber as recorded in the microscope at 440nm and 520nm; **bottom-right panel)** ratio signal obtained by dividing the fluorescence intensity at 440nm by the value at 520nm. The signal has a bi-functional behavior (in the panel, rigor ratio value at circa 1,35 and relax ratio value at circa 1,62).

In Figure 4.7. (lower-left panel), because of the blue shift of the probe emission, the fluorescence intensity emitted going from rigor to ATP buffer is greater at the blue side of the spectrum (DAPI filter: 440nm) than at the red side (GFP filter: 520nm). This effect is better highlighted in Figure 4.7. (right-lower panel). A ratio between the value obtained from the DAPI emission filter and the GFP emission filter is calculated and it is possible to transform a signal like the one shown in the left lower panel in a biphasic function like the one shown in Figure 4.7.
Changes in fluorescence intensity similar to those shown in Figure 4.7. were also observed in fibers where the native RLC had been exchanged with RLC-31 BIMANE and RLC-C81 BIMANE, see Table 4.2. and figures in the Supplementary Materials (section 8.3. Fluorescence data). In addition, several samples showed a decreased intensity, moving from rigor to ATP-relaxed, although the changes were smaller, and not always reversed by GTP, see Table 4.2. The observation of a number of spectral changes, together with the inhibition of the SRX by some probes, suggests that the region targeted here, the putative RLC-RLC interface and the N-terminal end are both involved in the formation of the SRX. A number of labeled mutants did not show spectral changes. In some cases this was not unexpected. Probes attached to RLC-C128, far from the interface showed no changes, with the exception of the sample with BIMANE which showed a small change, moving from rigor to ATP only (data not shown). Probes attached to RLC-C38 showed no changes (see Table 4.2), as expected because exchange of native RLC with this labelled mutant into fibers completely destabilized the SRX (data not shown).

Similar results were obtained for RLC-C44. Mutants labeled with MIANS showed few spectral changes, but MIANS also inhibited the formation of the SRX, due to its size and rigid attachment to the protein. A caveat in the interpretation of these results is required: the atomic structures used to select the probe sites were all from invertebrates, and the exact environment of a given probe in a mouse protein might be difficult to determine.

4.1.5. Spectral changes in EPR spectra.

Electron Paramagnetic Resonance (EPR) is a technique that is able to sense the orientation and mobility of paramagnetic probes. Since biological samples are, usually, not paramagnetic, a paramagnetic probe has to be added to the sample to perform EPR measurements. As described in the Introduction (Chapter 2.3. Electron Paramagnetic Resonance) such probes are composed of a ring, which stabilizes an unpaired electron, and a linker, which contains the reactive part of the molecule. The unpaired electron has a magnetic moment, which acts as a needle in a compass, giving rise to a spectrum. The mobility of the probe is related to the degrees of freedom in the linker region and to the topology of the surrounding environment. In addition to mobility, an ordered biological sample, such as muscle fibers, provides a good system to measure the orientation of the probes. A probe bound to the RLC will have a helical order due to the structure of the filaments. The spectrum of a probe in an EPR experiment is sensitive to the angle between the magnetic field direction and the principal axis of the probe (see Figure 4.8.).

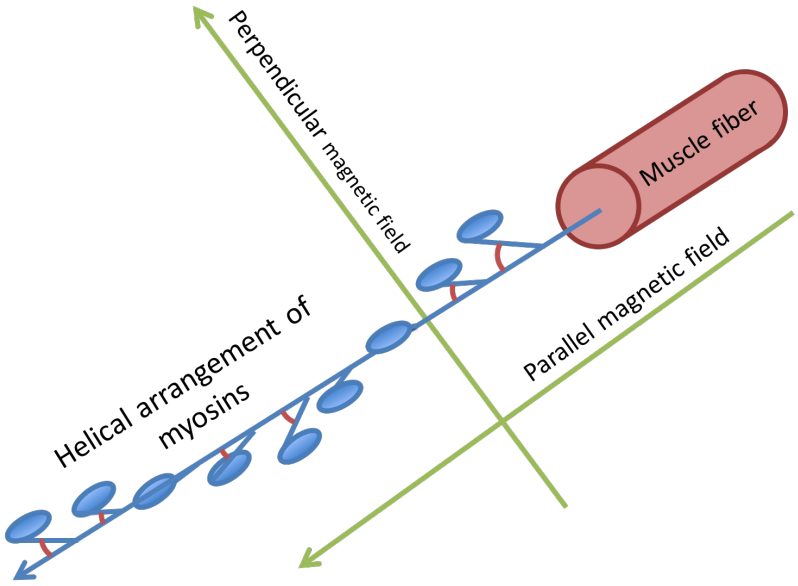

Figure 4.8. Scheme explaining the thick filament and the myosin heads arrangement respect to the parallel and perpendicular orientation of the external magnetic field. A magnetic field oriented parallel to the muscle fibers would lead to a constant angle between myosin and the field itself. A magnetic field oriented perpendicular to the muscle fiber would lead to several angles, the spectra is very similar to the one of a randomly oriented probe.

Thus the spectrum is dependent on the orientation of the fibers, either parallel or perpendicular to the magnetic field.

Myosin heads have a helical arrangement around the thick filament and, when the fiber is parallel to the magnetic field, the angle that each myosin experiences respect to the external field is constant. The signal sums up and the spectra is informative on that angle. In the case of myosin, several populations are usually present at the same time, each with its own structure and orientation, so, different angles would be present in the sample and reported in the spectrum. When the fiber is perpendicular to the magnetic field, the system lacks in order and the angle between myosin and field is very close to a random situation. Differences between parallel and perpendicular spectra of a muscle fiber indicate an ordered sample. Bundles of muscle fibers from rabbit psoas were dissected and placed in a flat cell that was observed with the fiber axis either parallel or perpendicular to the magnetic field. Spectra were obtained in rigor or in the presence of ATP with the SRX stabilized by addition of blebbistatin.

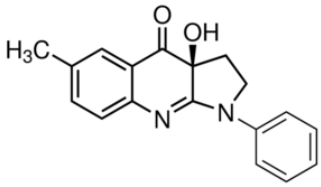

Figure 4.9. Blebbistatin molecule. Source: http://www.sigmaaldrich.com/content/dam/sigma-aldrich/structure2/130/mfcd08460907.eps/_jcr_content/renditions/mfcd08460907-medium.png

Blebbistatin is a myosin II inhibitor which binds to the 50kDa cleft in the head region of myosin and, by preventing the cleft from closing, it stabilizes a conformation of the nucleotide pocket which inhibit hydrolysis and release of nucleotides[57,58]. Blebbistatin also stabilizes the binding of myosin heads to the core of the thick filament in the helical array[59,60]. Blebbistatin was needed to maintain the SRX during the long incubations required for data collection, 10-20 minutes[61]. One mutant-probe pair gave appreciable spectral changes between rigor and the ATP relaxed state, RLC-C31-MMTS (see Figure 4.10.). The difference was clearly detectable in the low field region of the spectrum. This probe was oriented in the ATP-blebbistatin state, with more probe immobilization relative to rigor. The probe on RLC-81-MMTS was also more immobilized in the ATP-blebbistatin state than in rigor, and slightly oriented in both states. MSL was highly immobilized on both RLC-

31 and RLC-81, but showed no changes in orientation or mobility. IASL was more mobile on all sites, and did not show spectral changes between parallel and perpendicular or between rigor and ATP-blebbistatin. All the probes on RLC-C5 and RLC-C6 showed more mobility than those discussed above, and did not show spectral changes with orientation or state of myosin. As expected, probes on RLC-C128, RLC-C38 or RLC-C44 did not show spectral changes in different myosin states as also seen with fluorescent probes (Supplementary Materials 8.5. EPR Spectra).

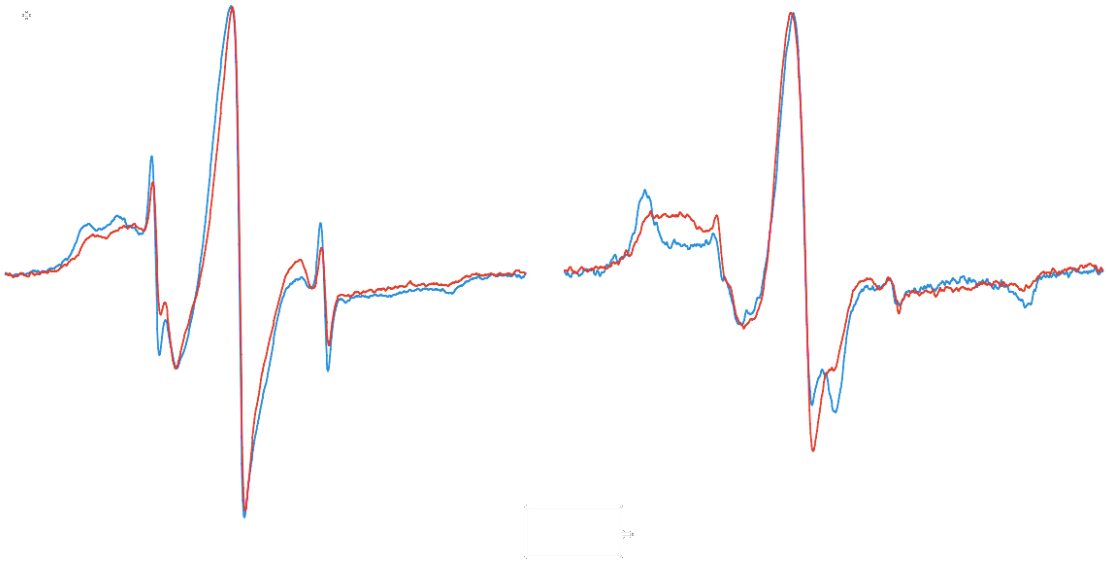

Figure 4.10. EPR spectra of fibers exchanged with RLC-C31-MMTS with the fiber axis either parallel (blue line) or perpendicular (red line) to the magnetic field. The derivative of absorption is shown as a function of the magnetic field strength. The fibers are in rigor solution (left spectra) and relaxing solution, ATP plus bebbistatin (right spectra). The difference between the parallel and perpendicular spectra in the top figure show that the paramagnetic probes are oriented in relaxation and the SRX. In rigor there is less orientation. The center-fields of the spectra are 0.3490 T and the sweep width is 10 mT.

4.2. Disrupting the SRX State: the high throughput screening.

4.2.1. Introduction

It is possible to speculate that the SRX state evolved as a mechanism to save energy in skeletal muscle. When muscle fibers are relaxed, the SRX state minimizes ATP consumption. Low ATP and energy consumption is perfectly functional in a condition where access to food is scarce or uncertain. Nowadays, many people consume more food than needed in relation to their energy consumption. On this basis, we identified, in this new state, a novel therapeutic target. Obese and diabetic

patients may largely benefit from the increase in the metabolic rate achieved by increasing ATP hydrolysis even in resting or relaxed conditions.

Based on the difference in time constant measured by mantATP, the metabolic rate should increase up to 10 times by shifting myosin heads from the SRX state to the disordered relax state. The question was how to achieve this, or better which compound can shift the myosin head distribution from SRX to DXR in a resting muscle fiber. The work described in the previous chapter "Spectroscopic Studies of the Super Relaxed State of Skeletal Muscle" was a fundamental step for the development of the high throughput screening presented here. The shift in fluorescence intensity provided by the A6C mutant of the RLC labeled with MDCC going from the rigor state to the SRX state allowed us to carry out a high throughput screen of 2240 compounds aimed to finding a molecule able to disrupt the SRX state.

4.2.2. The High Throughput (HT) screening: piperine

The use of high throughput screens to search for small molecules to destabilize the SRX is complicated by a number of factors. Primary among these is the fact that the SRX state can only be visualized in an intact filament array of skinned muscle fibers. To carry out these screens we labeled purified mutant A5C-RLC with fluorescent probe coumarin maleimide (MDCC), exchanged the mutated and labelled RLC for the endogenous RLC in skinned fast skeletal muscle fibers of rabbit.
The plates have been prepared as described in the Supplementary matherials (paragraph 5.2.1. Brief description of how the screening was run). The number of fibers in each well varied widely from 20 or less to more than 100 (see Figure 4.11.). As fibers were sedimented at the bottom of the well but not attached to it, they could move during the assay. Moreover, the fluorescent excitation intensity was not precisely uniform across the well. All of the above problems, however, were alleviated to a sufficient degree by our prior discovery of a fluorescent probe attached to a RLC exchanged into the fibers whose emission intensity both increased and moved to lower wavelengths upon the transition from the DRX to the SRX. The fluorescent probe was MDCC, attached to a single cysteine at aa 5 located near the N-terminus. As above described (Results, paragraph 4.1.4. Changes in the spectra of

fluorescent probes on the RLC), the intensity obtained at shorter wavelengths, 440nm, was divided by that obtained at longer wavelengths, 520nm, to produce a ratio that was intrinsic to the state of myosin and independent from the number of fibers being viewed, intensity of excitation and photobleaching.

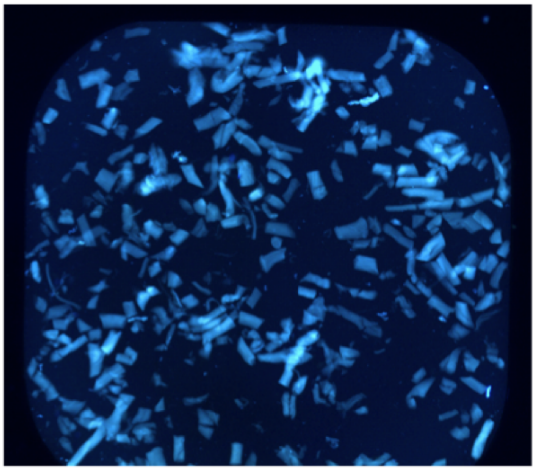

Figure 4.11. Fluorescent picture of RLC-C5 MDCC exchanged muscle fibers, chopped and loaded in a 384 wells plate.

Plates were set up using the labeled and chopped fiber preparation and loaded following the specifications described above. Results are reported in the following Figure 4.12.

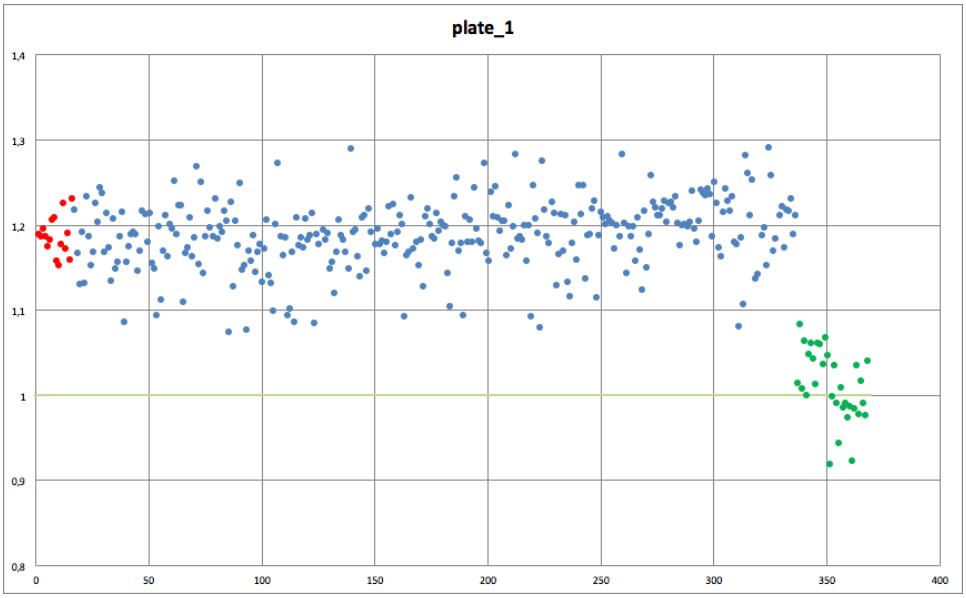

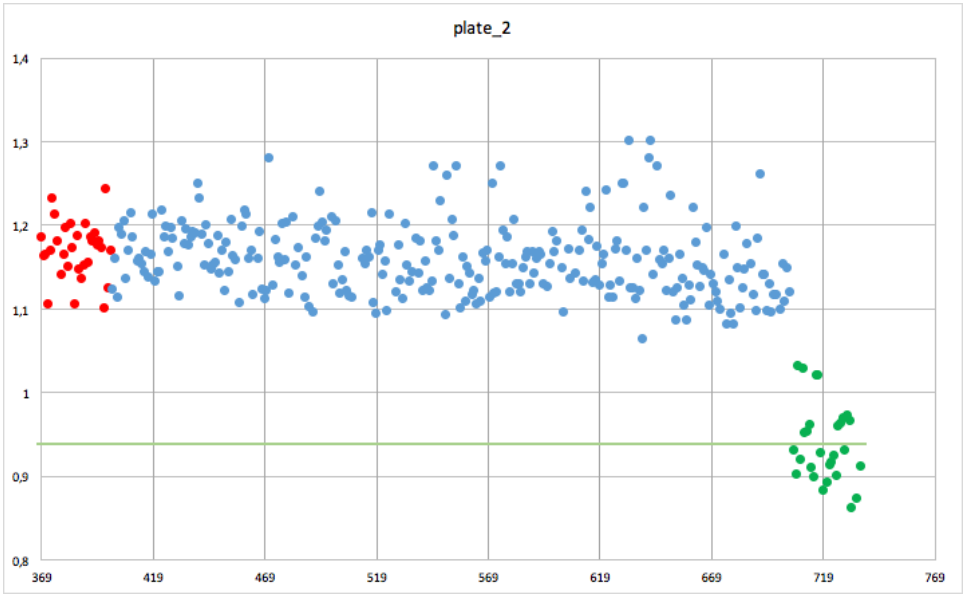
plate_2
1,4
1,3
1,2
1,1
1
0,9
0,8
369
419
469
519
569
619
669
719
769

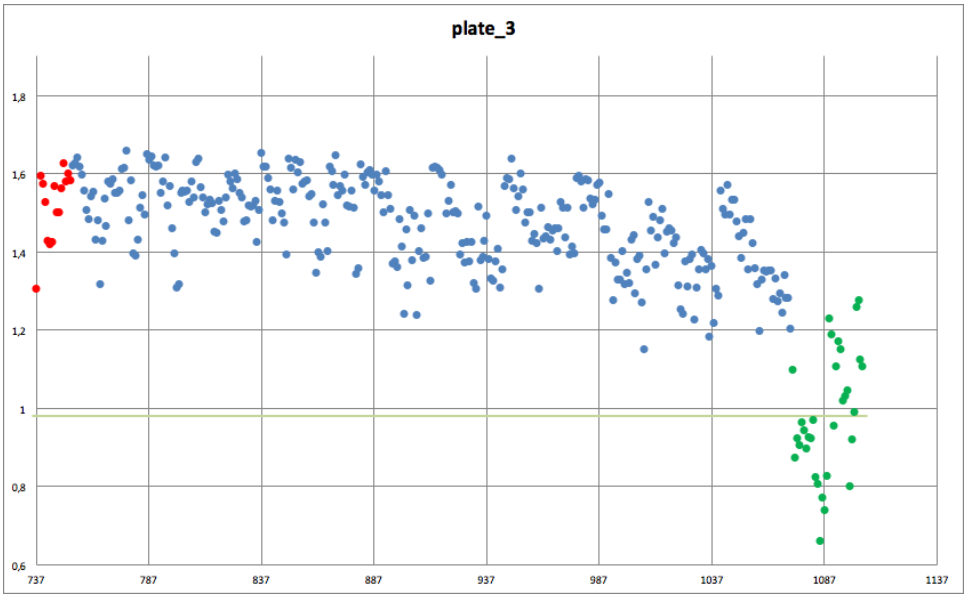
plate_3
1,8
1,6
1,4
1,2
1
0,8
0,6
737
787
837
887
937
987
1037
1087
1137

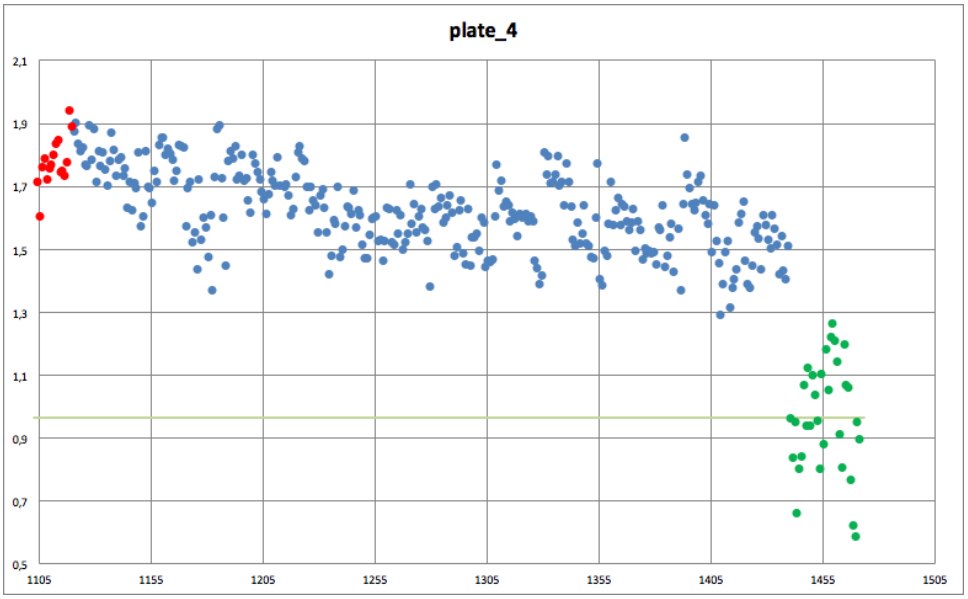
plate_4
2,1
1,9
1,7
1,5
1,3
1,1
0,9
0,7
0,5
1105
1155
1205
1255
1305
1355
1405
1455
1505

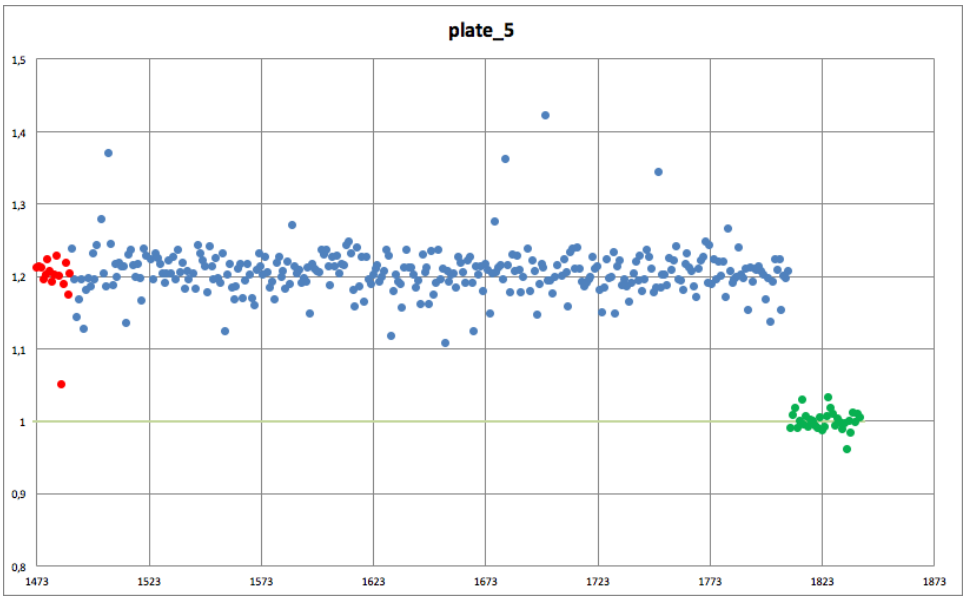
plate_5
1,5
1,4
1,3
1,2
1,1
1
0,9
0,8
1473
1523
1573
1623
1673
1723
1773
1823
1873

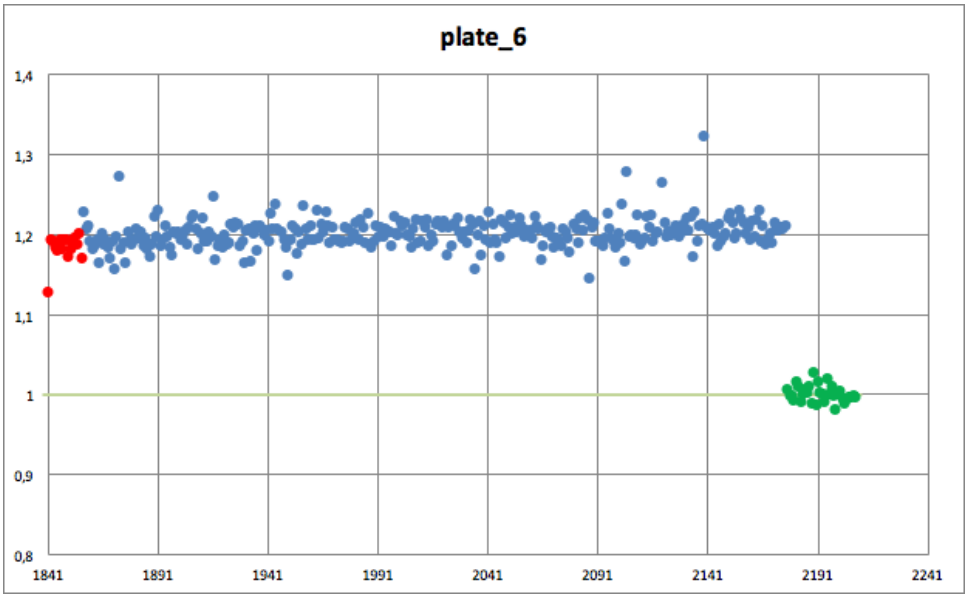
plate_6
1,4
1,3
1,2
1,1
1
0,9
0,8
1841
1891
1941
1991
2041
2091
2141
2191
2241

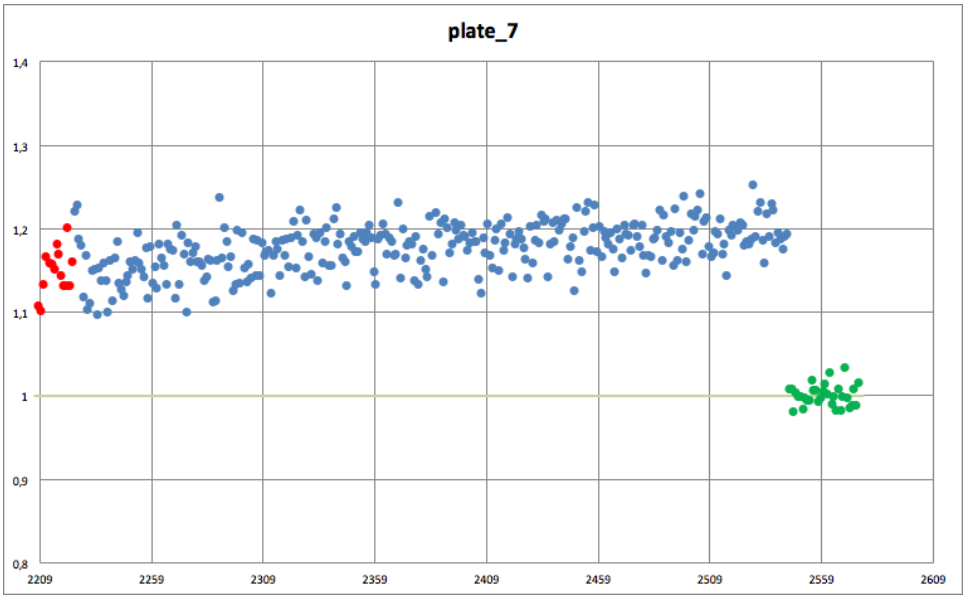
plate_7
1,4
1,3
1,2
1,1
1
0,9
0,8
2209
2259
2309
2359
2409
2459
2509
2559
2609

Figure 4.12. Results of the HT screening: plate 1 to 7. Negative control wells, containing fibers in relax solution (red dots). Sample wells (blue dot). Positive control wells, containing rigor solution (green dots). The straight light green line is the average of the positive control values.

After the analysis and the clean-up were complete there was only one well whose intensity ratios indicated that the SRX of the fibers have been destabilized by the presence of the compound present in that well.

The compound contained in the well was piperine (see Figure 4.13.). The compound piperine derives from an extract of black pepper. It is a compound well known in ayurvedic medicine and has been shown to interact with a number of targets in biological systems. Of particular interest, it has been implicated in attenuating weight gain and type 2 diabetes in rodent studies. These effects are discussed in more detail in the Discussion (paragraph 6.2.3. Literature about use of piperine to treat overweight rodents).

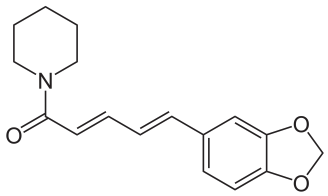

Figure 4.13. Piperine molecule. Source: *https://upload.wikimedia.org/*

4.2.3. Concentration dependence

Following the identification of piperine as a potentially interesting compound in the HT screening, the next step was to verify that this was a true hit using the in vitro assays of the SRX. Skinned fibers were mounted in flow cells and the ratios of their fluorescence intensities observed over time during solution changes. A typical trace is shown in Figure 4.14 where the fibers started in rigor. ATP was added to relax the fibers and populate the SRX producing an increase in the ratio of fluorescence intensities of about 15%. The solution was replaced by a relaxing solution containing 100μM piperine, and this caused a drop of approximately 7% in the intensity ratio, indicating that piperine has destabilized approximately 50% of the previously existing myosin in the SRX. The solution was again exchanged for a

relaxing solution without piperine, and the ratio returned to its previous level showing that the effect of piperine is reversible.

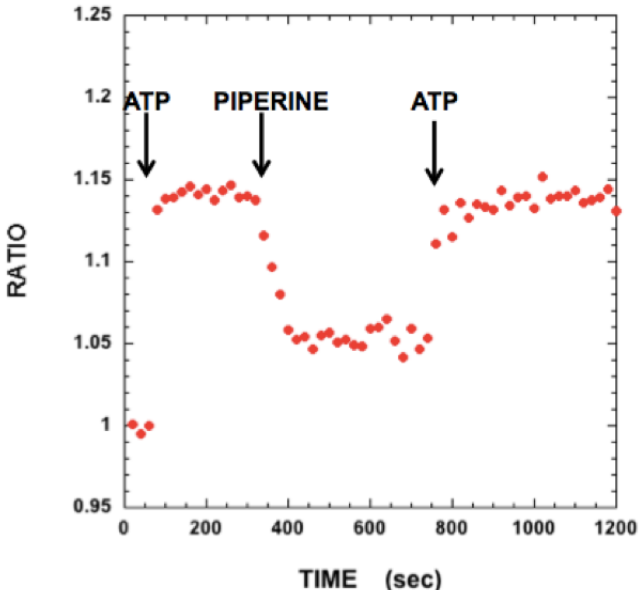

Figure 4.14. Muscle fiber exchanged with RLC-C5 MDCC. The fiber is mounted in a flow cell at the microscope to register the fluorescence at both 440 and 520nm. The fiber started in rigor buffer (ratio=1), in the relax solution (ATP) the ratio is circa 1,15. Piperine in relax solution lowered the value to circa 1,05. Piperine is washed with relax buffer at approx. 800s to restore the ratio to circa 1,15.

A correct estimation of the affinity for the binding of piperine to its target is complicated because piperine binds slowly to inhibit the SRX state. The full effect of piperine requires about 80 seconds at a concentration of 100µM, and the required time was found to be inversely proportional to its concentration. It takes almost an hour at concentrations smaller than 1µM. Because of this behavior, experiments like mantATP chasing were not ideal to measure the inhibition effect on the SRX state at low piperine concentrations, keeping fibers in 250µM mantATP for so long would hydrolyze all the fluorescent nucleotide. For the same reason and because the experiment was carried out at room temperature, ATPase activity and force measurements have only been done using 100µM piperine, to prevent fibers deterioration.

Due to this slow binding behavior, RLC-C5 MDCC exchanged fiber in a plate was the best method to measure the affinity of the molecule. We ran plates with wells containing several concentrations of piperine. Results are reported in Figure 4.15. The inhibition achieved reaches a plateau of about 50% at approximately 10µM

piperine. The ratio of the low salt rigor is lower than the usual rigor, being the ratio calculated as DAPI emission (440nm) over GFP emission (520nm), a lower ratio value corresponds to a higher GFP emission or a lower DAPI emission. In both those situations the probe has to be exposed to water, causing less blue shift than in the regular rigor buffer.

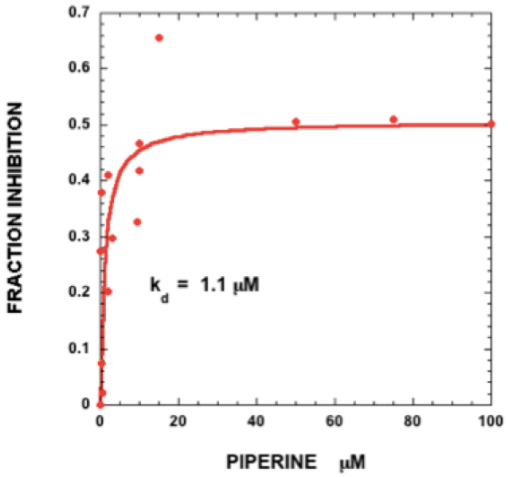

Figure 4.15. Percentage of SRX state inhibition plotted as a function of piperine concentration. Data have been fitted using a Michaelis Menten function to obtain a k_d.

The data described above uses the fluorescent signal of a labeled subunit of myosin to monitor the population of the SRX. A more definitive experiment is to directly measure the rate of nucleotide turnover in the fibers using the mantATP chasing experiment (Introduction 2.2.1. Measuring the stability of the SRX state).

In these experiments the fiber is first incubated in a fluorescent analogue of ATP, mantATP, and this is followed by the chase phase using unlabeled ATP to displace the fluorescent nucleotides. The fluorescence decays in two phases, a fast phase involving the release of mant nucleotides from proteins with rapid turnover rates followed by a slow phase which arises from the release of mant nucleotides from myosin heads in the SRX. Typical data are shown in Figure 4.16. (left panel) where the decay in fluorescence intensity for the control fiber shows a slow component that corresponds to a fraction of 30% of the initial fiber fluorescence and that is released with a lifetime of 250 seconds. As can be seen in the presence of 100µM piperine both the size of this component and its lifetime are decreased by about a factor of 2. This indicates definitively that piperine destabilizes the SRX. The HT

screening along with all of the fiber experiments discussed above were carried out using fibers isolated from rabbit psoas muscle. Rabbit psoas is a fast twitch fiber which mainly uses the myosin 2B isoforms. The experiment was repeated using fibers isolated from the soleus muscle, which expresses a slow type 1 myosin isoform. As can be seen in Figure 4.16. (right panel) piperine had no effect on the SRX in the slow twitch fibers. This result has important consequences for the development of piperine as a therapeutic compound. Slow twitch skeletal fibers share the same myosin isoform as cardiac ventricle cells. Thus, these data show that piperine is unlikely to affect cardiac cells, which would have been a very undesirable trait for a therapeutic agent targeted to skeletal muscle metabolism.

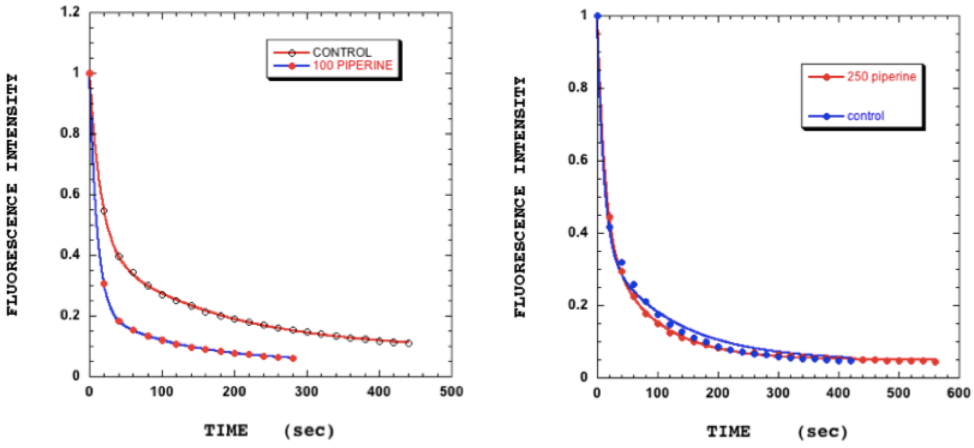

Figure 4.16. Chasing experiment on a fast muscle fiber from rabbit psoas (left panel, 100μM piperine) and on a slow muscle fiber from rabbit soleus (right panel, 250μM piperine).

Once a compound with the desired properties has been identified in a HT screening, a customary next step is to examine similar compounds for further drug development. Piperine (A) consists of 2 ring systems connected by a short 5 carbon leash. The compound is easily broken down into 2 components: piperic acid (B) and piperidine (C) as shown in Figure 4.17. The effects of both of these compounds were examined using the single nucleotide turnover protocols. Neither the compounds nor their combination at concentrations up to 200μM had any effect on either the population or the lifetime of the SRX. Thus the action of piperine requires that the two ring systems are connected together in order to produce an effect.

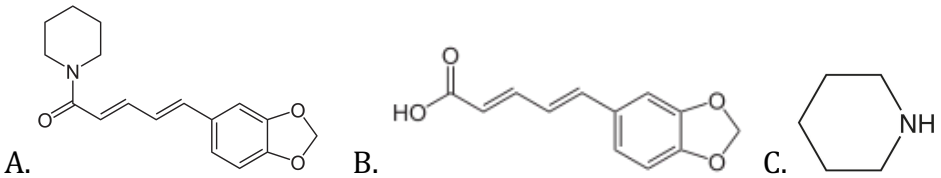

Figure 4.17. A) Piperine. B) Piperic acid. C) Piperidine.

4.2.4. ATPase activity in the presence of piperine

The data described above show that piperine destabilizes the SRX state such that about half of the myosin heads in SRX is shifted into the DRX in skinned muscle fibers. As the ATPase activity of myosin heads in the DRX is about ten fold greater than that in the SRX this destabilization would be expected to increase fiber ATPase activity. To explore this possibility, the ATPase activities of single skinned fibers were measured directly by the amount of phosphate produced over time by performing a malachite green assay[62]. The resulting ATPase activities at rest are shown in Figure 4.18.

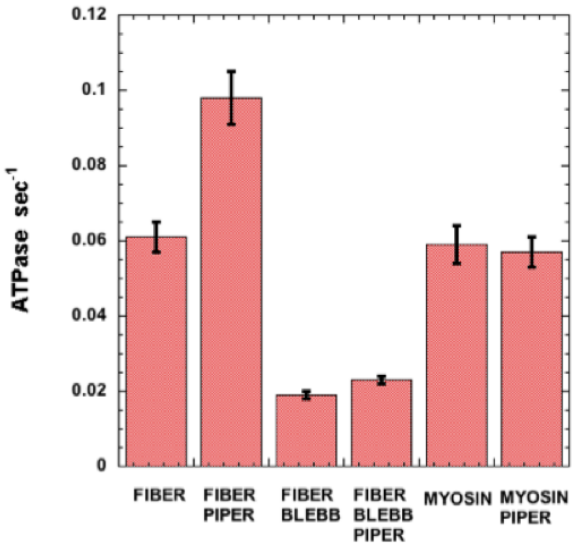

Figure 4.18. ATPase measurements. Piperine has been used at a concentration of 100μM while blebbistatin was 40μM.

The addition of 100μM piperine to the solution bathing the fibers produced a 60% increase in the ATPase activity of the fibers in relaxed condition. Skinned fibers observed here are complex systems containing a number of enzymes that use ATP in addition to myosin. Some of this complexity can be addressed by using a small molecule inhibitor of myosin ATPase activity, blebbistatin[63]. Blebbistatin is specific for myosin and inhibits its ATPase activity by about 90%. Thus in the presence of

blebbistatin the remaining ATPase activity comes almost entirely from other enzymes. The third and the fourth columns in Figure 4.18 show that non-myosin ATPase activity accounts for about one third that of the skinned fibers and further that piperine has little effect on the activity of these other enzymes. The last two columns in Figure 4.18 show that piperine has little effect on the ATPase activity of purified myosin. Together the data indicate that piperine increases the ATPase activity of skinned fibers by destabilizing the SRX.

4.2.5. Tension in the presence of piperine

To be an effective therapeutic agent for metabolic diseases a compound must increase the metabolic rate of resting fibers without any effect on the mechanics of active fibers. Any significant effect on active fibers would be an unacceptable side effect. To explore this possibility single skinned muscle fibers were mounted on a tensiometer, which could measure tension and shortening velocities. Each fiber was observed in the presence or absence of 100μM piperine. In a typical experiment, fibers were initially activated at 5°C for several minutes to allow equilibration of calcium and nucleotides. The fiber was, then, rapidly moved to an activating solution at 25°C and isometric tensions and/or shortening velocities were recorded before returning to the cooler solution. The solutions in both baths were then exchanged for ones that contained 100μM piperine and the experiment was repeated. The order in which the solutions were used was varied.

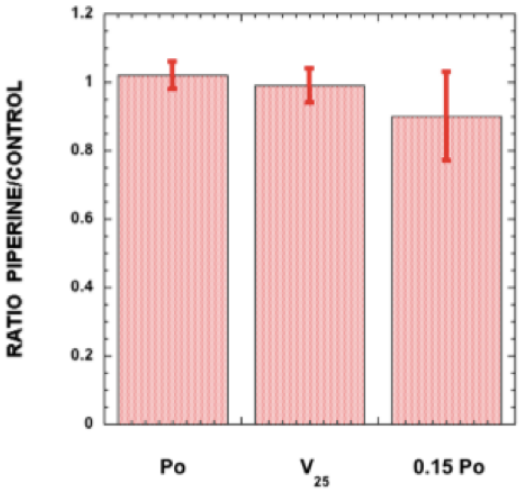

Figure 4.19. Tension measurements in 100μM piperine. Values are normalized by the control measurements without piperine.

In Figure 4.19. it is possible to observe that the addition of 100μM piperine had no significant effect on isometric tension of fully activated fibers, ratio of piperine/control = 1.05 ± 0.05. To measure shortening velocities, fibers were activated isometrically in the warm bath and the tension was then dropped to 25% of the isometric value, allowing the fiber to shorten over a period of 50ms. Addition of 100μM piperine had no significant effect on the shortening velocity at 25% of isometric tension, ratio of piperine/control = 0.97 ± 0.08. The phosphorylation of the myosin regulatory light chain is known to disorder the structure of the thick filament and to destabilize the SRX. It is also known to potentiate the tension in partially activated fibers, but have no effect on the tension generated by fully activated fibers. To check whether piperine had a similar effect, fibers were activated at pCa 5.8 where they generated 15% of the tension of fully activated fibers. Addition of 100μM piperine had no effect on the isometric tension generated by partially activated fibers, ratio of piperine/control = 0.9 ± 0.1. Thus, piperine has no significant effect on any of the parameters of active fibers measured here and, apparently, there is a fundamental difference in how thick filament structures are destabilized by RLC phosphorylation and by piperine.

4.3. A simpler SRX state complex

As said, the SRX state has only been visualized and measured in intact muscle fibers. Only one model is available and it has been obtained by fitting structures into a 3D electron density map. In order to have simpler complex, we tried the coexpression of RLC with a small portion of myosin heavy chain (HCC). We aimed to generate a complex to pursue crystallographic study and to use it in a HT screening instead of intact muscle fibers. The idea was to obtain a dimer of RLC and the portion of HCC which is able to bind to another equal dimer through the coiled coil alpha helix of the HCC (see Figure 4.20.). The structure should keep the two RLC at the right distance and still able to close the interface. To overcome low protein solubility issues, the complex was obtained by the co-expression of both proteins.

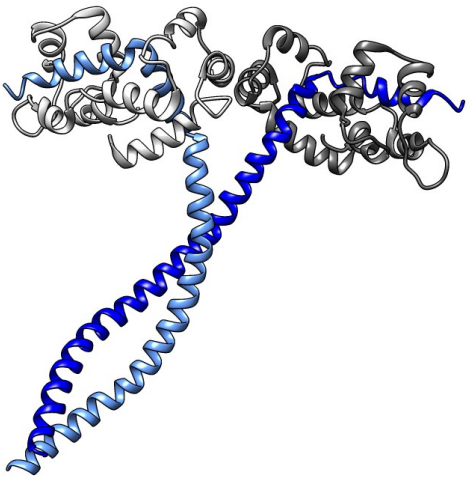

Figure 4.20. Complex formed by two RLC-HCC dimers. Structure adapted from the PDB entry 3J04. Myosin heavy chain in blue and light blue, RLCs in white and gray. Obtained using UCSF Chimera software[22].

4.3.1. How the HCC sequence has been chosen

To identify the RLC binding sequence on the myosin heavy chains, six structures from the PDB has been analyzed (3J04, 1I84, 2W4H, 3DTP, 2MYS and 1B7T)[65, 66, 20, 67, 68] and the RLC binding sequences aligned.

In the cited structures the RLC binding sequence length ranged from 32 to 37 aa (see Supplementary Materials 8.7. RLC binding sequences). Those sequences have been compared with mouse myosin heavy chain 2 sequence to identify the mammal sequence (ERRESIFCIQYNIRAFMNVKHWPWMKLFFKIKPLLKS) (in green in Figure 4.21. The complete sequence is in Supplementary Materials 8.8. Mouse complete myosin sequence: HCC highlighted). Three amino acids were added to the sequence N-terminus in order to have a short spacer (see Figure 4.21.).

KMVERRESIFCIQYNIRAFMNVKHWPWMKLFFKIKPLLKSAETEKEMATMKEEFQKTKD
DLAKSEAKRKELEEKMVSLLKEKNDLQLQVQAEAEGLADAEERCDQLIKTKIQLEAKIK
EVTERAEDEEEINAELTAKKRKLEDECSELKKDIDDLELTLAKVEKEKHATENKVKNLT
EEMAGLDETIAKLTKEKKALQEAHQQTLDDLQAEEDKVNTLTKAKIKLEQQVDDLEGSL
EQEKKLRMDLERAKRKLEGDLKLAQESTMDIENEKQQLDERLKKKEFEMSNLQSKIEDE
QAIGIQLQKKIKELQARIEELEEEIEAERASRAKAEKQRSDLSRELEEISERLEEAGGA
TSAQIEMNKKREAEFQKMRRDLEEATLQHEATAATLR

Figure 4.21. Portion of the mouse myosin heavy chain sequence (GenBank: AAH08538.1). Hydrophobic residues that are in frame with a hydrophobic first-fourth motif are highlighted in purple. In the figure, the spacer region is yellow, the RLC binding region is in green and the region selected for the coiled-coil construct is highlighted in light blue. The coiled-coil region is underlined.

Our purpose was to coexpress a protein which contains the RLC binding region, so, it was quite easy to decide where the sequence should start. It is definitely more challenging to decide where the sequence should end. The myosin heavy chain is not a very soluble protein, getting even less soluble out of the S2 region, where the heavy chains pack up all together to build the thick filament. The myosin heavy chain is responsible for the stability of the myosin dimer, so, the final structure is a coiled coil of the two alpha helices. It is well known that the leucine zipper motif stabilizes the coiled coil structures. Leucine zipper is a common secondary structure motif which contains a leucine in every fourth position of a 7-residues repetition. The first residue of the repetition is often hydrophobic. Myosin heavy chain sequence do not contain a clear leucine zipper pathway but a regular distribution of hydrophobic residues is identifiable. The reason may be that this part of the myosin heavy chain needs to be flexible and adapt to the head movements. Some papers even suggest an unstructured region adjacent to the head-rod junction[69, 70]. We arbitrarily decided to pick the portion containing four complete hydrophobic residues patterns (first and fourth residue). The total HCC construct contains the spacing region, the RLC binding region and the coiled coil region (yellow, green and light blue regions in Figure 4.21.). The picked region after the RLC binding site is 85aa, which results in an α helix approximately 130 Å long. Each RLC is nearly 60 Å long, so the complete complex would have a T shape, 120 Å at the top and around the same size in the coiled coil heavy chain.

4.3.2. Complex expression and purification

The RLC and HCC proteins were coexpressed as specified in Material and Methods (5.3.1. RLC-HCC co-expression). Due to poor HCC expression of the mouse wild type sequence in *E. coli*, the sequences were optimized using Life Technology service (GeneOptimizer®) and the data provided are shown in the Supplementary Materials (8.9. HCC codon optimization). The proteins were co-expressed in *E. coli* Rosetta cells with a polyhistidine tag and purified using a Nickel affinity column. Each construct contained a cleavage site to cut the tag, the RLC protein is expressed with a Thrombin cleavage site while the HCC construct contains a TEV protease site.

This system allows to cleave the excess protein in column and obtain a cleaner protein complex. In all the trials, RLC was more expressed than HCC. The HCC protein weights 18KDa while the RLC weights 21KDa. Two bound dimers in a native page should run as a complex of approximately 78KDa, as shown in Figure 4.22.

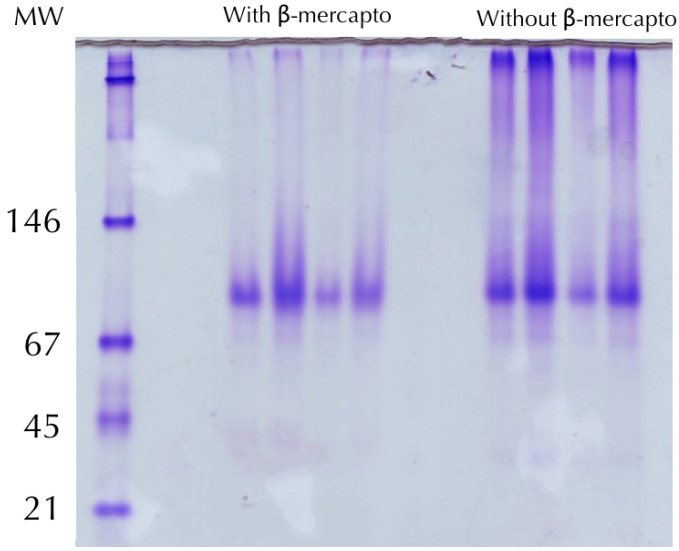

Figure 4.22. Native page of the purified complex. The difference between the lanes with and without the reducing agent suggests that the sample is prone to aggregation through cysteine reactivity. The sample loaded has been expressed with the wt HCC sequence, not the optimized one.

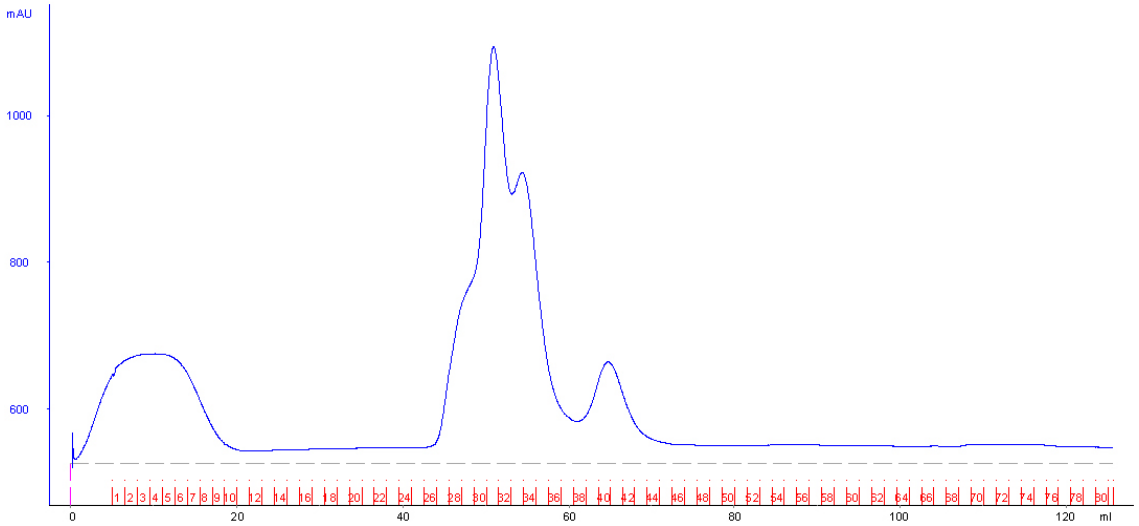

Figure 4.23. Size exclusion chromatography. Chromatographic profile of a RLC-HCC co-expression sample run after Qiagen Ni-NTA purification. At the very beginning the precipitated/aggregated protein is eluted. The compose peak has a higher molecular weight component which is the complex. The separation obtained with the HiLoad Superdex 200 PG column was not optimal for this sample.

In Figure 4.23. a chromatographic profile of a RLC-HCC co-expression sample is reported. As a first trial, the separation achieved with that column is not enough to

obtain a clean complex sample, probably because of the small size differences between the several components. The peak contains several components but the left shoulder at higher molecular levels represent the complete complex.

The HCC-RLC complex has been expressed not only for crystallization trials, the HCC portion has been co-expressed together with a double mutant RLC with cysteines in positions A55 and G102. The RLC has been labeled with a mixture of IAEDANS and Fluorescein to perform FRET measurements on the complex. Our hope was to be able to sense the RLC-RLC interface formation and disruption in a soluble protein preparation. Unfortunately, we were not able to achieve any signal change in any condition.

5. Material and Methods

5.1. Methods for “Spectroscopic Studies of the Super Relaxed State of Skeletal Muscle”

5.1.1 Chemicals and solutions.

The solution used to induce in muscle fiber the different states (Rigor, Contraction, Relaxation) had the following composition: 1) Rigor buffer is a solution of 50mM 3-(N-morpholino)propanesulfonic acid (MOPS), 120mM potassium acetate, 5mM magnesium chloride, 5mM EGTA, 5mM potassium phosphate, pH=6.8 adjusted at room temperature). 2) Relaxing buffers were obtained by addition of 4mM ATP or 250μM mantATP to the Rigor buffer. For the EPR experiments the relaxing buffer was obtained by adding to the rigor buffer ATP and blebbistatin from a high concentration stock in order to make the solution 4mM ATP and 40μM blebbistatin. Blebbistatin ((±)-1-Phenyl-1,2, 3,4-tetrahydro-4-hydroxypyrrolo [2.3-b]-7-methylquinolin-4-one), was obtained from Toronto Research Chemicals, Inc., 2 Brisbane Road, North York, ON M3J 2J8 Canada. 3) Contraction or Activation solution was obtained by adding to a Relaxing solution (EGTA concentration 1mM instead of 5mM of the usual rigor solution) $CaCl_2$ at the concentration of 0.6mM to obtain a pCa=5.8 (partially activated fibers) and 1mM to obtain a pCa=4 (full activated fibers). All activating solutions contained 10mM creatine phosphate and 1mg/ml creatine kinase. The RLCs were exchanged into fibers using exchange buffer (50mM MOPS, 20mM EDTA, 50mM KAC, 10mM potassium phosphate, pH7.0).

The spin labels: 4-maleimido-2,2,6,6,-tetramethyl-l-piperidinyloxy (MSL), 4-iodo acetamido-2,2,6,6,-tetramethyl-l-piperidinyloxy (IASL) (1-oxyl-2,2,5,5-tetramethyl pyrroline-3-methyl) methanethiosulfonate (MMTS or MTSL) were purchased from Sigma Aldrich (USA) Chemical Co. All fluorescent probes: 3-(bromomethyl)-2,5,6 -trimethyl-1*H*,7*H*-pyrazolo[1,2-*a*]pyrazole-1,7-dione (BIMANE); 7-Diethylamino -3-

[*N*-(2-maleimidoethyl)carbamoyl] coumarin (MDCC); 2-(4'-maleimidylanilino) naphthalene-6-sulfonic acid (MIANS) were obtained from Sigma Aldrich (USA) Chemical Co. A stock of 20 mM of each was prepared in DMF and stored in the freezer at -20°C. P-6 spin columns were purchased from Bio-Rad. Thrombin was purchased from Sigma Aldrich (USA) Chemical Co. The proteins were visualized on 18% SDS gels obtained from NOVAX using either Instant blue stain (Expedeon) or silver stain that was prepared in the lab. Troponin C was kindly provided by the Dong Lab (WSU). Other chemicals were purchased from Sigma (USA) Chemical Co. The proteins were visualized on 18% or 4-20% SDS gels obtained from NOVAX using either instant blue stain (Expedeon) or silver stain that was prepared in the lab.

5.1.2. Preparation of muscle fibers.

White New Zealand rabbit (*Oryctolagus cuniculus*) were sacrificed according to the protocols approved by the Institutional Animal Care and Use Committee. Skeletal muscle fibers were harvested and stored in cold skinning solution (120mM KAc, 50mM MOPS, 5mM MgOAc, 5mM DTT, 5mM EGTA, 50% glycerol, pH 7.0) tied with silk threads to wood sticks. Psoas muscle provided fast fibers, and soleus provided slow fibers. The muscles were kept 24h at 4°C shaking in skinning solution, the solution was replaced with some fresh the day after. The muscle fibers were then transferred at -20°C until the day of use. The procedure of skinning is taken from Salviati (1982) [ref. Salviati, G, MM Sorenson, and AB Eastwood. "Calcium accumulation by the sarcoplasmic reticulum in two populations of chemically skinned human muscle fibers. Effects of calcium and cyclic AMP." The Journal of general physiology 79.4 (1982): 603-632.].

5.1.3. RLC mutant preparation: molecular biology and protein purification

The mouse RLC sequence comes from a cDNA kindly provided by the Di Lisa's Lab (University of Padova). The cysteines present in the sequence, positions C128 and C157, were mutated to alanines and the other cysteines were added using Qiagen Quickchange II mutagenesis kit (K5C, A6C, K31C, D38C, I44C, T81C and C128). The media used for cellular growth is indicated as super LB (20g/L tryptone, 10g/L yeast

extract and 5g/L Sodium Chloride). The induction was done using Isopropyl β-D-1-thiogalactopyranoside (IPTG) when the Optical Density (OD) of the culture was between 0.6 and 0.8. The cysteine-mutants RLC were expressed overnight at 18°C in BL21 Rosetta cells kindly provided by the Narlikar Lab (UCSF) as a N-terminal fusion protein with a histidine tag and thrombin protease site from a Novagen pET28a vector. Cells were collected by centrifuging for 15min at 5000g and resuspended in wash buffer (200mM NaCl, 50mM TES buffer, 20mM imidazole, 2mM MgCl2, 1mM DTT, 10% sucrose, ph 8.0). Cells were broken by cycling the resuspension into a temperature controlled AVESTIN EmulsiFlex-C3 homogenizer for 12 to 15 min, temperature set at 5°C. The supernatant was collected by centrifuging the samples at 40000g for 45 minutes at 4°C and, then, loaded on a Qiagen Ni-NTA Agarose resin column previously equilibrated in wash buffer. After the flow through was gone, the resin was washed extensively with wash buffer (10 to 20 column volumes). Protein binding the resin was then washed with 10ml of wash buffer without DTT and eluted with elution buffer (wash buffer with 300mM imidazole, 100μM DTT and pH 7.6). The protein from the column was diluted to a concentration of approximately 100μM with dilution buffer (200mM NaCl, 50mM TES buffer, 2mM MgCl2, pH 7.6) before being labeled overnight at 4°C in the presence of 300μM of paramagnetic or fluorescent probes (stocks of probes are at concentrations 10 to 20mM in DMF, stored at -20°C). The unreacted probe was quenched with 1mM DTT (in fluorescent probe samples only) and, followed by digestion with thrombin, if desired, to remove the HIS-tag, see below. Finally, the RLC was dialyzed in exchange buffer and used or stored at -20°C.

5.1.4. Cleavage of the RLC with thrombin.

To obtain the protein without the histidines tag, RLC mutants were treated with thrombin immediately after the labeling overnight. Before proceeding with the cleavage, the extra fluorescent probe was quenched with 1mM dithiothreitol (DTT). DTT was not used on sample labelled with spin probes, since the unpaired electron can be reduced by the chemical. The protein was left at room temperature for 20 minutes to let the reduction happens. One unit of thrombin (Sigma Aldrich, Thrombin from human plasma T7009-250UN) and 200μM $CaCl_2$ were added to the

elution/dilution buffer, the solution was left at 30°C for 3 hrs. The reaction was stopped by adding 300µM EDTA solution to remove calcium. Depending on the amount of protein that was cut, the buffer was then exchanged into the fiber exchange buffer either by dialysis of by using P-6 spin columns (Bio Rad, Micro Bio-Spin Columns With Bio-Gel P-6).

5.1.5. Exchanging RLC on muscle fibers.

Small bundles of 8-10 rabbit psoas fibers, approximately 10 mm long, were dissected and washed with exchange buffer (50mM MOPS, 20mM EDTA, 50mM KAC, 10mM potassium phosphate, pH7.0) for 1 hr at 4°C. About 10 bundles of fibers were incubated with 50µl of exchange buffer containing 100 µM of labeled RLC. The mixture was again left shaking on ice for another 1 hr then incubated at 30°C for 30 minutes. The bundles were transferred to a rigor solution containing 0.4 mg/ml solution of Troponin C and left shaking on ice for 1 hr. In the end, the bundles were placed into a rigor solution with 50% glycerol, left shaking on ice for another 1-2 hrs and stored at -20ºC for use. The extent of RLC exchange was determined by SDS gel electrophoresis which allowed the quantification of the decrease in the endogenous RLC and the increase in the mutant RLC.

5.1.6. Measurement of Fluorescence.

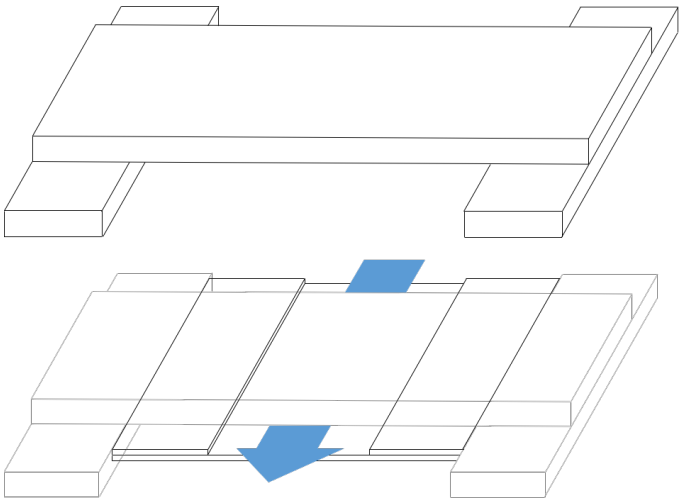

Figure 5.1. Flow-cell scheme. The upper part (thick glass) has been made out of microscope slides glued together using an epoxy glue. The thin part (thin glass) has been made of coverslips. The thin glasses were kept together by adhesion with silicon grease.

Single muscle fibers were mounted on a coverslip and the ends were secured with small amounts of silicone grease. A simple flow cell (see Figure 5.1.) was constructed by mounting the coverslip with the fiber on a glass slide between two other coverslips forming a small cell, which had a thickness of ~270μm. The device allows to flow solution in from one side and suck the old solution from the other side to exchange them rapidly. The fluorescent signal was detected using a Nikon TE2000 microscope at the Nikon Imaging Center @ UCSF/QB3 at University of California San Francisco, Genentech Hall. Temperature was 25ºC.

5.1.7. EPR spectroscopy.

EPR measurements were performed with a Bruker EMX EPR spectrometer (Billerica, MA). Continuous Wave (CW), X-band spectra were recorded in a high-sensitivity microwave cavity using 50s, 10 mT-wide magnetic-field sweeps. The instrument settings were as follows: microwave power, 25 mW; time constant, 164 ms; frequency, 9.83 GHz; modulation, 0.1 mT at a frequency of 100 kHz. Each spectrum used in data analysis was an average of 10–50 sweeps from an individual experimental preparation. Temperature was 24±2ºC and was monitored using a thermistor placed close to the experimental sample.

5.1.8. EPR experiments on RLC exchanged fibers.

Fibers exchanged with paramagnetic labeled RLC were aligned on an EPR flat cell. The EPR spectra of the fibers were obtained with the cell aligned either parallel or perpendicular to the magnetic field. Random spectra were obtained using minced fibers. The relaxed spectra of fiber in the SRX state were obtained by incubating the fibers for 15 min in a rigor solution containing 40μM blebbistatin, followed by 15 minutes in relaxing solution with 40μM blebbistatin. The fibers were shaken in each solution, the extra solution was removed, and the fibers were remounted in the flat cell which was set in the spectrometer cavity.

5.2. Methods for "Disrupting the SRX State: the high throughput screening"

5.2.1. Brief description of how screen was run

Skinned muscle fibers were chopped using a common razor blade in fragments approximately 50-200μm in length, were exchanged with coumarin labeled RLC-C5 as described previously. The wells in column 1 were filled with 60μL of rigor buffer plus 0.02% Triton X-100, and used to obtain an average picture of the illuminated background. Chopped fibers were manually distributed in columns 2 to 24 by pipetting 50μL of resuspension in rigor buffer plus Triton. Wells in column 2 were used as negative controls, so 10μL of ATP (in rigor buffer) were added in order to obtain a concentration of 4mM, in those wells no compound will be added. Wells in columns 23 and 24 were used as positive controls, so 10μL of rigor buffer were added to keep the volume constant. Compounds were pinned in wells of columns 3 to 22 in a volume to obtain a final concentration of 10μM, so each plate contained 320 different compounds. Those wells will be defined as "samples" wells. The final volume is 60μL for each well. Pictures of the wells were taken and analyzed as described below.

5.2.2. Images

The data were collected in form of fluorescent pictures on a Nikon 6D High-Throughput fluorescent microscope in the NIC - Nikon Imaging Center at the University of California, San Francisco. The excitation and emission filters were from a DAPI set, excitation wavelength (377/11nm) and emission filters set at 420-460nm (DAPI emission) and 510-540nm (GFP emission). The shutter time used was 500ms for each picture, so 1s of total illumination per well.

5.2.3. Fiji Macro

A Fiji[48] macro was developed to analyze all the pictures (complete code in supplementary Materials, 8.6. Example of the Fiji macro (code)). To obtain a ratio, the macro had to analyze two picture at a time, one coming from the DAPI emission

and the other one from the DAPI-GFP fret emission. The pictures were first corrected by subtracting an average backgrounds taken in empty wells, one for each channel. This procedure was added to make the intensity of the light even, especially at the corners, and to improve the reliability of the following steps. Dust and other objects on occasion provided bright images that altered analysis. These were detected by a high cutoff filter and all regions of the picture much brighter than expected were removed by setting those pixels to zero (black). The brightest picture (among the two channels) was used to auto-threshold the fibers in the well (Figure 5.2.), the selection was then saved to measure the intensity of the same regions in the other picture. To obtain a reliable background, the fiber selection was enlarged by 20 pixels before inverting it, to select the background, this was to avoid diffraction and scattering of light in the region close to the fibers. The final output contains 5 values for each couple of pictures, fluorescence intensities for both channels, background intensities for both channels and a correction coefficient. This last number represent the amount of pixels that had to be taken to zero because of the high brightness, by comparing this value with the size of a picture a reliability value can be estimated. Wells in which the compound is autofluorescent in one of the two channels will be much intense even after subtracting the background.

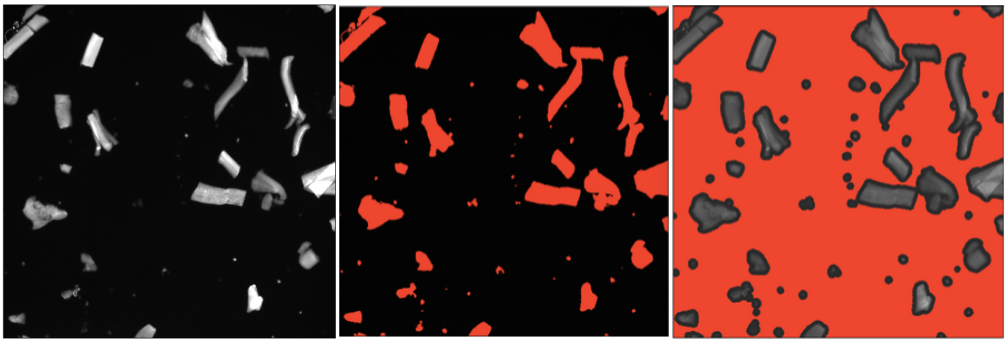

Figure 5.2. Example of a picture analyzed by the Fiji macro. Original picture (left picture), fiber selected by the auto-threshold algorithm (middle picture). Background selected as the opposite of the fiber selection (right picture). The fiber selection is enlarged by 20 pixels before doing the opposite selection. This is to avoid the portion of background too close to the fibers which may be affected by the fiber light.

5.2.4. How to clean up results

As mentioned previously, some of the 2240 molecules used in the screening were fluorescent in the range 420-460nm (DAPI emission) or the 510-540nm (GFP

emission). The concentration of these molecules is 10μM in the well and this lead to a bright emission which does not come from muscle fibers. Furthermore, in case of autofluorescence, the pattern of objects in the picture was lost: chopped fiber fluorescence was concentrated in small areas approximately 100x60μm, diffused autofluorescence made the thresholding procedure hard and uneffective. The ratio measured in those wells was completely unreliable and, so, those compounds were discarded. The results of the macro were corrected by either considering the autofluorescent compounds and by manually measuring fibers. The pictures of the sample wells that were characterized by a lower ratio (closer to the positive control) were analyzed by picking fibers and background manually. Due to on-the-way improvement of both fibers preparation and macro analysis, the first results were manually checked well by well. Even the first macro was able to do almost all the expected analysis, leaving only dozens of wells with a low ratio to be manually checked.

5.3. Methods for "A simpler SRX state complex"

5.3.1. RLC-HCC co-expression

The mouse heavy chain sequence (named HCC) was extracted from mouse skeletal muscle cDNA and inserted into a pCDFduet-1. Due to the very low yields in trial purifications, the optimized sequence have been ordered from Life Technologies (Thermo Fisher Scientific) as a GeneArt Strings DNA Fragments service. The sequence has been chosen as described in 4.3.1. How the HCC sequence has been chosen. The sequence has been inserted into a pCDFduet-1 plasmid by using FastCloning technique[71] in a way to be suitable of a co-expression with the pool of RLC mutants in pET28a. The construct contains a TEV protease site to cleave the histidines tag present at the N-terminus of the protein for purification purposes.

The co-expression of RLC and HCC was achieved by the co-transfection of a pET28-RLC plasmid and a pCDFduet-HCC plasmid in BL21 Rosetta cells. Plates and liquid media for co-expression contained 50μg/ml kanamycin (pET28a resistance), 25 μg/ml spectinomycin (pCDFduet resistance) and 25 μg/ml chloramphenicol. The

last antibiotic is needed because the Rosetta strain contains an additional plasmid for the improvement of *E. coli* codon usage by expressing poorly used tRNAs (argU, argW, glyT, IleX, leuW, metT, proL, thrT, thrU, and tyrU). The growing and purification procedure for the co-expression is similar to the one previously described for the RLC mutants.

6. Discussion

6.1. Our work

6.1.1. Introduction

Our goal in this study was three-fold. First was to understand the role of the RLC in the structure of the IHM. Second was to find a signal that would allow the use of high throughput screens to search for small molecules that would change the stability of the IHM and SRX, and thereby alter the energy economy of muscle to influence whole body metabolism. Third, was to run a screen in a library of 2200 compounds to discover new molecules to disrupt the SRX. The ultimate goal of this approach was the discovery of compounds that increase resting muscle metabolic rate.

6.1.2. Developing spectroscopic probes

We used the atomic model, 3DTP, derived from the cryo-EM structure[20] to provide a low-resolution picture of the RLC–RLC structure, and we refined the region of interest by examining the pattern of conserved amino acids on the surface of the protein. We placed single cysteines within this patch of conserved amino acids or adjacent to it. In addition we placed single cysteines in the N-terminal segment of the protein, as this segment is unstructured in all crystal structures and contains the phosphorylated serine, which is known to influence the stability of the IHM.

The mutations alone had a small effect on the stability of the SRX as measured by our chase experiments. A single mutation would not be expected to have a large effect on the stability of the SRX as the interfaces that form this complex involve an extensive area. In addition to the RLC-RLC interface the interacting head motif is also stabilized by two additional interfaces involving, intramolecularly, the two myosin heads and, intermolecularly, by additional interfaces with adjacent IHM complexes. The only mutation which showed a sizable effect, probably did so by destabilizing a divalent cation bound to the RLC.

Addition of probes to the sites on the RLC exerted larger changes to the stability of the SRX. One site RLC-C128 accommodated all of the probes as expected as it was

chosen to be a control, far away from the crucial interface region. Two of the mutants, RLC-C44 and RLC-C38 did not tolerate even the smallest probes. Among the remaining 6 mutants there was a rough correlation between the size of the label and its effect. BIMANE is the smallest of our probes as it adds a two ring planar structure that is not much larger than the side chain of tryptophan. The label that is expected to have the largest effect is MIANS which has a multi-ring moiety attached fairly rigidly to the cysteine. MIANS had an appreciable effect on all sites. Although the ring structure of coumarin is fairly large, it is linked through a flexible leash to the cysteine, and this label was reasonably well tolerated at all sites. The spin labels have an intermediate size, their ring structures are not planar and the addition of methyl groups forms a roughly cylindrical structure, which might be expected to interfere with an interface. The smallest of these labels, MMTS, was fairly well tolerated at most sites, while the other two labels inhibited at some sites and were accepted by others. We conclude from the data described above that the regions in which we have placed our probes are involved in the stability of the IHM. In particular, they show that the N-terminal end and the divalent cation each play an important role. The observation that the addition of a probe to a site within the RLC-RLC interface destabilizes this interface provides a proof of concept that the binding of small molecules could decrease the stability of the SRX. Although the structure of the IHM involves multiple interfaces, the steric disruption of one of these interfaces by an attached probe is sufficient to destabilize the entire complex. Because full inhibition was found for some samples, in which only 50% of the RLC's were exchanged, the data further show that the sub-stoichiometric binding of an inhibitor can destabilize the SRX completely. The SRX is completely destabilized in spite of the fact that 25% or more of the myosins in the array have not been modified. Thus destabilization of one molecule also destabilizes adjacent molecules, and the myosin heads in the array are interacting in a cooperative fashion. Destabilization of a fraction of them destabilizes the entire array, which then acts as a unit. A cooperative inhibition of the SRX has previously been observed for RLC phosphorylation where inhibition is achieved when less than 50% of the myosins are phosphorylated, but all the myosins have a shorter lifetime. A cooperative interaction is implicated by the observation that the inhibition of the lifetime of the

SRX is linearly proportional to the inhibition of the population of the SRX as shown in Results (4.1.3. Effect of RLC mutants on the SRX state). If there were no cooperative interactions between heads in the array, the destabilization of a fraction of the SRX would leave the remaining heads in the SRX with a T2 that was unchanged. A similar correlation between P2 and T2 was seen for destabilization of the SRX by RLC phosphorylation and temperature[10]. However, there are also examples where T2 changes without changes in P2[72]. A variety of results obtained by other studies have suggested that the formation of the array of myosin heads bound to the core of the thick filament involves cooperative interactions between the heads. Some of the most compelling evidence comes from small angle X-ray diffraction measurements where myosin heads in the array give rise to a series of myosin layer lines in the diffraction pattern. If the myosin heads are disordered the layer lines are lost. When a skeletal muscle fiber is activated the myosin layer lines are lost much more rapidly than the increase in force[73].

This result shows that some signal has been transmitted from the activated thin filament to the resting thick filament that causes the release of the ordered myosin heads from the core of the thick filament. Even more compelling evidence comes from experiments in which the muscle fibers are activated at longer sarcomere lengths, where a large fraction of the myosin heads are not in the overlap zone[74, 75]. Even though half or more of the myosin heads have no thin filaments to interact with, upon activation all of the myosin heads become very rapidly disordered. This observation shows that there has been a signal passed from the myosin heads in the overlap zone to other distant myosin heads causing them to become disordered. A cooperative mechanism has also been demonstrated for the activation of tarantula thick filaments by phosphorylation[76, 77].

A number of the fluorescent probes showed spectral changes on the transition from the rigor state to the ATP-relaxed state and on the transition from the ATP relaxed state to the GTP-relaxed state. No spectral changes were seen for the mutants C-44 and C-38, in which the formation of the super relaxed state is strongly inhibited, and with one exception changes were not seen for the control position, C-128. Of the remaining combinations, more than half of them showed fluorescence changes in their fluorescence spectra. For the majority of these probes, fluorescence intensity

increased going from the rigor state to the ATP-relaxed state and this change was reversed going from the ATP relaxed state to the GTP-relaxed state. This observation shows that for these samples the probes were in a more nonpolar environment in the ATP-relaxed state, as expected if the probes were involved in an interface between the RLC's in the interacting heads motif. However there were also samples, in which fluorescence decreased going from the rigor state to the ATP-relaxed state, although the changes were smaller and some were not reversed in the GTP-relaxed state. Finally, there were probe mutant combinations that showed no changes. In summary we can conclude that the pattern of spectral changes supports the conclusion that the residues targeted are involved in the formation of the IHM, and that the diversity of spectral response is due to the details of the interaction between the probe and the surrounding protein structure. In the presence of a magnetic field, TEMPO probes give rise to a spectrum consisting of three lines. The splitting between the spectral peaks depends on the angle between the principal axis of the probe and the magnetic field, the wider the spectral splitting the smaller the angle.

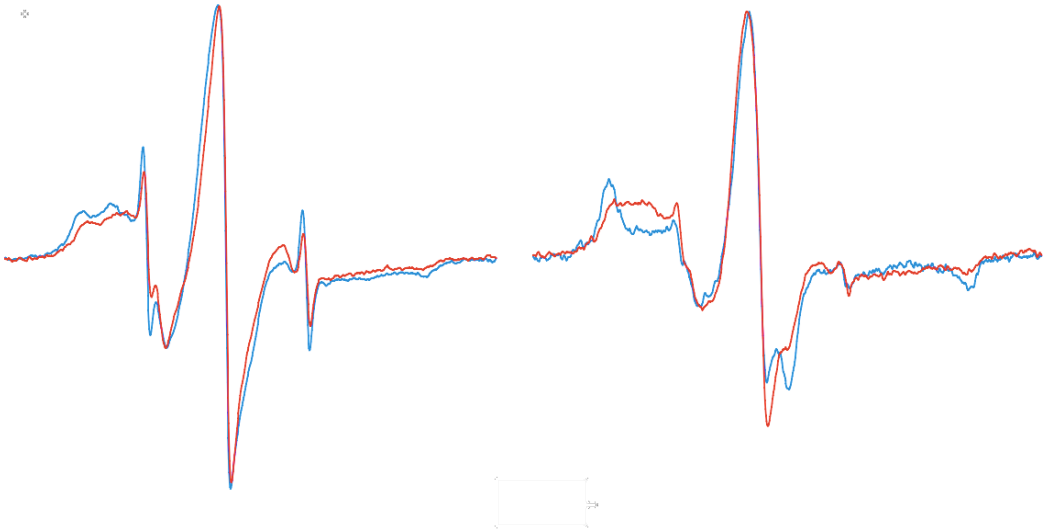

Figure 6.1. (also Figure 4.1.) EPR spectra of fibers exchanged with RLC-C31-MMTS with the fiber axis either parallel (blue line) or perpendicular (red line) to the magnetic field. The derivative of absorption is shown as a function of the magnetic field strength. The fibers are in rigor solution (left spectra) and relaxing solution, ATP plus bebbistatin (right spectra). The difference between the parallel and perpendicular spectra in the top figure show that the paramagnetic probes are oriented in relaxation and the SRX. In rigor there is less orientation. The center-fields of the spectra are 0.3490 T and the sweep width is 10 mT.

A comparison of the spectra taken with the long axis of the fiber parallel or perpendicular to the magnetic field provides information on the orientation

distribution of the probes. By looking at the differences between the parallel spectra and the perpendicular spectra it is possible to say that the sample with the best orientation is the RLC-C31 MMTS. In this sample, the change from rigor to relax-blebbistatin buffer, corresponds to a shift of a population that becomes more immobilized in the SRX state. In the spectra this is highlighted by the peak in the low-field region. More quantitative interpretation of the orientation is difficult as the two RLC's of a given myosin molecule have two different orientations, and in addition we do not know how the probe is oriented relative to the protein. However, we note that oriented probes even in muscle fibers are rare.

In the tarantula IMH of the 3DTP model, the residue number 31 seems to be in an ideal position to sense the changes in the conformation of the complex. The original lysines (K31) are at the interface between the two RLC, facing each other. The surface is not tight and a small probe may fit in the empty space, which is left by removal of the lysines. Furthermore, in chase of very close spin probes an effect called “spin-spin interaction” happens and it changes the spectra in a very clear way. We did not see any spin-spin interactions in none of the spectra, so, it may be that the probes are not close in the structure or that one of the RLC is easier to exchange than the other. We can conclude that the paramagnetic probes, like the fluorescent probes, show spectral shifts between rigor and the relaxed state. The presence or absence of spectral shifts appears to vary widely with different probe combinations due to the specific details of the interaction between probe and protein. For our purposes, IASL probe failed to show any difference in the spectra, probably because of its floppy nature. Because of the helical nature of the thick filament and because of the different orientation of the two RLC in the SRX state structure, our EPR experiments are more prone to be informative on the immobilization of the probe rather than on its orientation. Based on what said, we can speculate that MSL probe gave poor results because of its rigid structure. Samples labeled with MSL gave immobilized spectra when bound to RLC but even before the exchange of the protein into muscle fibers.

Taken together, we can conclude that the results show that the targeted regions are involved in the formation of the SRX.

There is one structural model of a conformational change in the N-terminal region of the RLC upon the transition from the dephosphorylated form (presumably the SRX conformation) to the phosphorylated form (presumably in the DRX)[49, 51, 53, 55, 78]. This involves a transition from a compact region lacking secondary structure to an alpha-helical region that is more solvent exposed. Our data show that there is a tendency for the probes in the N-terminal region to be less solvent exposed in the SRX, thus providing some support for the model, but more detailed conclusions cannot be made. Observation of the polarization of bi-functional fluorescent probes on the RLC has provided information on the structure of this region in muscle fibers. The orientations of the probes in relaxed fibers show that there is an appreciable population of the RLCs that are in the IHM[77, 80]. This population is also seen in active and even in rigor fibers. Thus the RLC region is still structured in rigor. Because the dimension of the myosin is sufficient to bridge the span from the thin filament to the thick filament, the RLCs could still be interacting with the core of the thick filament[80]. This conclusion might help to explain the observation that some of our probes had no spectral response on the transitions between rigor, the SRX and the DRX. Although conformational changes do occur in these transitions, they are not global.

The changes in spectral intensity of the fluorescent probes discussed above did provide a signal that has been used for high throughput (HT) screenings. The variation in intensity of the signal happened to be only 15 to 20% in the best cases. Fortunately, the blue-shift observed in the emission spectrum of coumarin attached to RLC-C5 provided a solution to this problem. Because two fluorescence emissions arise from the excitation of one probe, the ratio function is independent of the amount of material being observed, excitation intensity and photobleaching.

To summarize, mutants and probe sites have been chosen to monitor a putative RLC-RLC interface in the SRX state complex. The inhibition of the state and the spectral changes associated with it strongly suggests that the putative interface exist. The data shown that the N-terminal region participates in the formation and, probably, determines the stability of the surface. This information proves that the SRX state complex can be disrupted by small molecules.

6.2 High throughput screens

6.2.1 Motivation for high throughput screens

There is currently an epidemic of obesity and type 2 diabetes affecting the developed countries and increasingly the developing countries. Many factors have contributed to this but primarily it is attributed to an overconsumption of food coupled with a reduction in physical activity. In addition there are significant genetic factors, which also play a role. A natural antidote to both obesity and type 2 diabetes is to choose a healthy lifestyle, including a low-calorie diet and increased activity. However, many patients do not choose this option and for some patients increased physical activity is not possible. The response to overfeeding in humans is diverse, some store the excess calories almost entirely while others burn them off. As strenuous activity was limited in some people resistant to overweight in the presence of overfeeding, the diversity of weight gain was attributed to light activities, such as fidgeting. This has led to the concept that low-level activity distributed throughout the day might be more effective in combating obesity than periods of high intensity activity, which are usually of limited duration. Alternatively the diversity may be due to variation in the metabolic rate of resting muscles, and to how this responds to activity.

A pharmacological approach to combating obesity has been of limited value. A number of approaches have been tried including targeting appetite, affecting nutrient uptake, etc. and several pharmaceuticals have been developed but withdrawn due to adverse side effects. Currently Orlistat, a lipase inhibitor that reduces the uptake of fatty acids by the digestive system is the only drug approved in most countries.

We believe that skeletal muscle may be a new target for combating obesity and type 2 diabetes by increasing the resting metabolic rate. The metabolic rate of resting, living skeletal muscle is variable responding to stretch and to hormones including leptin and epinephrine, for review see Cooke (2011)[81]. Although the resting metabolism of muscle is low compared to other tissues, due to its large mass, ~40% of body weight, its contribution to whole body metabolic rate at rest is appreciable,

approximately 25%. In this thesis we propose the destabilization of the SRX state as a way to exploit myosin increased ATP turnover to burn more energy. Measuring single cycle ATP turnover rates in skinned resting muscle we showed that myosin can be in two relaxed states, one with a turnover time of ~20 seconds, similar to the rate for purified myosin and one with a much slower turnover time, ~200 seconds. That the myosin ATPase activity in resting skeletal fibers was highly inhibited had been shown many years earlier by a comparison between in vivo rate of resting muscle and the activity of purified myosin[9]. The low metabolic rate of resting skeletal muscle requires that the vast majority of myosin heads spend most of their time in the SRX in both animals and in humans. A simple calculation shows that if all myosin heads were transferred from the SRX to the DRX that human whole body metabolic rate would increase by approximately 2-4 MJ/day. Thus, a pharmaceutical that did so would significantly alter the balance between energy intake (diet) and energy consumption and become an effective therapy for obesity and type 2 diabetes. Skeletal muscle is an ideal organ for increasing thermogenesis, as it has a large reserve metabolic capacity. A major hurdle to discovering small molecules that destabilize the SRX has been the limitations imposed by the single nucleotide turnover measurement previously used to observe it. In this work we showed that this obstacle can be overcome by using the A6C mutant labelled with MDCC that, as described, showed a spectral shift upon the transition from the SRX to the DRX. We used this signal to carry out a high throughput screen of 2240 compounds approved for human consumption by the FDA. This screen identified one compound, piperine, as described below.

6.2.2 The results of the high throughput screen.

Using the spectral shift of of the C5-MDCC labeled fibers we were able to achieve the accuracy in determining the population of the SRX required for screens. We were also able to solve the technical problems of pipetting fiber suspensions into 384 well plates. The images were analyzed by the Fiji[48] macro and the outliers could be assessed manually. Surprisingly, at the end of this process there was only one hit. The experience of prior investigators was that at least several hits would be found in the screen of the library since it consists of 2200 compounds approved for human

use by the FDA in the USA. A library of biologically active compounds as the one used is expected to have a hit rate higher than a usual screening and about 1%. The only hit was piperine, an alkaloid of black pepper. Piperine was approved by the FDA as a supplement that improved the bioavailability of other medicines (see Discussion 6.2.4. Piperine treatment: *in vivo* experiments).

6.2.3. Literature about use of piperine to treat overweight rodents

After discovering piperine in the HT screening and its effect on muscle fibers, we were pleased to find in the literature that piperine had already been associated with attenuation of weight gain in rodents. In a typical experiment rats or mice are fed a high fat chow for an extended time (weeks). All animals gain weight, but those also receiving piperine gain less than the controls. The difference in weight gain varied widely in different studies. In Okumura et al.[82] mice were fed a high-fat diet and high glucose, the treatment with 0.05% piperine reduced body weight by approx. 10% over control mice. That amount of piperine corresponds to approximately 3.6μM, if evenly distributed in the body, at that concentration the reported effect is a reduction in mesenteric, perinephric and epididymal white adipose tissue of about 500mg while the food intake is comparable with the controls. In the paper by Choi et al.[83] the reduction of body weight of high-fat diet mice over controls is 20% at a dose of 50mg/kg which corresponds approximately to 5.3μM piperine, an effect similar to the one observed using sibutramine. Some other beneficial effects highlighted are a decrease in insulin resistance and an increase in fatty acid oxidation. In the same paper they observed that piperine is more effective in prevent hepatic steatosis caused by high fat diet than to cure a pre-existing condition.

The available literature does not clarify the mechanism by which piperine promotes weight loss. Data have suggested the structural similarity to melanocortin-4 agonists[84], enhanced leptin sensitivity[85], antagonizing PPARγ activity[86], metabolic alteration[87], promotion of satiety[88], or regulation of lipid metabolism and activation of AMP-activated protein kinase[89]. Any kind of muscle activation promote AMPK phosphorylation, in that frame, our model agrees with the paper by Kim et al., the enhanced muscle metabolism due to piperine effect on myosin may lead to higher levels of p-AMPK. Since most of these models are proposing piperine as a hormone-

like or signalling-like molecule, a model in which piperine is mechanically acting on a motor protein has never been proposed before but it does not disagree with the others. In the cited paper, Kim and coworkers reported an increased expression of uncoupling proteins (UCP2 and UCP3) in L6 myocytes exposed to black pepper alkaloids. In this case, piperine seems to only promote UCP3 expression, the skeletal muscle homologue of UCP1. In other papers, it is described the agonistic effect of piperine on TRPV1 receptors[90]. Since TRPV1 activation is known to increase UCP1 content in brown adipose tissue[91], it is possible to speculate piperine thermogenic effect. Several authors have pointed out the obvious connection between piperine-induced weight loss and increased total-body thermogenesis. Our data show that piperine enhances thermogenesis via a perturbation of the SRX/DRX ratio in resting muscle. Resting muscle is extremely efficient with a slow ATPase turnover rate. Thus it may at first seem counterintuitive that it could be a major player in whole-body thermogenesis. However, skeletal muscle is also the largest organ in the human body, comprising 36%/42% (female/male) of the body mass[92]. Thus efficiency is high, but mass results in a high total output. As originally recognized by Ferenczi et al.[9] over 30 years ago, *in vivo* ATP turnover requires almost all myosin in relaxed skeletal muscle to be in what we now term the SRX. A transfer of only 20% of the myosin in relaxed muscle from the SRX to the DRX would cause thermogenesis to double[81]. Could the activation of resting muscle metabolism by piperine found here explain the difference in fat gain produced by piperine in rodents fed high-fat chow for an extended period? In the experiments by BrahmaNaidu et al.[87], rats were fed high-fat chow for 42 days. All rats gained fat during this time, but those who were also fed piperine gained approximately 80g less fat than controls. Similar changes were seen by other investigators[82, 83, 89]. The energy involved in the metabolism of fat is known, 37 kJ/gm, thus 80 grams is equivalent to 2.8×10^6 J. We compare this value to the amount of energy that could be mobilized by piperine. We first calculate how much energy would be produced by all myosin heads if they were in the DRX, where they have an ATPase activity similar to that of pure myosin. Rat myosin has an ATPase activity of about 0.65 s^{-1}. The weight of lean mass in these rats was 350g. Assuming half of this is muscle and multiplying by the concentration of myosin heads, ~250μM, we obtain the number of moles of myosin. Multiplying this times

the ATPase activity, the duration of the experiment and the energy involved in metabolism of 1 ATP, we find that $9x10^6$ J would be consumed if all myosin heads were in the DRX. This shows that the capacity of resting muscle metabolism to consume excess energy is large. This energy is about 3 times greater than the energy involved in the difference in fat gain observed by BrahmaNaidu et al.[87]. Thus if the piperine transferred one third of the myosin heads from the SRX to the DRX, it would explain the difference in fat gained. The dissociation constant of piperine in the fibers is 3μM. Thus, a concentration of approximately 1.5μM piperine would shift 30% of the myosin heads out of the SRX and into the DRX explaining the change in fat gain. Serum levels of piperine measured in other experiments are approximately 5μM, although much of this piperine has been conjugated, and its activity is unknown.

Thus we conclude that the beneficial impact of piperine observed in rodents could be explained by its effect on the SRX. Although it requires a number of assumptions, the above calculation shows that the metabolic changes found here for piperine are of the right magnitude to explain its effect on weight gain. We propose that this is a major factor in the effect of piperine in attenuating weight gain. As the proposed mechanism would activate muscle metabolism, it could also be a factor in the observed improvement of insulin resistance.

6.2.4. Piperine treatment: *in vivo* experiments

It is hard to estimate the concentration of active piperine in the body for several reasons, as it is not really known the uptake at the muscular level and, not less important, in some papers piperine has been addressed as a substrate of glucuronidase enzymes, and in some others it is represented as a glucuronidase inhibitor. According to Bahat et al.[93] rats have been feeded with piperine enriched food to check in which organs the molecule would accumulate. They conclude that piperine is not excreted much in urines but it has been associated with an increasing in the excretion of conjugated glucuronides, sulphates and phenols. In that paper the presence of conjugated phenols is correlated with demethylation of piperine. The relation between piperine and glucuronidation processes may play an important

role in piperine disposition in vivo, but it is still unclear. Some results suggest that piperine induces detoxification enzymes as UDP-glucuronosyl transferase[94], while other results suggest that other compounds are more available because of piperine direct inhibition on that class of enzymes and by lowering UDP-glucuronic acid concentration, the substrate of glucuronidases[95, 96]. In humans, Volak et al.[97] reported that piperine itself is not measurable in blood plasma without preventive deconjugation with b-glucuronidase/sulfatase. Furthermore, other alkaloids similar to piperine have shown to be stronger in promoting uncoupling protein expression (UCP2 and UCP3) and peroxisome proliferator-activated receptors. Results obtained in COS-7 cell line shown that, both dehydropipernonaline and pipernonaline have an effect much greater than piperine in triggering the PPARδ receptor[89], responsible for changing body fuel preference from glucose to lipids[98]. Certainly the fact that piperine and, in general, alkaloids from black pepper have so many effects *in vivo* does not facilitate the understanding the mechanism of its weight loss action.

6.3. Potential for further development

Piperine was picked from a high throughput screen designed to identify compounds that would destabilize the SRX increase energy consumption in skeletal muscle and thus treat metabolic diseases. A subsequent literature search showed that piperine has the properties we were searching for because it was already associated with an attenuation of weight gain and amelioration of type 2 diabetes. Piperine as many of the qualities that would be required for any compound to be useful as a therapeutic treatment for metabolic diseases in humans. First, it destabilizes the SRX and can lead to substantial thermogenesis. Secondly, it functions only in fast twitch muscle fibers with no effect in slow twitch muscle fibers, strongly suggesting that it would also not affect cardiac muscle fibers, which share a myosin isoform with the slow skeletal muscle. Third, it has no effect on active muscle fibers. Such an action would produce unacceptable side effects. Although its affinity is reasonably high it is probably not high enough for to be an effective therapy in humans. Furthermore, the effect of glucuronidation of piperine in humans has still to be clarified. Piperine has been identified as binding to a number of other molecular targets with a similar

affinity, which would probably lead to unfavorable side effects if taken at the quantities that would be necessary for effective thermogenesis. Although piperine is probably not an effective therapeutic, it is an excellent lead compound, which could be used to find similar compounds whose properties could be optimized using our *in vitro* muscle assay systems.

7. Conclusions

Energy management and energy economy are important elements in evolution. To survive, animals need to move and to do so, muscles have been developed. Muscles are powerful tools optimized for moving, mating, fighting, hunting and escaping. Because of the large amount of muscle tissue in an animal body it is logical to think that it needs multiple modes of regulation. In particular, an important function is to manage energy expenditure. The SRX provides a mechanism whereby striated muscle can achieve higher energy economy.

The goal of this research was twofold, to explore the nature of the interface between the two RLC's in the SRX, and to obtain a signal that could be used in high throughput screens to find molecules that destabilize this complex. Probe sites were picked to be within a putative interface identified by structural data, or in structural elements adjacent to this interface that might play a role in its formation. The attachment of probes to many of these sites altered the stability of the SRX and conversely formation of the SRX altered the spectra of the probes. Thus the data show that the regions targeted by the probes are involved in the formation of the SRX. Probes within a structural motif which binds divalent cations, showed that this site has a strong influence on the formation of the SRX. Probes on the N-terminal end of the RLC showed that this region is also involved in the formation of the SRX. Thus the first goal of these experiments was accomplished. The second goal was also fulfilled with the discovery of one probe, which provided a ratiometric spectral signal that can be used to carry out high throughput screens.

The discovery that a small molecule can disrupt the SRX has far reaching consequences, both for the field of muscle and for the treatment of type 2 diabetes and obesity. The disruption of the SRX in theory has the potential of raising metabolic rate by 500-1000 calories per day. Even if the effect is less, say 25% of the theoretical, it will have a large impact on the human race. Its most immediate effect is likely to be in diabetes. Even a modest increase in physical activity can improve type 2 diabetes, however many are unwilling or unable to take this route. Disrupting the SRX will increase the use of glucose by resting muscle and thus decrease the

insulin resistance which leads to diabetes. Thus the fundamental problem that produces diabetes, the consumption of more glucose than the body can metabolize, is fixed. Thus it is in diabetes that this approach will have the greatest and most immediate effects. Currently, in the USA type 2 diabetes affects about 13 million people and costs 150 billion dollars per year. Alleviating this condition would be a spectacular step forward in medical treatment of human health. Obesity can also be treated, but as it involves the metabolism of greater amounts of energy than does diabetes it will require a greater increase in metabolism. However, disrupting the SRX will again provide an effective treatment by addressing the basic problem in obesity that more calories are consumed than are metabolized. Currently 65% of the American public are overweight and 31% are obese.

The disruption of the SRX can have a huge impact on human health.

8. Supplementary Materials

8.1. RLC multi alignment

```
Oryctolagus_cuniculus MAP--KKAKRRAAAEGG--------------------------SSNVFS 21
Ovis_aries            MAP--KKAKRRAAAEGG--------------------------SSNVFS 21
Mus_musculus          MAP--KKAKRRAGAEG---------------------------SSNVFS 20
Sus_scrofa            MAP--KKAKRRAAAEG---------------------------SSNVFS 20
Homo_sapiens          MAP--KRAKRRTVAEGG--------------------------SSSVFS 21
Gallus_gallus         MAP--KKAKRRA-AEG---------------------------SSNVFS 19
chicken_smooth        MSS--KRAKAKTTKKRPQ-------------------------RATSNVFA 24
turkey                MSS--KRAKAKTTKKRPQ-------------------------RATSNVFA 24
Bombyx_mori           MADKDKKVKKKKAKEDAPAEEAPAAAAPAGDRQSSRGSRKAKRTGSNVFS 50
tarantula             MGDDEKKEKKKKSKKKAEEEGGDAPAAPPAPKPPSQ-KRRAQRSGSNVFA 49
                      *.   *: * :   :                                *.**:

Oryctolagus_cuniculus MFDQTQIQEFKEAFTVIDQNRDGIIDKEDLRDTFAAMGRLNVKNEELDAM 71
Ovis_aries            MFDQTQIQEFKEAFTVIDQNRDGIIDKEDLRDTFAAMGRLNVKNEELDAM 71
Mus_musculus          MFDQTQIQEFKEAFTVIDQNRDGIIDKEDLRDTFAAMGRLNVKNEELDAM 70
Sus_scrofa            MFDQTQIQEFKEAFTVIDQNRDGIIDKEDLRDTFAAMGRLNVKNEELDAM 70
Homo_sapiens          MFDQTQIQEFKEAFTVIDQNRDGIIDKEDLRDTFAAMGRLNVKNEELDAM 71
Gallus_gallus         MFDQTQIQEFKEAFTVIDQNRDGIIDKDDLRETFAAMGRLNLKNEELDAM 69
chicken_smooth        MFDQSQIQEFKEAFNMIDQNRDGFIDKEDLHDMLASMGK-NPTDEYLEGM 73
turkey                MFDQSQIQEFKEAFNMIDQNRDGFIDKEDLHDMLASMGK-NPTDEYLEGM 73
Bombyx_mori           MFSQKQVAEFKEAFQLMDHDKDGIIGKNDLRATFDSLGRLASEKE-LDEM 99
tarantula             MFTQHQVQEFKEAFQLIDQDKDGFISKNDIRATFDSLGRLCTEQE-LDSM 98
                      ** * *: ****** ::*:::**:*.*:*::  : ::*:     .* *: *

Oryctolagus_cuniculus MKEASGPINFTVFLTMFGEKLKG-ADPEEVITGAFKVLDPEGKGTIKKQF 120
Ovis_aries            MKEASGPINFTVFLTMFGEKLKG-ADPEDVITGAFKVLDPEGKGTIKKQF 120
Mus_musculus          MKEASGPINFTVFLTMFGEKLKG-ADPEDVITGAFKVLDPEGKGTIKKQF 119
Sus_scrofa            MKEAGGPINFTVFLTMFGEKLKG-ADPEDVITGAFKVLDPEGKGTIKKHF 119
Homo_sapiens          MKEASGPINFTVFLTMFGEKLKG-ADPEDVITGAFKVLDPEGKGTIKKKF 120
Gallus_gallus         IKEASGPINFTVFLTMFGEKLKG-ADPEDVIMGALKVLDPDGKGSIKKSF 118
chicken_smooth        MSEAPGPINFTMFLTMFGEKLNG-TDPEDVIRNAFACFDEEASGFIHEDH 122
turkey                MSEAPGPINFTMFLTMFGEKLNG-TDPEDVIRNAFACFDEEASGFIHEDH 122
Bombyx_mori           VGEASGPINFTQLLTLFANRMSGGSDEDDVVINAFKTFDE--EGKIDSER 147
tarantula             VAEAPGPINFTMFLTIFGDRIAG-TDEEDVIVNAFNLFDEG-DGKCKEET 146
                      : ** ****** :**:*.::: * :* ::*: .*:  :*   .*  ..

Oryctolagus_cuniculus LEELLTTQCDRFSQEEIKNMWAAFPPDVGGNVDYKNICYVITHGDAKDQE 170
Ovis_aries            LEELLTTQCDRFSQEEIRNMWAAFPPDVGGNVYYKNICYVITHGDAKDQE 170
Mus_musculus          LEELLTTQCDRFSQEEIKNMWAAFPPDVGGNVDYKNICYVITHGDAKDQE 169
Sus_scrofa            LEELLTTQCDRFSQEEIKNMWAAFPPDVGGNVDYKNICYVITHGDAKDQE 169
Homo_sapiens          LEELLTTQCDRFSQEEIKNMWAAFPPDVGGNVDYKNICYVITHGDAKDQE 170
Gallus_gallus         LEELLTTQCDRFTPEEIKNMWAAFPPDVAGNVDYKNICYVITHGEDKEGE 168
chicken_smooth        LRELLTTMGDRFTDEEVDEMYREAPIDKKGNFNYVEFTRILKHG-AKDKD 171
turkey                LRELLTTMGDRFTDEEVDEMYREAPIDKKGNFNYVEFTRILKHG-AKDKD 171
Bombyx_mori           LRHALMTWGDKFSADEVDEAYDQMDIDDKGYIDTTKLIAMLTASAEEEEG 197
tarantula             LKRSLTTWGEKFSQDEVDQALSEAPIDGNGLIDIKKFAQILTKGAKEEGA 196
                        *.. * *  ::*: :*: :      *  * .   ::  ::. .  ::

Oryctolagus_cuniculus  ----
Ovis_aries             ----
Mus_musculus           ----
```

```
Sus_scrofa              ----
Homo_sapiens            ----
Gallus_gallus           ----
chicken_smooth          ----
turkey                  D--- 172
Bombyx_mori             GEAA 201
tarantula               ----
```

8.2. Mouse - Tarantula mutants numbering (3DTP structure)

Tarantula numbering	**Mouse numbering**
Proline 34	Lysine 5
Serine 35	Alanine 6
Alanine 40	Glycine 11
Glutamine 41	Alanine 12
Lysine 60	Lysine 31
Phenylalanine 63	Phenylalanine 34
Leucine 65	Valine 36
Aspartic Acid 67	Aspartic Acid 38*
Phenylalanine 73	Isoleucine 44*
Aspartic Acid 84	Alanine 55
Tyrosine 109	Tyrosine 81
Glycine 155	Cysteine 128
Aspartic Acid 84 - Asparagine 131	Alanine 55-Glycine 102

*residues coordinating calcium ions in the EF-hand

8.3. Fluorescence data

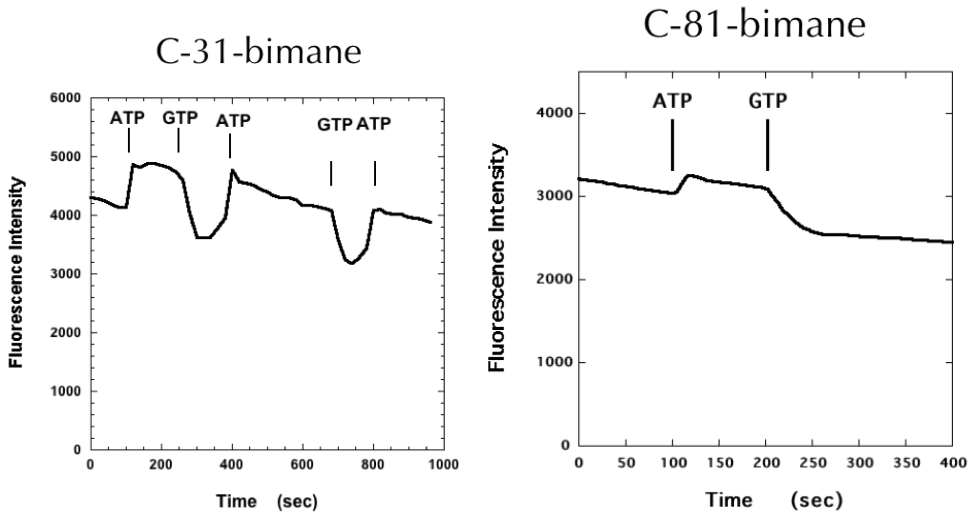

8.4. Coumarin excitation spectra

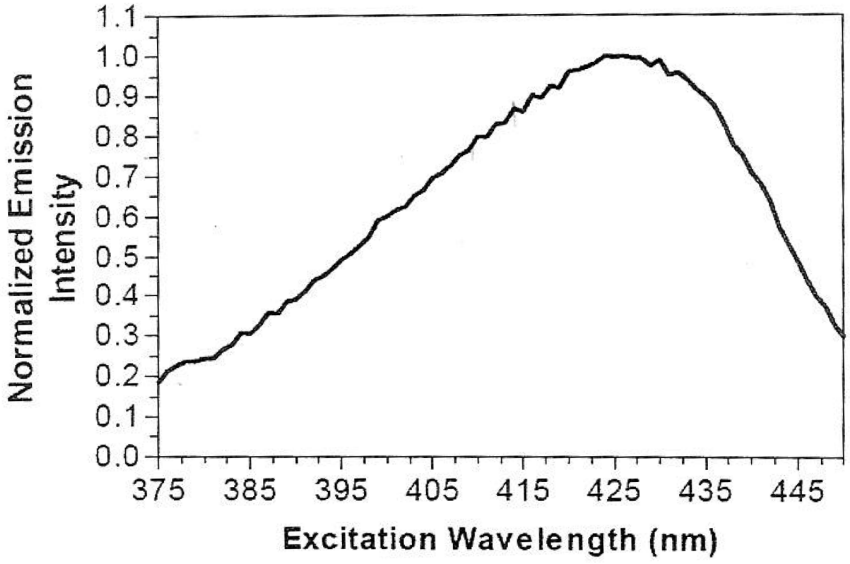

8.5. EPR spectra

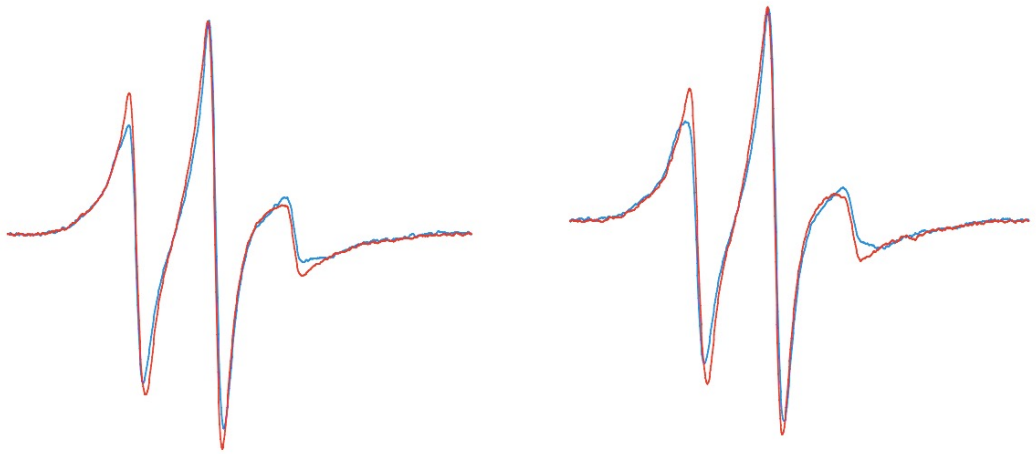

RLC-31 labelled with IASL spin probe. Rigor buffer (left panel) and relax ATP blebbistatin buffer (right panel), parallel (blue) and perpendicular (red) magnetic field.

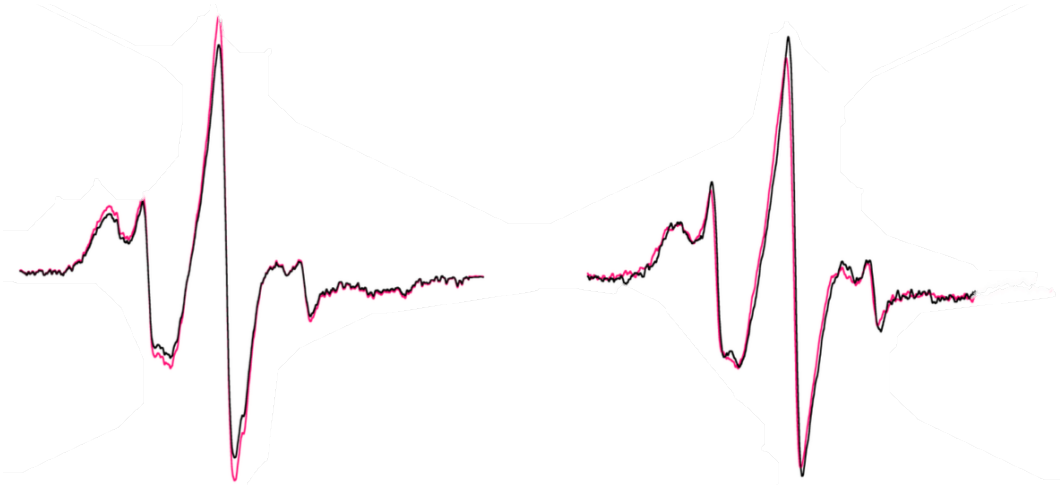

RLC-31 labelled with MSL spin probe. Rigor buffer (left panel) and relax ATP blebbistatin buffer (right panel), perpendicular (black) and parallel (red) magnetic field.

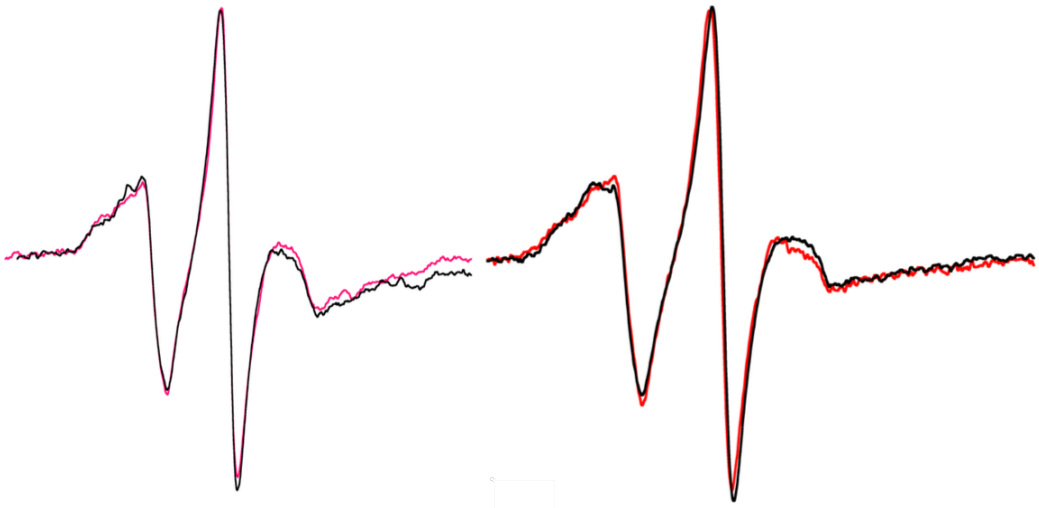

RLC-44 labelled with MSL spin probe. Rigor buffer (left panel) and relax ATP blebbistatin buffer (right panel), perpendicular (black) and parallel (red) magnetic field.

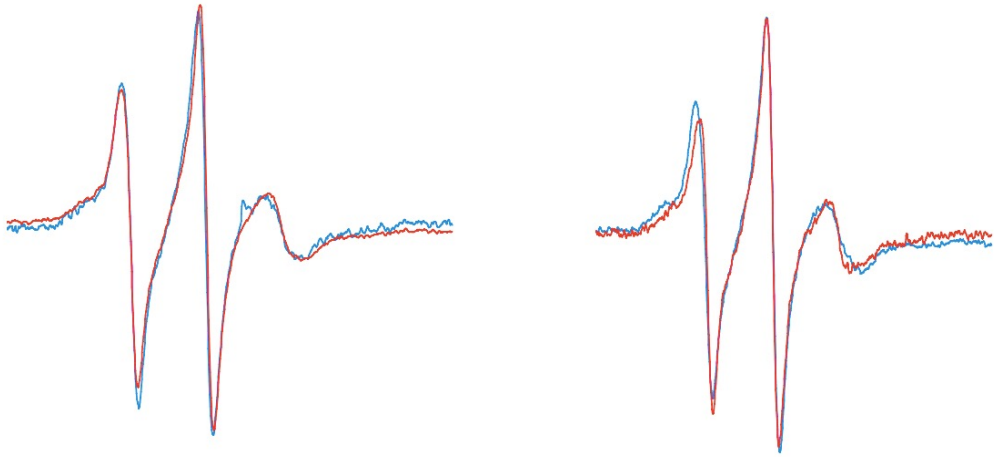

RLC-81 labelled with IASL spin probe. Rigor buffer (left panel) and relax ATP blebbistatin buffer (right panel), perpendicular (red) and parallel (blue) magnetic field.

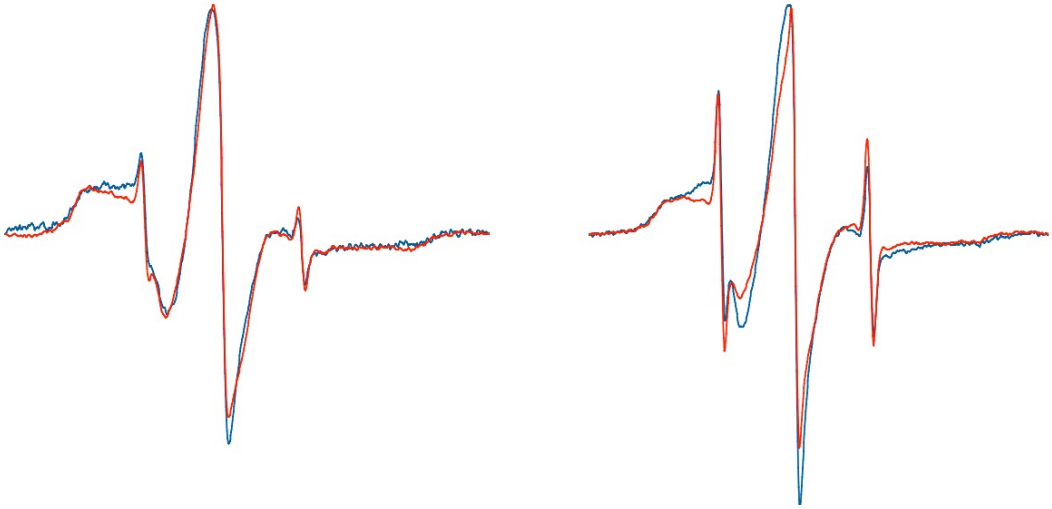

RLC-81 labelled with MMTS spin probe. ATP blebbistatin buffer (left panel) and rigor buffer (right panel), perpendicular (red) and parallel (blue) magnetic field.

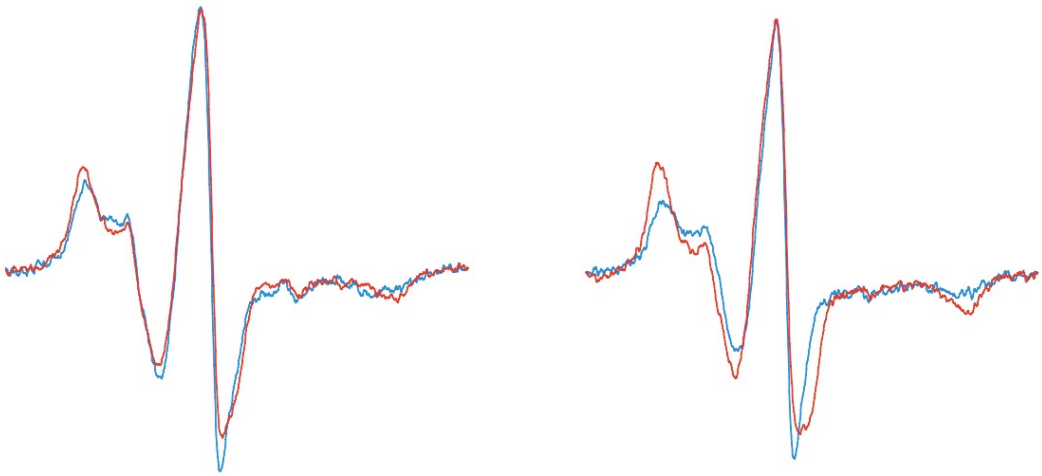

RLC-81 labelled with MSL spin probe. Rigor buffer (left panel) and relax ATP blebbistatin buffer (right panel), perpendicular (red) and parallel (blue) magnetic field.

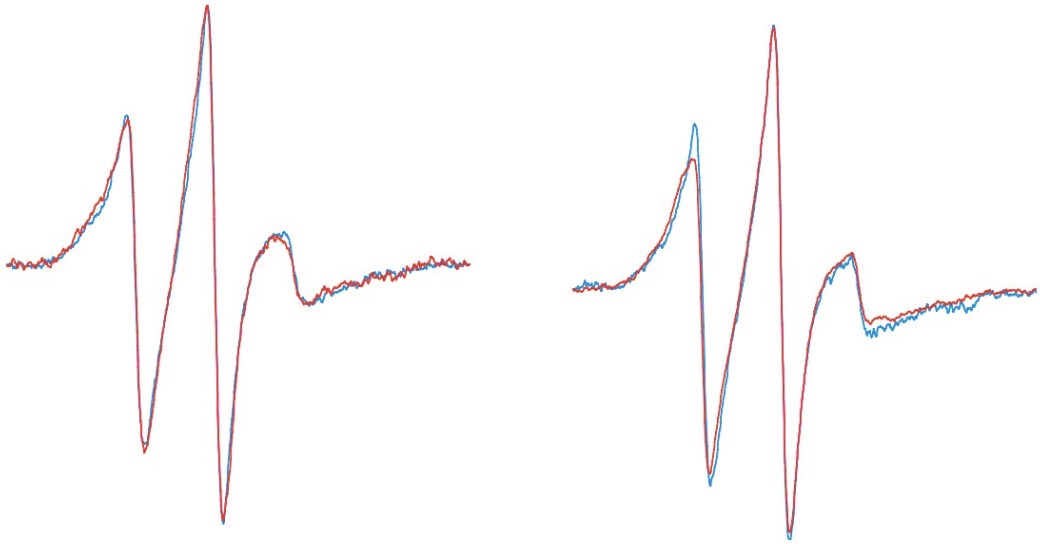

RLC-128 labelled with IASL spin probe. Rigor buffer (left panel) and relax ATP blebbistatin buffer (right panel), perpendicular (red) and parallel (blue) magnetic field.

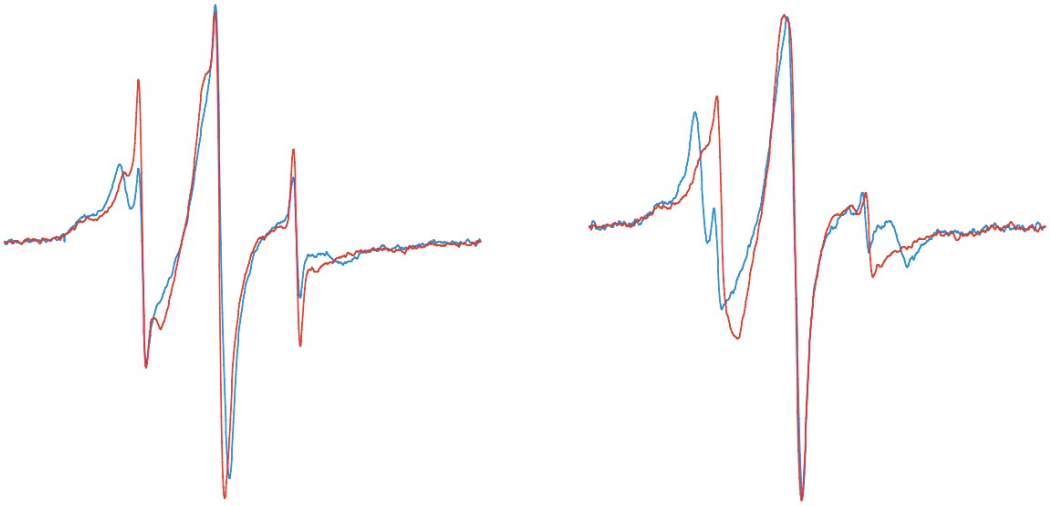

RLC-128 labelled with IASL spin probe. Rigor buffer (left panel) and relax ATP blebbistatin buffer (right panel), perpendicular (red) and parallel (blue) magnetic field.

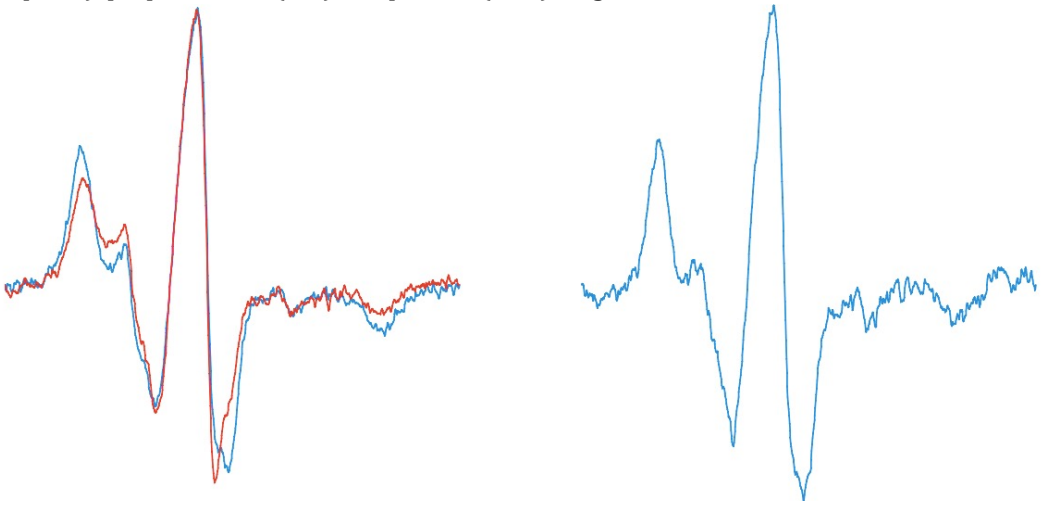

RLC-128 labelled with MSL spin probe. Rigor buffer (left panel) and relax ATP blebbistatin buffer (right panel), perpendicular (red) and parallel (blue) magnetic field.

8.6. Example of the Fiji macro (code)

```
inputFolder = getDirectory("select input folder");
list = getFileList(inputFolder);
for (i=0; i<list.length; i++) {
       roiManager("Reset");
       j=i+1;
       open(inputFolder + list[i]);
       rename("picture.tif");
       open("/Users/leonardonogara/Desktop/back_c1_pip.tif");
       imageCalculator("Subtract","picture.tif", "back_c1_pip.tif");
       close("back_c1_pip.tif");
       getStatistics(area, mean, min, max, std, histogram);
       if (min>1000) {
              makeRectangle(100, 100, 1400, 1400);
              roiManager("Add");
              print("DAPI-GFP autofluorescence compound alert:",i);
       } else {
    if (max>5000) {
       setThreshold(5000, max);                //particles dapi-gfp
       run("Create Selection");
       run("Enlarge...", "enlarge=20 pixel");
       roiManager("Add");                                  //0
              } else {
                    makeRectangle(80, 80, 1, 1);
                    roiManager("Add");                     //0
              };
              };
    close();

    open(inputFolder + list[j]);
    rename("picture.tif");
       open("/Users/leonardonogara/Desktop/back_c2_pip.tif");
       imageCalculator("Subtract","picture.tif", "back_c2_pip.tif");
       close("back_c2_pip.tif");
    getStatistics(area, mean, min, max, std, histogram);
     if (min>1000) {
              makeRectangle(100, 100, 1400, 1400);
               roiManager("Add");
               print("DAPI autofluorescence compound alert:",j);
        } else {
              if (max>3500) {
              setThreshold(3500, max);      //hair in dapi
          run("Create Selection");
          run("Enlarge...", "enlarge=20 pixel");
                    roiManager("Add");                     //1
              } else {
                    makeRectangle(85, 85, 1, 1);
                    roiManager("Add");                     //1
              };
              };
    close();

//fibers selection
    open(inputFolder + list[j]);
    rename("picture.tif");
       open("/Users/leonardonogara/Desktop/back_c2_pip.tif");
       imageCalculator("Subtract","picture.tif", "back_c2_pip.tif");
```

```
      close("back_c2_pip.tif");
    roiManager("Select", newArray(0,1));
    roiManager("Combine");
    roiManager("Add");                  // 2 all corrections
    setBackgroundColor(0, 0, 0);
    roiManager("Select",2);
    run("Clear", "slice");
    run("Measure");
    run("Select None");
    run("Auto Threshold", "method=Huang ignore_black white");
    run("Create Selection");
    run("Make Inverse");
      roiManager("Add");                //3 fibers
    close();

   //background selection
   open(inputFolder + list[i]);
   roiManager("Select",3);
   run("Enlarge...", "enlarge=20 pixel");
   roiManager("Add");                           //4 fiber enlarged
   roiManager("Select", newArray(4,2)); //4 background-corr
   roiManager("Combine");
   run("Make Inverse");
   roiManager("Add");                           //5 real background
   close();

    //measurements
    open(inputFolder + list[i]);
    rename("picture.tif");
      open("/Users/leonardonogara/Desktop/back_c1_pip.tif");
      imageCalculator("Subtract","picture.tif", "back_c1_pip.tif");
      close("back_c1_pip.tif");
    roiManager("Select",3);
    run("Measure");
    roiManager("Select",5);
    run("Measure");
      close();
            j = i+1;
            open(inputFolder + list[j]);
            rename("picture.tif");
            open("/Users/leonardonogara/Desktop/back_c2_pip.tif");
      imageCalculator("Subtract","picture.tif", "back_c2_pip.tif");
            close("back_c2_pip.tif");
            roiManager("Select",3);
         run("Measure");
       roiManager("Select",5);
       run("Measure");
          close();
       i = i+1;
       };
exit();
```

8.7. RLC binding sequence

PDB ID	sequence	sequence length	organism
3JO4	TAMKVIQRNC AAYLKLRNWQ WWRLFTKVKP LLQVTRQ	37	Gallus gallus
1I84	RQQQLTAMKV IQRNCAAYLK LRNWQWWRLF TKVKPLL	37	Gallus gallus
2W4H	MVERRESIFCIQ YNVRSFMNVK HWPWMKLFFK IKPLLK	38	Gallus gallus
3DTP	TAMKVIQRNC AAYLKLRNWQ WWRLFTKVKP LL	32	tarantula
2MYS	VERRESIFCI QYNVRSFMNV KHWPWMKLFF KIKPLLK	37	Gallus gallus
1B7T	KKLQDQRIGL SVIQRNIRKW LVLRNWQWWK LYSKVKP	37	scallop

8.8. Mouse complete myosin sequence: HCC highlighted

Myosin 2 [Mus musculus] GenBank: AAH08538.1

>gi|14250231|gb|AAH08538.1| Myh2 protein [Mus musculus]
MSSDAEMAVFGEAAPYLRKSEKERIEAQNRPFDAKTSVFVAEPKESFVKGTIQSKDAGKVTVKTEAGATL
TVKEDQIFPMNPPKYDKIEDMAMMTHLHEPAVLYNLKERYAAWMIYTYSGLFCVTVNPYKWLPVYNPEVV
AAYRGKKRQEAPPHIFSISDNAYQFMLTDRENQSILITGESGAGKTVNTKRVIQYFATIAVTGDKKKEEA
TSGKMQGTLEDQIISANPLLEAFGNAKTVRNDNSSRFGKFIRIHFGTTGKLASADIETYLLEKSRVTFQL
KAERSYHIFYQITSNKKPELIEMLLITTNPYDYPFVSQGEISVASIDDQEELMATDSAIDILGFTNDEKV
SIYKLTGAVMHYGNMKFKQKQREEQAEPDGTEVADKAAYLQGLNSADLLKALCYPRVKVGNEYVTKGQTV
EQVTNAVGALAKAMYEKMFLWMVTRINQQLDTKQPRQYFIGVLDIAGFEIFDFNSLEQLCINFTNEKLQQ
FFNHHMFVLEQEEYKKEGIEWTFIDFGMDLAACIELIEKPMGIFSILEEECMFPKATDTSFKNKLYEQHL
GKSANFQKPKVVKGKAEAHFSLIHYAGTVDYNITGWLDKNKDPLNETVVGLYQKSSVKTLAYLFSGAQTA
EAEASSGGAAKKGAKKKGSSFQTVSALFRENLNKLMTNLRSTHPHFVRCIIPNETKTPGAMEHELVLHQL
RCNGVLEGIRICRKGFPSRILYADFKQRYKVLNASAIPEGQYIDSKKASEKLLGSIDIDHTQYKFGHTKV
FFKAGLLGLLEEMRDDKLAQLITRTQAMCRGFLARVEYQKMVERRESIFCIQYNIRAFMNVKHWPWMKLF
FKIKPLLKSAETEKEMATMKEEFQKTKDDLAKSEAKRKELEEKMVSLLKEKNDLQLQVQAEAEGLADAEE
RCDQLIKTKIQLEAKIKEVTERAEDEEEINAELTAKKRKLEDECSELKKDIDDLELTLAKVEKEKHATEN
KVKNLTEEMAGLDETIAKLTKEKKALQEAHQQTLDDLQAEEDKVNTLTKAKIKLEQQVDDLEGSLEQEKK
LRMDLERAKRKLEGDLKLAQESIMDTENEKQQLDERLKKKEFEMSNLQSKIEDEQAIGIQLQKKIKELQA
RIEELEEEIEAERASRAKAEKQRSDLSRELEEISERLEEAGGATSAQIEMNKKREAEFQKMRRDLEEATL
QHEATAATLRKKHADSVAELGEQIDNLQRVKQKLEKEKSEMKMEIDDLASNVETVSKAKGNLEKMCRTLE
DQVSELKSKEEEQQRLINDLTSQRGRLQTESGEFSRQLDEKEALVSQLSRGKQAFTQQIEELKRQLEEEV
KAKNALAHALQSSRHDCDLLREQYEEEQESKAELQRALSKANSEVAQWRTKYETDAIQRTEELEEAKKKL
AQRLQAAEEHVEAVNAKCASLEKTKQRLQNEVEDLMLDVERTNAACAALDKKQRNFDKILAEWKQKYEET
HAELEASQKEARSLGTELFKMKNAYEESLDQLETLKRENKNLQQEISDLTEQIAEGGKRIHELEKIKKQV
EQEKCELQAALEEAEASLEHEEGKILRIQLELNQVKSEIDRKPAMQKRKPRKPSLMPP

Spacer region
RLC binding region
Hydrophobic residues in a zipper domain pattern
Myosin heavy chain (S2 region)
HCC construct picked region

8.9. HCC codon optimization

HCC sequence before optimization

```
aagatggtggagagaagggagtccatcttctgcatccagtacaacatccgcgccttcatg
 K  M  V  E  R  R  E  S  I  F  C  I  Q  Y  N  I  R  A  F  M
aacgtcaagcactggccctggatgaaactcttcttcaagatcaaacccctgctgaagagc
 N  V  K  H  W  P  W  M  K  L  F  F  K  I  K  P  L  L  K  S
gcagagaccgagaaggagatggccaccatgaaggaggagttccagaaaaccaaagatgac
 A  E  T  E  K  E  M  A  T  M  K  E  E  F  Q  K  T  K  D  D
cttgccaagtcagaggcaaagaggaaggaacttgaagaaaagatggtgtccctcttgaaa
 L  A  K  S  E  A  K  R  K  E  L  E  E  K  M  V  S  L  L  K
gaaaaaaatgacttgcaacttcaagttcaggctgaagctgaaggcttggccgatgcagag
 E  K  N  D  L  Q  L  Q  V  Q  A  E  A  E  G  L  A  D  A  E
gagcgatgcgaccagctgatcaaaaccaaaatccagctggaggccaaaatcaaagaggtg
 E  R  C  D  Q  L  I  K  T  K  I  Q  L  E  A  K  I  K  E  V
accgagagggccgag
 T  E  R  A  E
```

HCC sequence after optimization

```
aaaatggttgaacgtcgtgaaagcattttcgtgattcagtataatgtgcgtgcctttatg
 K  M  V  E  R  R  E  S  I  F  V  I  Q  Y  N  V  R  A  F  M
aacgttaaacattggccgtggatgaaactgtatttcaaaatcaaaccgctgctgaaatca
 N  V  K  H  W  P  W  M  K  L  Y  F  K  I  K  P  L  L  K  S
gccgaaaccgaaaaagaaatggccaacatgaaagaagaatttgaaaaagccaaagaaaac
 A  E  T  E  K  E  M  A  N  M  K  E  E  F  E  K  A  K  E  N
ctggcaaaagcagaagccaaacgtaaagaactggaagaaaaaatggtggccctgatgcaa
 L  A  K  A  E  A  K  R  K  E  L  E  E  K  M  V  A  L  M  Q
gaaaaaaatgatctgcaactgcaggttcagagcgaagcagatagcctggcagatgcagaa
 E  K  N  D  L  Q  L  Q  V  Q  S  E  A  D  S  L  A  D  A  E
gaacgtagcgatcaactgattaaaaccaaaattcagctggaagctaaaatcaaagaagtt
 E  R  S  D  Q  L  I  K  T  K  I  Q  L  E  A  K  I  K  E  V
accgaacgcgcagaa
 T  E  R  A  E
```

Life Technology GeneOptimizer® analysis of the sequences

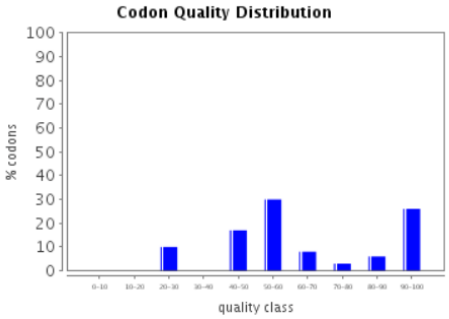

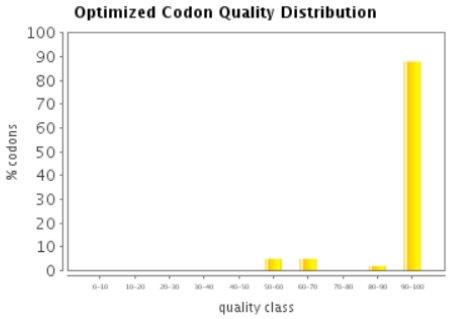

The histograms show the percentage of sequence codons which fall into a certain quality class. The quality value of the most frequently used codon for a given amino acid in the desired expression system is set to 100, the remaining codons are scaled accordingly (Sharp et al.[99]).

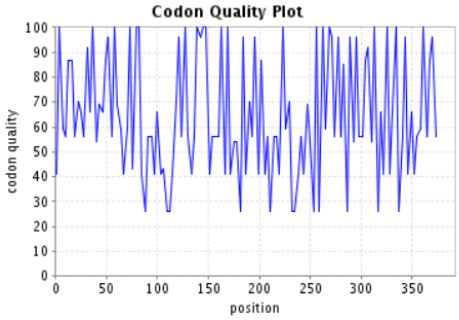

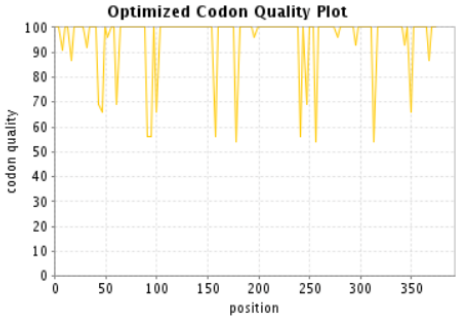

The plots show the quality of the used codon at the indicated codon position.

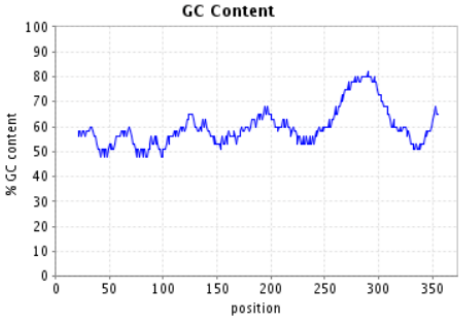

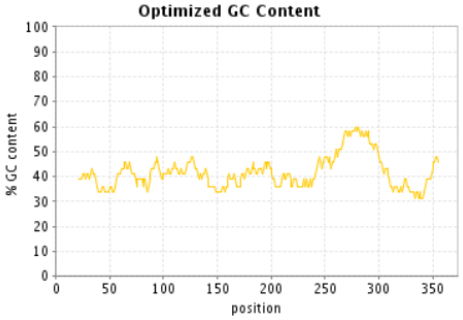

The plots show the GC content in a 40 bp window centered at the indicated nucleotide position.

8.10. Probe used

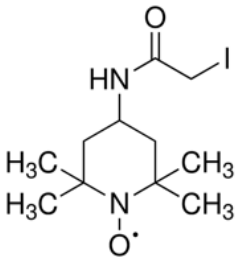

IASL (4-(2-Iodoacetamido)-TEMPO) MW: 339.19

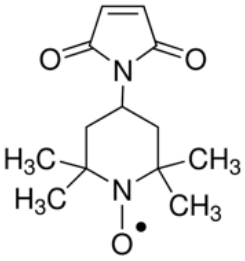

MSL (4-Maleimido-TEMPO) MW: 252.31

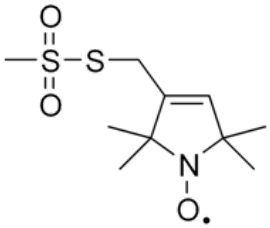

MTSL (1-oxyl-2,2,5,5-tetramethylpyrroline-3-methyl)methanethiosulfonate)

MW: 264.38

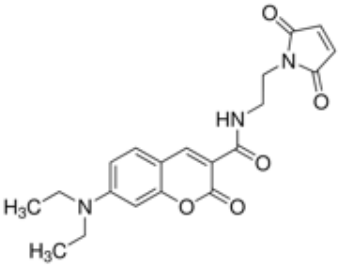

MDCC or COUMARIN (7-Diethylamino-3-[N-(2-maleimidoethyl)carbamoyl]coumarin)

MW: 383.40

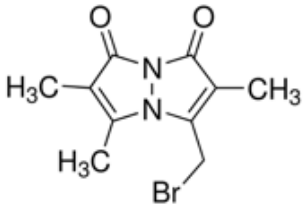

Bromobimane MW: 271.11

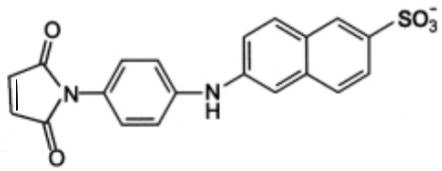

MIANS MW: 361.39

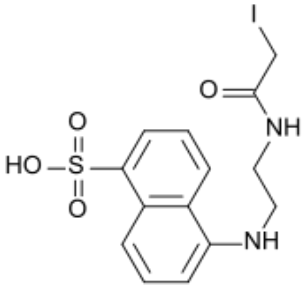

IAEDANS MW: 434.25

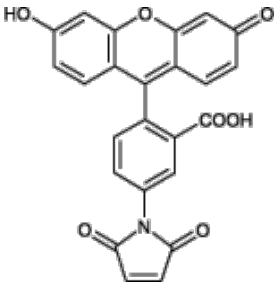

Fluorescein (Fluorescein-5-Maleimide) MW: 427.36

9. References

1. McArdle, William D, Frank I Katch, and Victor L Katch. Exercise physiology: nutrition, energy, and human performance. Lippincott Williams & Wilkins, 2010.
2. Takeda, Soichi et al. "Structure of the core domain of human cardiac troponin in the Ca2+-saturated form." Nature 424.6944 (2003): 35-41. Lehman, William et al. "Structural basis for the activation of muscle contraction by troponin and tropomyosin." Journal of molecular biology 388.4 (2009): 673-681.
3. Gordon, AM, E Homsher, and M Regnier. "Regulation of contraction in striated muscle." Physiological reviews 80.2 (2000): 853-924.
4. Galińska-Rakoczy, Agnieszka et al. "Structural basis for the regulation of muscle contraction by troponin and tropomyosin." Journal of molecular biology 379.5 (2008): 929-935.
5. Huxley, Andrew F, and R Niedergerke. "Structural changes in muscle during contraction." Nature 173.4412 (1954): 971-973.
6. Schliwa, Manfred, and Günther Woehlke. "Molecular motors: Switching on kinesin." Nature 411.6836 (2001): 424-425.
7. Ebashi, Setsuro, Makoto Endo, and Iwao Ohtsuki. "Control of muscle contraction." Quarterly reviews of biophysics 2.04 (1969): 351-384.
8. Kushmerick, MJ, and RJ Paul. "Aerobic recovery metabolism following a single isometric tetanus in frog sartorius muscle at 0 degrees C." The Journal of physiology 254.3 (1976): 693.
9. Ferenczi, MICHAEL A et al. "Reaction mechanism of the magnesium ion-dependent adenosine triphosphatase of frog muscle myosin and subfragment 1." Biochem. J 171 (1978): 165-175.
10. Stewart, M. A., Franks-Skiba, K., Chen, S. & Cooke, R. (2010). Myosin ATP turnover rate is a mechanism involved in thermogenesis in resting skeletal muscle fibers. Proc Natl Acad Sci U S A 107, 430-5.
11. Lowey, Susan, Guillermina S Waller, and Kathleen M Trybus. "Skeletal muscle myosin light chains are essential for physiological speeds of shortening." 365.6445 (1993): 454-456.

12. VanBuren, Peter et al. "The essential light chain is required for full force production by skeletal muscle myosin." Proceedings of the National Academy of Sciences 91.26 (1994): 12403-12407.
13. Vandenboom, Rene et al. "Myosin phosphorylation and force potentiation in skeletal muscle: evidence from animal models." Journal of muscle research and cell motility 34.5-6 (2013): 317-332.
14. Cremo, C. R., Neuron, J. M. & Yount, R. G. (1990). Interaction of myosin subfragment 1 with fluorescent ribose-modified nucleotides. A comparison of vanadate trapping and SH1-SH2 cross-linking. Biochemistry 29, 3309-19.
15. Woodward, S. K., Eccleston, J. F. & Geeves, M. A. (1991). Kinetics of the interaction of 2'(3')-O-(N-methylanthraniloyl)-ATP with myosin subfragment 1 and actomyosin subfragment 1: characterization of two acto-S1-ADP complexes. Biochemistry 30, 422-30.
16. Huxley, HE. "Low-angle X-ray diffraction studies on muscle." Disc. Faraday Soc 11 (1951): 148.
17. Xu, Sengen et al. "X-ray diffraction studies of the thick filament in permeabilized myocardium from rabbit." Biophysical journal 91.10 (2006): 3768-3775.
18. Wendt, T., Taylor, D., Messier, T., Trybus, K. M. & Taylor, K. A. (1999). Visualization of head-head interactions in the inhibited state of smooth muscle myosin. J Cell Biol 147, 1385-90.
19. Woodhead, J. L., Zhao, F. Q., Craig, R., Egelman, E. H., Alamo, L. & Padron, R. (2005). Atomic model of a myosin filament in the relaxed state. Nature 436, 1195-9.
20. Alamo, L., Wriggers, W., Pinto, A., Bartoli, F., Salazar, L., Zhao, F. Q., Craig, R. & Padron, R. (2008). Three-dimensional reconstruction of tarantula myosin filaments suggests how phosphorylation may regulate myosin activity. J Mol Biol 384, 780-97.
21. Craig, R. & Woodhead, J. L. (2006). Structure and function of myosin filaments. Curr Opin Struct Biol 16, 204-12.

22. Pettersen, Eric F et al. "UCSF Chimera—a visualization system for exploratory research and analysis." *Journal of computational chemistry* 25.13 (2004): 1605-1612.
23. Thomas, DD, and R Cooke. "Orientation of spin-labeled myosin heads in glycerinated muscle fibers." Biophysical journal 32.3 (1980): 891.
24. Sale, Ken et al. "Structural determination of spin label immobilization and orientation: A Monte Carlo minimization approach." Journal of Magnetic Resonance 156.1 (2002): 104-112.
25. Lakowicz, Joseph R. "Solvent effects on emission spectra." Principles of fluorescence spectroscopy (1999): 185-210.)
26. Förster, Th. "Zwischenmolekulare energiewanderung und fluoreszenz." Annalen der physik 437.1-2 (1948): 55-75.
27. Broussard, Joshua A et al. "Fluorescence resonance energy transfer microscopy as demonstrated by measuring the activation of the serine/threonine kinase Akt." Nature protocols 8.2 (2013): 265-281.
28. Roy, Rahul, Sungchul Hohng, and Taekjip Ha. "A practical guide to single-molecule FRET." Nature methods 5.6 (2008): 507-516.
29. Rodgers, R John, Matthias H Tschöp, and John PH Wilding. "Anti-obesity drugs: past, present and future." Disease models & mechanisms 5.5 (2012): 621-626.
30. McPherson, Klim, Tim Marsh, and Martin Brown. Tackling obesities: future choices: Modelling future trends in obesity and the impact on health. Department of Innovation, Universities and Skills, 2007.
31. Freedman, David S et al. "Relationship of childhood obesity to coronary heart disease risk factors in adulthood: the Bogalusa Heart Study." Pediatrics 108.3 (2001): 712-718.
32. Daniels, Judi. "Obesity: America's Epidemic: What goes up does not always come down. Is there a solution?." AJN The American Journal of Nursing 106.1 (2006): 40-49.).
33. Flegal, Katherine M et al. "Cause-specific excess deaths associated with underweight, overweight, and obesity." Jama 298.17 (2007): 2028-2037.

34. Definition, WHO. "diagnosis and classification of diabetes mellitus and its complications: report of a WHO consultation." Geneva: World Health Organization (1999).
35. Ripsin, Cynthia M, Helen Kang, and Randall J Urban. "Management of blood glucose in type 2 diabetes mellitus." Am Fam Physician 79.1 (2009): 29-36.
36. Alwan, Ala. Global status report on noncommunicable diseases 2010. World Health Organization, 2011.
37. Morrish, NJ et al. "Mortality and causes of death in the WHO Multinational Study of Vascular Disease in Diabetes." Diabetologia 44.2 (2001): S14-S21.
38. World Health Organization. "Global data on visual impairments 2010." URL: http://www. who. int/blindness/GLOBALDATAFINALforweb. pdf [accessed 2013-02-28][WebCite Cache] (2012).
39. Roglic, Gojka et al. "The Burden of Mortality Attributable to Diabetes Realistic estimates for the year 2000." Diabetes care 28.9 (2005): 2130-2135.
40. Dansinger, Michael L et al. "Comparison of the Atkins, Ornish, Weight Watchers, and Zone diets for weight loss and heart disease risk reduction: a randomized trial." Jama 293.1 (2005): 43-53.
41. LeBlanc, Erin S et al. "Effectiveness of primary care–relevant treatments for obesity in adults: a systematic evidence review for the US Preventive Services Task Force." Annals of internal medicine 155.7 (2011): 434-447.
42. Wing, Rena R et al. "A self-regulation program for maintenance of weight loss." New England Journal of Medicine 355.15 (2006): 1563-1571.
43. Li, Zhaoping et al. "Meta-analysis: pharmacologic treatment of obesity." Annals of internal medicine 142.7 (2005): 532-546.
44. Bray, George A, and Frank L Greenway. "Pharmacological treatment of the overweight patient." Pharmacological reviews 59.2 (2007): 151-184.
45. Fleury, Christophe et al. "Uncoupling protein-2: a novel gene linked to obesity and hyperinsulinemia." Nature 15 (1997): 269-272.
46. Hamilton, Marc T, Deborah G Hamilton, and Theodore W Zderic. "Role of low energy expenditure and sitting in obesity, metabolic syndrome, type 2 diabetes, and cardiovascular disease." Diabetes 56.11 (2007): 2655-2667.

47. Baskin, Kedryn K, Benjamin R Winders, and Eric N Olson. "Muscle as a “mediator” of systemic metabolism." Cell metabolism 21.2 (2015): 237-248.
48. Schindelin, Johannes et al. "Fiji: an open-source platform for biological-image analysis." *Nature methods* 9.7 (2012): 676-682.
49. Nelson, Wendy D et al. "Site-directed spin labeling reveals a conformational switch in the phosphorylation domain of smooth muscle myosin." Proceedings of the National Academy of Sciences of the United States of America 102.11 (2005): 4000-4005.
50. Naber, N., Cooke, R. & Pate, E. (2011). Slow myosin ATP turnover in the super-relaxed state in tarantula muscle. J Mol Biol 411, 943-50.
51. Brito, R., Alamo, L., Lundberg, U., Guerrero, J. R., Pinto, A., Sulbaran, G., Gawinowicz, M. A., Craig, R. & Padron, R. (2011). A molecular model of phosphorylation-based activation and potentiation of tarantula muscle thick filaments. J Mol Biol 414, 44-61.
52. Alamo, L., Li, X. E., Espinoza-Fonseca, L. M., Pinto, A., Thomas, D. D., Lehman, W. & Padron, R. (2015). Tarantula myosin free head regulatory light chain phosphorylation stiffens N-terminal extension, releasing it and blocking its docking back. Mol Biosyst 11, 2180-9.
53. Espinoza-Fonseca, L. M., Alamo, L., Pinto, A., Thomas, D. D. & Padron, R. (2015). Sequential myosin phosphorylation activates tarantula thick filament via a disorder-order transition. Mol Biosyst 11, 2167-79.
54. Espinoza-Fonseca, L. M., Colson, B. A. & Thomas, D. D. (2014). Effects of pseudophosphorylation mutants on the structural dynamics of smooth muscle myosin regulatory light chain. Mol Biosyst 10, 2693-8.
55. Kast, D., Espinoza-Fonseca, L. M., Yi, C. & Thomas, D. D. (2010). Phosphorylation-induced structural changes in smooth muscle myosin regulatory light chain. Proc Natl Acad Sci U S A 107, 8207-12.
56. Xu, S., Offer, G., Gu, J., White, H. D. & Yu, L. C. (2003). Temperature and ligand dependence of conformation and helical order in myosin filaments. Biochemistry 42, 390-401.
57. Straight, Aaron F et al. "Dissecting temporal and spatial control of cytokinesis with a myosin II Inhibitor." Science 299.5613 (2003): 1743-1747.

58. Allingham, John S, Robert Smith, and Ivan Rayment. "The structural basis of blebbistatin inhibition and specificity for myosin II." Nature structural & molecular biology 12.4 (2005): 378-379.
59. Xu, Sengen et al. "Stabilization of helical order in the thick filaments by blebbistatin: further evidence of coexisting multiple conformations of myosin." Biophysical journal 96.9 (2009): 3673-3681.
60. Zhao, Fa-Qing, Raúl Padrón, and Roger Craig. "Blebbistatin stabilizes the helical order of myosin filaments by promoting the switch 2 closed state." Biophysical journal 95.7 (2008): 3322-3329.
61. Wilson, C., Naber, N., Pate, E. & Cooke, R. (2014). The myosin inhibitor blebbistatin stabilizes the super-relaxed state in skeletal muscle. Biophys J 107, 1637-46.
62. Kodama, Takao, Kazuhiro FUKUI, and Kaoru KOMETANI. "The initial phosphate burst in ATP hydrolysis by myosin and subfragment-1 as studied by a modified malachite green method for determination of inorganic phosphate." Journal of biochemistry 99.5 (1986): 1465-1472.
63. Straight, Aaron F et al. "Dissecting temporal and spatial control of cytokinesis with a myosin II Inhibitor." Science 299.5613 (2003): 1743-1747.
64. Baumann, Bruce AJ et al. "Phosphorylated smooth muscle heavy meromyosin shows an open conformation linked to activation." Journal of molecular biology 415.2 (2012): 274-287.
65. Wendt, Thomas et al. "Three-dimensional image reconstruction of dephosphorylated smooth muscle heavy meromyosin reveals asymmetry in the interaction between myosin heads and placement of subfragment 2." Proceedings of the National Academy of Sciences 98.8 (2001): 4361-4366.
66. Wu, Shenping et al. "Structural changes in isometrically contracting insect flight muscle trapped following a mechanical perturbation." PloS one 7.6 (2012): e39422-e39422.
67. Rayment, Ivan et al. "Three-dimensional structure of myosin subfragment-1: a molecular motor." Science 261.5117 (1993): 50-58.

68. Houdusse, Anne et al. "Atomic structure of scallop myosin subfragment S1 complexed with MgADP: a novel conformation of the myosin head." Cell 97.4 (1999): 459-470.
69. Málnási-Csizmadia, András et al. "Dimerization of the head–rod junction of scallop myosin." Biochemical and biophysical research communications 252.3 (1998): 595-601.
70. Tama, Florence et al. "The requirement for mechanical coupling between head and S2 domains in smooth muscle myosin ATPase regulation and its implications for dimeric motor function." Journal of molecular biology 345.4 (2005): 837-854.
71. Li, Chaokun et al. "FastCloning: a highly simplified, purification-free, sequence- and ligation-independent PCR cloning method." BMC biotechnology 11.1 (2011): 92.
72. Colson, B. A., Petersen, K. J., Collins, B. C., Lowe, D. A. & Thomas, D. D. (2015). The myosin super-relaxed state is disrupted by estradiol deficiency. Biochem Biophys Res Commun 456, 151-5.
73. Brunello, E., Bianco, P., Piazzesi, G., Linari, M., Reconditi, M., Panine, P., Narayanan, T., Helsby, W. I., Irving, M. & Lombardi, V. (2006). Structural changes in the myosin filament and cross-bridges during active force development in single intact frog muscle fibres: stiffness and X-ray diffraction measurements. J Physiol 577, 971-84.
74. Reconditi, M., Brunello, E., Fusi, L., Linari, M., Martinez, M. F., Lombardi, V., Irving, M. & Piazzesi, G. (2014). Sarcomere-length dependence of myosin filament structure in skeletal muscle fibres of the frog. J Physiol 592, 1119-37.
75. Haselgrove, J. C. (1975). X-ray evidence for conformational changes in the myosin filaments of vertebrate striated muscle. J Mol Biol 92, 113-43.
76. Sulbaran, G., Biasutto, A., Alamo, L., Riggs, C., Pinto, A., Mendez, F., Craig, R. & Padron, R. (2013). Different head environments in tarantula thick filaments support a cooperative activation process. Biophys J 105, 2114-22.
77. Woodhead, J. L. & Craig, R. (2015). Through Thick and Thin--Interfilament Communication in Muscle. Biophys J 109, 665-7.

78. Espinoza-Fonseca, L. M., Kast, D. & Thomas, D. D. (2007). Molecular dynamics simulations reveal a disorder-to-order transition on phosphorylation of smooth muscle myosin. Biophys J 93, 2083-90.)
79. Fusi, L., Huang, Z. & Irving, M. (2015). The Conformation of Myosin Heads in Relaxed Skeletal Muscle: Implications for Myosin-Based Regulation. Biophys J 109, 783-92.
80. Kampourakis, T., Sun, Y. B. & Irving, M. (2015). Orientation of the N- and C-terminal lobes of the myosin regulatory light chain in cardiac muscle. Biophys J 108, 304-14.
81. Cooke, Roger. "The role of the myosin ATPase activity in adaptive thermogenesis by skeletal muscle." Biophysical reviews 3.1 (2011): 33-45.
82. Okumura, Yukiko, Masataka Narukawa, and Tatsuo Watanabe. "Adiposity suppression effect in mice due to black pepper and its main pungent component, piperine." Bioscience, biotechnology, and biochemistry 74.8 (2010): 1545-1549.
83. Choi, Seoyoon et al. "Piperine reverses high fat diet-induced hepatic steatosis and insulin resistance in mice." Food chemistry 141.4 (2013): 3627-3635.
84. Shah, Shreya S et al. "Effect of piperine in the regulation of obesity-induced dyslipidemia in high-fat diet rats." Indian journal of pharmacology 43.3 (2011): 296.
85. Diwan, Vishal, Hemant Poudyal, and Lindsay Brown. "Piperine attenuates cardiovascular, liver and metabolic changes in high carbohydrate, high fat-fed rats." Cell biochemistry and biophysics 67.2 (2013): 297-304.
86. Park, Ui-Hyun et al. "Piperine, a component of black pepper, inhibits adipogenesis by antagonizing PPARγ activity in 3T3-L1 cells." Journal of agricultural and food chemistry 60.15 (2012): 3853-3860.
87. BrahmaNaidu, Parim et al. "Mitigating efficacy of piperine in the physiological derangements of high fat diet induced obesity in Sprague Dawley rats." Chemico-biological interactions 221 (2014): 42-51.
88. Rondanelli, Mariangela et al. "Improvement in insulin resistance and favourable changes in plasma inflammatory adipokines after weight loss

associated with two months' consumption of a combination of bioactive food ingredients in overweight subjects." Endocrine 44.2 (2013): 391-401.

89. Kim, Kyung Jin et al. "Piperidine alkaloids from Piperretrofractum Vahl. protect against high-fat diet-induced obesity by regulating lipid metabolism and activating AMP-activated protein kinase." Biochemical and biophysical research communications 411.1 (2011): 219-225.
90. Szallasi, Arpad. "Piperine: researchers discover new flavor in an ancient spice." Trends in pharmacological sciences 26.9 (2005): 437-439.
91. Iwasaki, Yusaku et al. "TRPV1 agonist monoacylglycerol increases UCP1 content in brown adipose tissue and suppresses accumulation of visceral fat in mice fed a high-fat and high-sucrose diet." Bioscience, biotechnology, and biochemistry 75.5 (2011): 904-909.
92. Mareib, EN, Hoehn, K. (2010) Human Anatomy & Physiology (8th ed.) San Francisco: Benjamin. p. 312. ISBN 978-0-8053-9569-3.
93. Bhat, B Ganesh, and N Chandrasekhara. "Studies on the metabolism of piperine: absorption, tissue distribution and excretion of urinary conjugates in rats." Toxicology 40.1 (1986): 83-92.
94. Thiel, Anette et al. "Black pepper constituent piperine: Genotoxicity studies in vitro and in vivo." Food and Chemical Toxicology 66 (2014): 350-357.
95. Shoba G et al. "Influence of piperine on the pharmacokinetics of curcumin in animals and human volunteers." Planta Med. 64 (1998): 353-356.
96. Singh, JASWANT, RK Dubey, and CK Atal. "Piperine-mediated inhibition of glucuronidation activity in isolated epithelial cells of the guinea-pig small intestine: evidence that piperine lowers the endogeneous UDP-glucuronic acid content." Journal of Pharmacology and Experimental Therapeutics 236.2 (1986): 488-493.
97. Volak, Laurie P et al. "Effect of a herbal extract containing curcumin and piperine on midazolam, flurbiprofen and paracetamol (acetaminophen) pharmacokinetics in healthy volunteers." British journal of clinical pharmacology 75.2 (2013): 450-462.

98. Brunmair, B et al. "Activation of PPAR-δ in isolated rat skeletal muscle switches fuel preference from glucose to fatty acids." Diabetologia 49.11 (2006): 2713-2722.
99. Sharp, Paul M, and Wen-Hsiung Li. "The codon adaptation index-a measure of directional synonymous codon usage bias, and its potential applications." Nucleic acids research 15.3 (1987): 1281-1295.

10. Acknowledgements.

I would like to thank Dr.ssa Marcella Canton and Prof. Carlo Reggiani for their support and for proposing me to work for this project, three years ago.

A special thanks goes to Prof. Roger Cooke and Nariman Naber for the scientific support during my three-episodes-adventure in San Francisco, they both taught me not science only. I would like to remember Prof. Edward Pate, who helped me with the design and analysis of experiments and recently passed away.

I would like to thank my parents, Antonella and Emiliano, and all my relatives. I feel so lucky I have so many people who love me and make me feel I am special. I would like to thank my roommates for being so kind during the crazy time I spent writing this thesis.

Data for this study were acquired at the Nikon Imaging Center at UCSF/QB3. I would like to thank Dr. Kurt Thorn and Ms. Delaine Larson for their generous help in using the microscopes. The screen was carried out in the SMDC at UCSF with the help of Kenny Ang. Troponin C was a gift from Dr. Dong, WSU; the mouse sequence was a gift from Prof. Fabio Di Lisa, Università degli Studi di Padova. I would also like to thank the many members of the laboratory of Dr. Geeta Narlikar, UCSF, and Dr. Elisabetta Bergantino for their help with the molecular biology. I would like to thank Fondazione Cassa di Risparmio di Padova e Rovigo and Fondazione Ing. Aldo Gini for its financial support.